THERMODYNAMIC AND STRUCTURAL RELATIONSHIPS IN THE LANTHANUM-NICKEL-OXYGEN SYSTEM

by

C.P. TAVARES BSc (Hons)

January 1981

A Thesis submitted for the Degree of Doctor of Philosophy of the University of London and for the Diploma of Imperial College.

Metallurgy and Materials Science Dept.
Imperial College
Prince Consort Road
London SW7 2AG.

A C K N O W L E D G M E N T S

I am grateful to my Supervisor Dr. B.C.H. Steele for his advice and encouragement throughout this project.

In the Laboratory my thanks go to Dr. J. Drennan who collected the Lattice Imaging Data, to Dr. J. Kilner for his all round advice and availability and M.J. Storey (now left) for the stimulating discussions we used to have. Mr. J.W. Wright and Mr. G. Hicks's rare qualities of helpfulness and willingness are greatly admired and respected.

Further afield, Dr. Goodgame (Chemistry Department) who advised on the preparation of the hexanitritonickelates is greatly indebted to.

Since I learnt a great deal about oxygen pumps and gauges at the E.N.P.G. (Grenoble) during my three months stay there, I am also indebted to Dr. M. Kleitz for receiving me.

Financial assistance from the S.R.C. for the project was gratefully received.

My wife Lullyn who typed the final script deserves a special mention. She provided support in most difficult times.

T H E S I S

ABSTRACT

Phases of the general formula $La_{N+1}Ni_NO_{3N+1}$ (where N = 1,2,3,4 and ∞) have been prepared and isolated in the La-Ni-O system. Structural and electronic properties of all the compounds and relates ones are discussed. The N = ∞ phase was prepared by a new route at 650-700°C from the precurser $NH_4La\ Ni(NO_2)_6 \times H_2O$ in addition to methods used by other workers. Of the intermediate phases, the N = 3 phase ($La_4Ni_3O_{10}$) was once previously reported. The other two compounds $La_3Ni_2O_7$ and $La_5Ni_4O_{13}$ were unknown prior to this work. They have the Fmmm structure similar to $La_4Ni_3O_{10}$. They have the following lattice constants :-

i) $La_3Ni_2O_7$ a = 5.397± 0.001Å, b = 5.448±0.001Å and c = 20.509±0.004Å

ii) $La_5Ni_4O_{13}$ a = 5.415Å, b = 5.456Å and c = 34.99Å

The perovskite $LaNiO_3$ was studied by thermogravimetry and the T.G.A. curve showed evidence of the N = 1, 2 and 3 phases being involved in the decomposition. Part of the T.G.A. curve was reproduced electrochemically employing a solid state oxygen pump and gauge. Two types of curves were produced by this technique :-

a) At constant temperature - the G(X) curve.

b) At constant partial pressure of oxygen - the T(X) curve.

Thermodynamic properties of all the compounds except $LaNiO_3$ were determined by measuring the variation of the oxygen partial pressure against temperature in solid state electromotiveforce (e.m.f.) cells based on Ytrria Stabilized Zirconia solid electrolyte. The values obtained read :-

i) N = 1, ΔG_f^o = - 2065.5 + 0.364T ± 13 kJmol^{-1} 1150K < T < 1340K

ii) N = 2, ΔG_f^o = - 3150 + 0.542T ± 13 kJmol^{-1} 1160K < T < 1460K

iii) N = 3, ΔG_f^o = - 4239 + 0.792T ± 13 kJmol^{-1} 1150K < T < 1310K

iv) $N = 4, \Delta G_f^o = -5330 + 0.915T \pm 13\ kJmol^{-1}$ $1100K < T < 1270K$

These properties correlate with the deductions made from the T.G.A. curve of $LaNiO_3$.

At high temperatures the nonstoichiometry of the compounds is discussed in terms of the formation of metastable or solid solution compounds. This is observed in the e.m.f. vs temperature curves as a change of slope and in the T(X) and G(X) curves as the broadening of triphasic regions. At low temperatures the nonstoichiometry in all the $La_{N+1}Ni_NO_{3N+1}$ compounds was studied by high resolution electron microscopy (lattice imaging). This technique showed that the nonstoichiometry is by the formation of coherent intergrowths of other neighbouring $La_{N+1}Ni_NO_{3N+1}$ phases sharing the perovskite sublattice.

C O N T E N T S

CHAPTER 0

Introduction

0.1 General Comments

Perovskite oxides that are electronic conductors have been well studied within the last decade or so notably as catalytic cathodes for the electrochemical burning of fuels[85]. One example of this class of compounds is $LaNiO_3$ which has the distorted perovskite ($R\bar{3}m$) structure. It has been tested in both high and low temperature fuel cells[1,2a] and has been tested as an electrochemical ethanol sensor[82].

The electrocatalytic effect as shown by $LaNiO_3$[17,36] embraces two properties. One is the property of the metallic continuum for charge transfer which is a bulk property. The other is due to the chemical nature of the transition metal ion which according to Sachlter[91] is restricted to the first few monolayers of the solid. Both of these are properties of stoichiometry. For a ternary oxide such as $LaNiO_3$ if one component, say oxygen, is removed or added defects may accumulate or crystal structure may change and the oxidation state of the catalytic ion will be affected.

A knowledge of the mechanism of defect accumulation is therefore invaluable. This description may, as suggested above, involve the formation of other phases. Accordingly relative phase stabilities and relationships i.e. the phase diagram, demands elucidation.

0.2 Anion Elimination in ABO_3 Perovskites

The ABO_3 (Pm3m) perovskite structure can be considered the end member of a family of oxides having the A_2BO_4 (I4mmm) structure as the other end member. Gross anion deficiency in the perovskite matrix is by the elimination of whole rows of BO_6 octahedra. This process produces structures and compositions intermediate between ABO_3

and A_2BO_4. The conditions to be satisfied can broadly be grouped into two categories :-

1) Crystallographic - by taking away slabs of BO_6 octahedra from the ABO_3 matrix coulombic forces may develop between two halves of the structure. One half of the structure is therefore displaced halfway along a diagonal [110] axis.

Geometrically structures of 1 octahedra in width and 2N+1 octahedra in height are possible - these are shown in Figure 8 of Chapter 1. When N = 1 we are at the extreme of anion elimination - alternate BO_6 sheets are removed - and we obtain the A_2BO_4 phase which as described above is furthest away from ABO_3. The A_2BO_4 structure is a layer structure of BO_6 octahedra sandwiching larger A cations; each layer being displaced halfway along the [110] axis.

When N = 2 layer thickness = 2 - the composition is $A_3B_2O_7$

" N = 3 " " = 3 - " " " $A_4B_3O_{10}$

" N = 4 " " = 4 - " " " $A_5B_4O_{13}$

and so on up to N = ∞ - perovskite (ABO_3). The generalised chemical formula is $A_{N+1}B_NO_{3N+1}$. The space group for all these intermediate phases is ideally I4mmm as it is for A_2BO_4 (N = 1).

2) Thermodynamic - The Gibbs phase rule must be obeyed. At fixed temperature and pressure anion elimination takes place within a three phase equilibrium. This equilibrium is formed between two ternary phases and a binary phase. From 1) above it is implicit that the line connecting ABO_3 and A_2BO_4 in the Gibbs ternary triangle is discontinuous. The three phase region is therefore bounded by one of the two binary oxides of the triangle and two ternary oxides along the discontinuous ABO_3 - A_2BO_4 line. This is shown in Figure 1. As we move towards the perovskite (N=∞) the differences in thermodynamic properties between two phases sharing a common tangent become smaller.

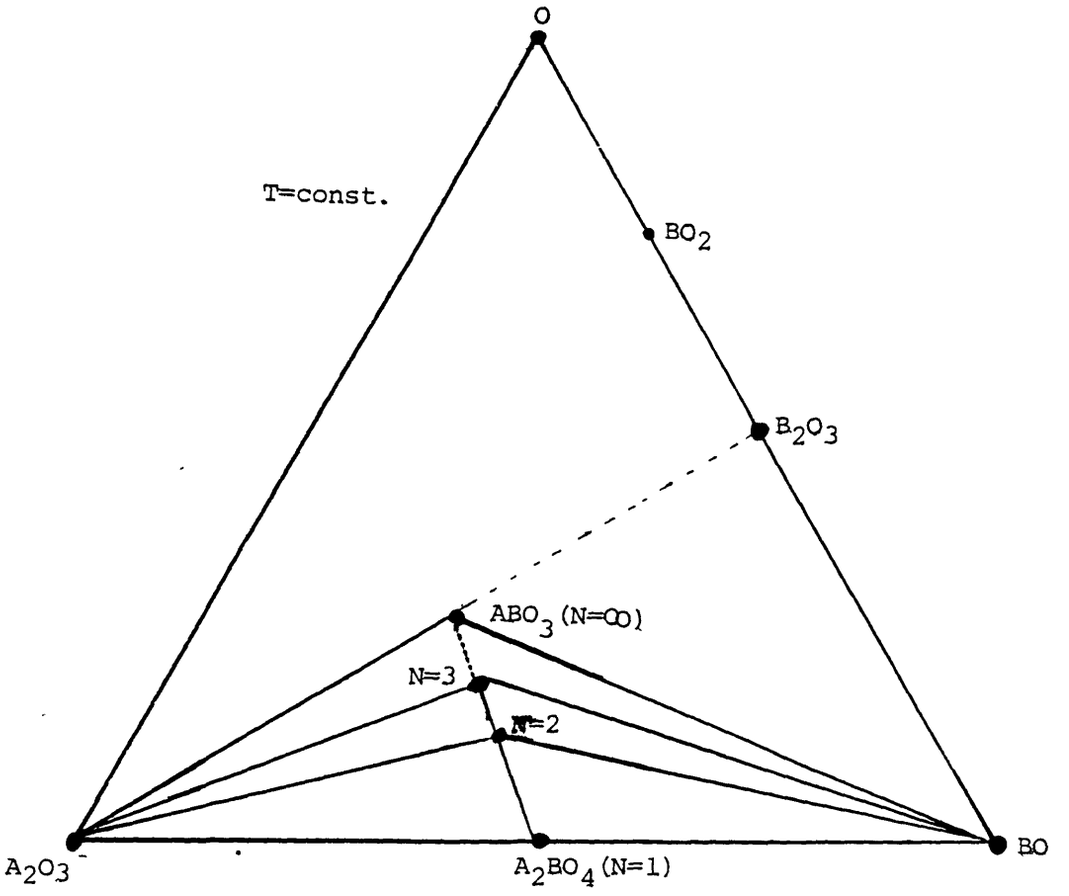

Figure 1 - Typical A-B-O 'phase diagram' showing $A_{N+1}B_NO_{3N+1}$ phases intermediate between ABO_3 & A_2BO_4.

The phases closest to A_2BO_4 ($N = 2 \longrightarrow N = 4$) are readily distinguishable by X-ray diffraction methods. For example Ruddlesden et al.[92] isolated and identified the N=2 and N=3 phases in the Sr-Ti-O system 23 years ago. Part of this project is devoted to the preparation and characterisation of similar phases in this 'easily accessible' range of the La-Ni-O phase diagram.

Synthesis and structural characterisation of phases nearer ABO_3 are difficult. The former by the very small changes in A:B that are required and the accurate control of preparation atmosphere (p_{O_2}) and temperature. Tackling these problems via ordinary ceramic preparation techniques may seem like cracking a nut with a sledgehammer. The latter problem appears to be more soluble using high resolution electron microscopy. However the larger perovskite building blocks may also impart new and different structural features. In addition the uncertainty as to when, where and if a point defect model successfully competes requires analysis outside the scope of this project. For these reasons no studies were carried out in this 'poorly

accessible' region of the La-Ni-O phase diagram.

0.3 Phase Study

The stable phases within a system are those arrangements of atoms that possess the minimum in Gibbs free energy G where G = H-TS. The properties of the constituent atoms such as bond lengths (near neighbour relationships) and therefore bond energies correlate more closely with the enthalpy H whereas properties related to disorder (non near neighbour relationships) correlate more closely with the entropy S[81]. This project in part entails the evaluation of G for La-Ni-O compounds at high temperatures.

In A-B-O systems G is more often than not measured in terms of μ_{O_2} - the chemical potential of the solid phases being assumed to be constant. The idealised μ- X curve is a step function in which $\left(\frac{\partial \mu}{\partial x}\right) = 0$ for 3 solid phase regions (system is invarient) and $\left(\frac{\partial \mu}{\partial x}\right) = \infty$ for 2 phase regions (system is univarient). In other words at a fixed temperature the tangent formed by three coexisting phases (any one of the triangles in Figure 1) demarcate a certain μ_{O_2}. For those regions therefore μ_{O_2} and in consequence G varies with temperature at fixed reference μ_{O_2} and the converse. The slope of the μ(T) curve defines the reaction entropy ΔS and its intercept the reaction enthalpy ΔH.

For oxide systems galvanic cells employing oxide ion conductors (such as Yttria Stabilised Zirconia (YSZ)) provides a very accurate technique for determining the μ_{O_2}(T) relationship at high temperatures. There is no need for a conventional noble metal electrocatalyst (eg Pt) on the sample side of such cells when using electrocatalytic oxides as those in the La-Ni-O system. This amounts to a simplification in the design of such cells. The limitation of such cells depends on whether the voltage that develops across the electrolyte results in partial electrolysis such that $t_{O^{2-}} < 1$. Normally $E \sim 1.5$ V at $T \sim 1200$K is the acceptable limit on YSZ[58]. For the $La_{N+1}Ni_NO_{3N+1}$ oxides, air, P_{O_2} = 21.3kPa was an adequate and accurate reference because P_{O_2} coexistence

ranges of the phases with N = 1,2,3,4 and ∞ were typically 0.1 pa-100kPa (ie E ∽ (150-5) mV at 1000K < T < 1460K.

The application of galvanic cell techniques although elegant is dependent absolutely on the ability to synthesise phases. The μ - T - X surface of a 3 component system will show a series of steps[52] smoothing out at higher temperatures where coexistence broadens. Each pair of steps constitutes two 3 phase regions joined by a common tangent (one phase common to both). Under these conditions the Gibbs-Duhem equation is applicable for the determination of thermodynamic properties for unisolated phases observable in both T-X and G-X curves. From any single pure ternary phase these profiles are obtainable electrochemically employing two cells :-

i) A pump so that the current $i = f(Q_{O_2})$

ii) A gauge so that the voltage $E = f(p_{O_2})$.

Pump and gauge modulation depends on the choice of experimental variables. We term the possible titrations as follows :-

a) Potentiocoulometric - P (Q) (G-X curve) - T constant

b) Thermocoulometric - T (Q) (T-X curve) - p_{O_2} constant.

The latter is well known as the conventional T.G.A. profile obtainable using a mass balance.

The electrochemical techniques for both triphasic and monophasic specimens clearly have advantages in accuracy and the size of specimens required over other techniques such as gas equilibration. One limitation however is the low ionic conductivity of the oxide electrolyte at temperatures below 650°C. This is partly traded off against extended equilibration times for the electrode processes. On the debit side phase resolution is sharper at lower temperatures and manifestly more in correlation with data from structure sensitive techniques such as X-ray and electron microscopy obtained by and large at 300K.

0.4 Non-Stoichiometry of Perovskite-Related Compounds

All the $A_{N+1}B_NO_{3N+1}$ compounds share the perovskite sublattice. Non-stoichiometric faults instead of random point defect can be introduced in any one compound by the insertion of rows or columns or blocks of another compound because the structures are geometrically compatible[3,87b,88]. Thus for 'common tangent' phases anion excess in one phase may be considered as anion deficiency in the other. In other words the perovskite type lattices intergrow coherently.

Lattice imaging is the direct method for studying such intergrowth or 'metastable' phases. Tilley[3] and Carpy et al.[88] have used the technique to study intergrowths in $Sr_{N+1}Ti_NO_{3N+1}$ and $CaNa_NNb_NO_{3N+1}$ compounds. These compounds (in both families) are insulating and have a high permittivity ϵ[3,8]. The former school[3] and Iguchi[86] suggested a high permittivity is diagnostic and defect accumulation by extended defect (intergrowth) formation. The large value of ϵ is due predominantly to the ionic polarisability term. This is large for small 'highly polarising' cations which can occupy a distorted polyhedron environment.

Intergrowth structures, as will be discussed later, are observed in all the $La_{N+1}Ni_NO_{3N+1}$ phases so far isolated. If ionic size is, in the final analysis, the operational criterion for extended defect formation, then it appears to be fulfilled for the $La_{N+1}Ni_NO_{3N+1}$ compounds. The $La_{N+1}Ni_NO_{3N+1}$ compounds are metallic or semiconductors of low activation energy. In addition Ni^{2+} which is larger than typical B^{4+} (e.g Ti^{4+}) is, to varying degrees, incorporated in these compounds. These observations suggest that extended defect formation cannot be explained purely on the basis of the ideas developed for insulating oxides. This topic will be further discussed in Chapter 6.

CHAPTER 1

Ternary Compounds in the System La-Ni-O

1.1 $LaNiO_3$ - Lanthanum Trioxonickelate III -

1.1.1 Structure :-

The oxide has the rhombohedrally distorted perovskite structure (either $R\bar{3}m$ or $R\bar{3}c$ - Figures 2a and 2b respectively - but changes to the ideal cubic form ($Pm3m$) at 1213K according to Obayashi et al[4]. We have found good agreement for the unit cell parameters as reported by Wold et al.[5] and Demazeau et al.[6] as is summarised in Table 1. There are however discrepances in the indexing of the X-ray powder diffraction pattern (Plate 1 B (i)) as reported by Wold et al.[5] Details of these are listed in the Appendix (Table A1).

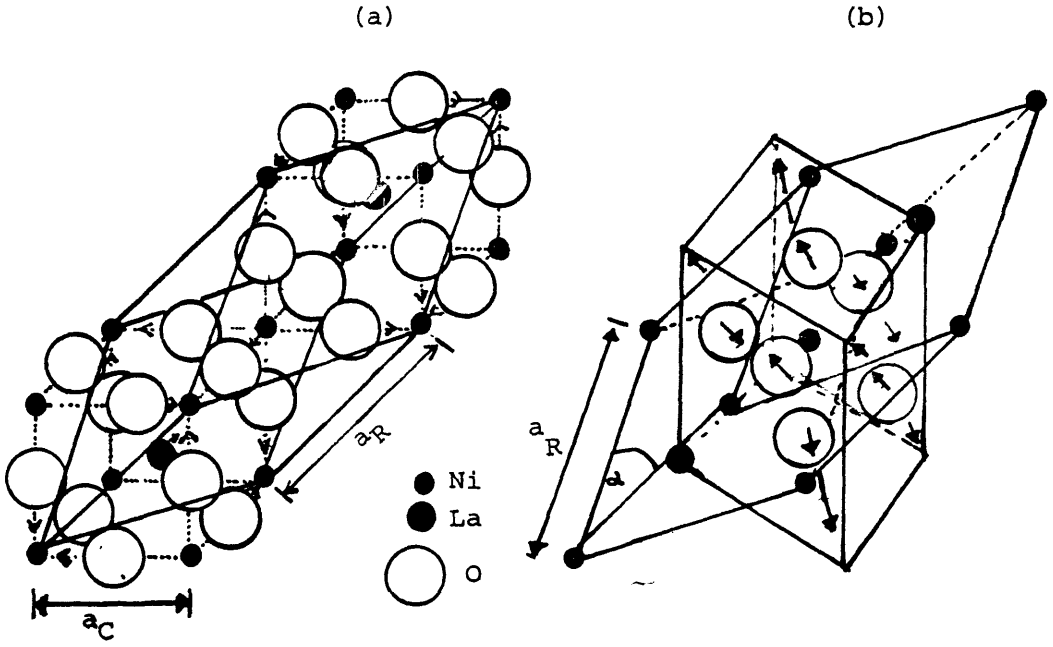

Figure 2 - Distorted Perovskite Structure of $LaNiO_3$
(a) $R\bar{3}m$ (b) $R\bar{3}c$

Plate 2(a) shows the electron diffraction pattern of $LaNiO_3$ indexed on the hexagonal basis. On the left of the picture is the indexing on the rhombohedral $R\bar{3}m$ basis. The very small distortion from cubic symmetry is apparent in the first picture (i.e. B = $[\bar{1}00]$ (rhombohedral) $\alpha \sim 90^\circ$).

PLATE I

A) $Sr_x La_{2-x} Li_y Ni_{1-y} O_4$ - I4MMM.

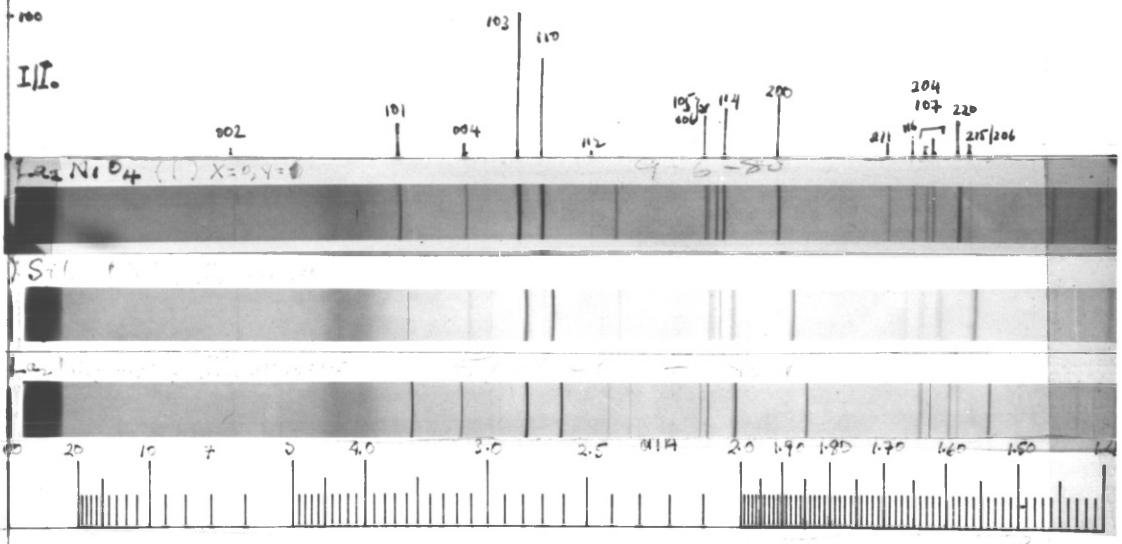

B) $La_{n+1} Ni_n O_{3n+1}$

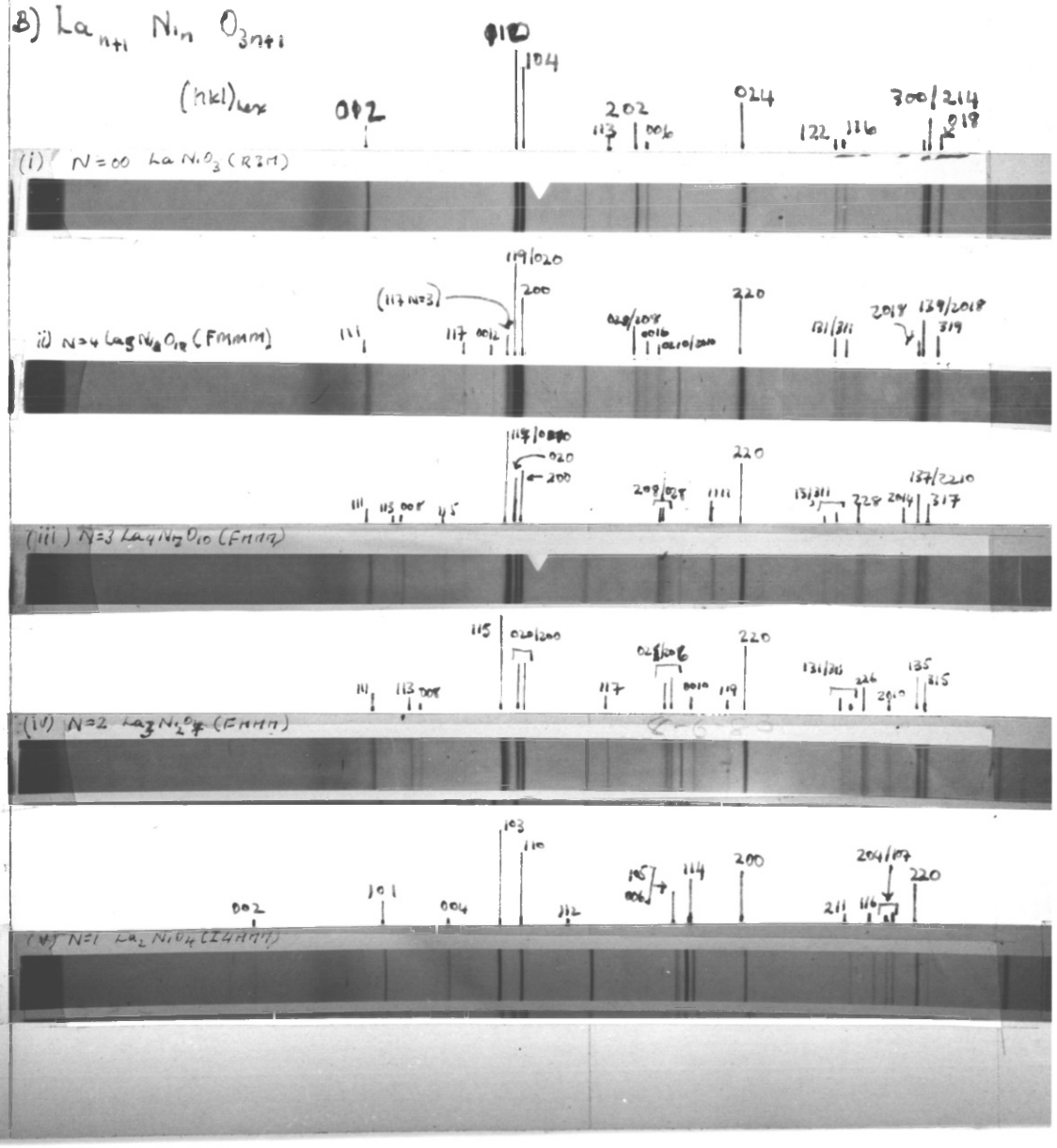

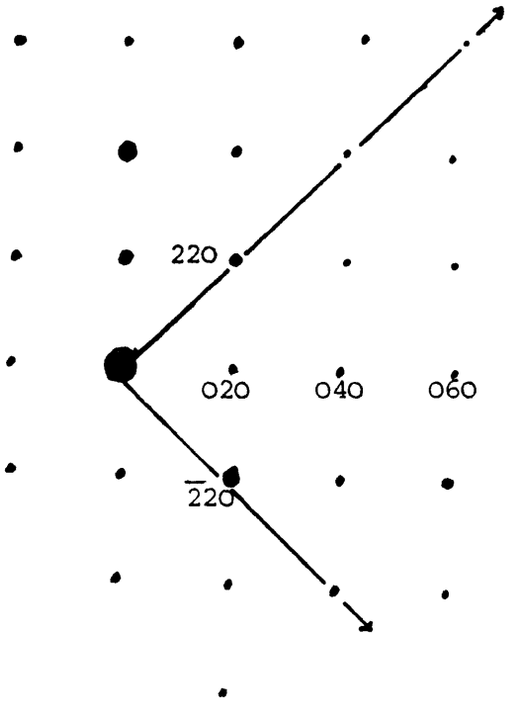

B = $[\bar{1}00]$ (hkl- $R\bar{3}m$)

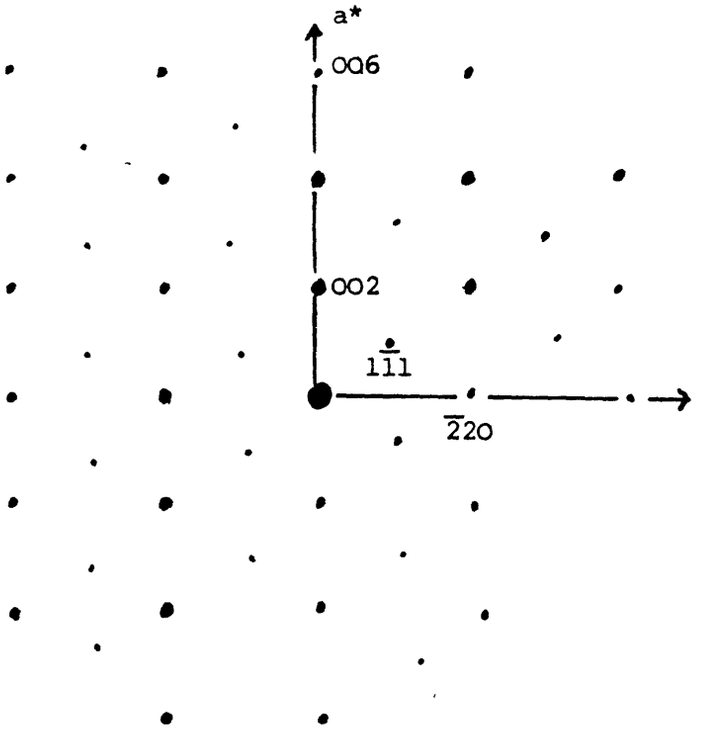

B = [110] (hkl- $R\bar{3}m$)

Plate 2a

Single crystal electron diffraction pattern of $LaNiO_3$ (R3m' indexed on the hexagonal basis.

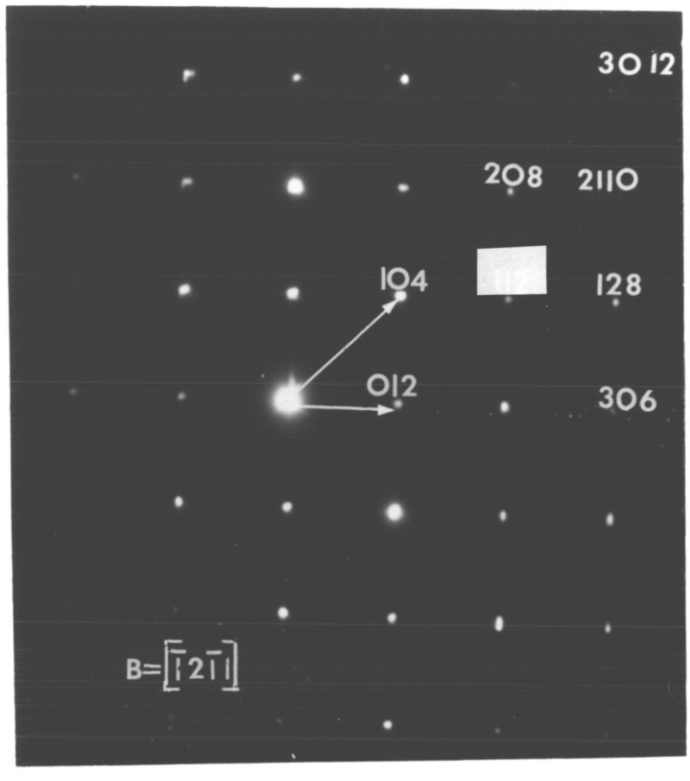

$\lambda = 0.037\text{Å}$ L = 144 cm.

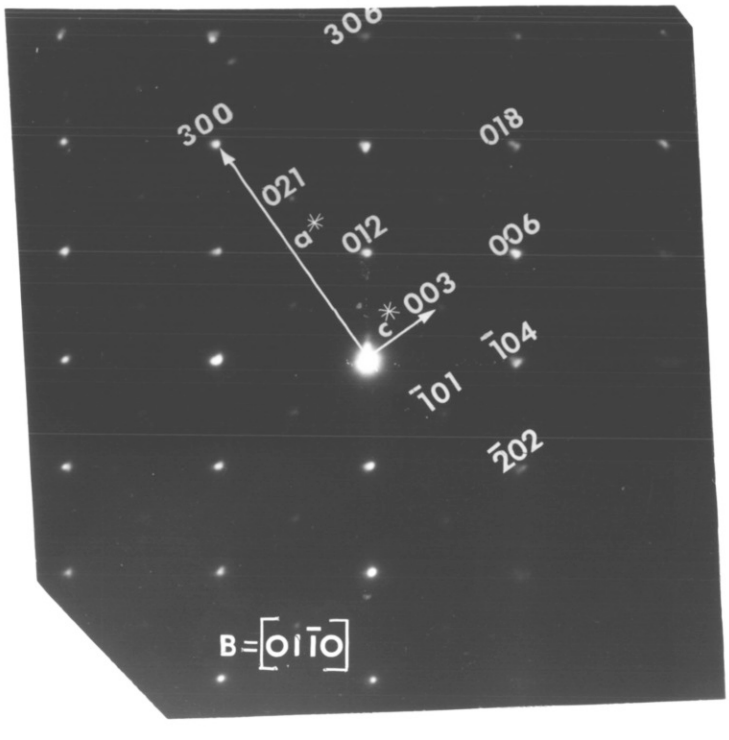

a = 5.453Å c = 13.128Å

TABLE 1 Lattice Parameter of $LaNiO_3$:-

Author		Wold et al.[5]	Demazeau et al.[6]	This work
$R\bar{3}m$	a/Å	7.676	-	7.672
	α/°	90°43'	-	90°32'
$R\bar{3}c$	a/Å	5.461	5.393	-
	α/°	60°49'	60°48'	-
Hexagonal	a/Å	5.456	5.459	5.453
	c/Å	13.122	13.131	13.128

It is uncertain whether $LaNiO_3$ adopts the $R\bar{3}c$ (Z = 1) or the $R\bar{3}m$ (Z=2) symmetry. In $R\bar{3}c$ all the Ni ions are equivalent. In $R\bar{3}m$ there are two distinguishable Ni positions - La displaced along [111] so that $d_{La-Ni} \neq d'_{La-Ni}$ (Figure 2). The physical reason for this would be unclear in pure $LaNiO_3$. According to Rao[7], Goodenough and Longo[8] $LaCoO_3$ changes from $R\bar{3}c$ where all the Co ions are in the low spin state (Co^{III} - t_{2g}^6 S = 0 -) to R3 at higher temperatures where there is nearly equal population of Co^{III} and Co^{3+} ($t_{2g}^4 e_g^2$, S = 2). As a result the compound shows localised $\longleftrightarrow$ electron behaviour.

The electrical and magnetic properties of $LaNiO_3$ (next section) shows no such 'spin cross-over' effect as is evident in $LaCoO_3$ by the semiconductor $\longleftrightarrow$ metal transition[7]. Indeed metallic conduction[4,6,7,9,10,22] and weak Pauli paramagnetism[9,13] are observed from liquid hydrogen temperatures to 1313K where, according to Obayashi et al.[4], it decomposes. By inference therefore Ni^{III} ($t_{2g}^6 e_g^1$, S = ½) and not Ni^{3+} ($t_{2g}^5 e_g^2$, S = $\frac{3}{2}$) is retained and the symmetry is $R\bar{3}c$ after Demazeau et al.[6] and Goodenough et al.[8]

However as will become evident later in this Chapter $La_{N+1}Ni_NO_{3N+1}$ oxides having distinguishable Ni positions (Ni^{III} and Ni^{2+}) have almost identical [001] zones - electron diffraction - to

the $[\bar{1}2\bar{1}1]$, $R\bar{3}m$, zone of $LaNiO_3$ (Plate 2(a)(1)). It is tentatively assumed therefore that under known and existing conditions of synthesis there is some population of Ni^{2+} ($t_{2g}^6 e_g^2$, S = 1) in which case the symmetry is $R\bar{3}m$ and not $R\bar{3}c$ and in accordance the composition is not $LaNiO_3$ but $La_{N+1}Ni_NO_{3N+1}$ where N is large but less than infinity. The purest of pure might be $R\bar{3}c$ or even cubic ($Pm3m$). The argument (to be elucidated later) is also supported firstly by the fact that we have observed phases of the above type having N = 6 or 7 at the same temperature where $LaNiO_3$ is supposed to be cubic[4]. Secondly, by Ganguly and Rao's[10] work showing signigicant differences in conductivity and Seebeck Coefficient measurements of samples prepared by the two old and established methods of Wold et al.[5] and Goodenough et al.[11] Thirdly, and this point should become clearer in Chapters 3 and 4, thermodynamic measurements on samples hitherto thought of as pure $LaNiO_3$ - having an X-ray powder pattern similar, if not identical, to those reported in the literature - showed that they were in fact $La_{N+1}Ni_NO_{3N+1}$. Fourthly the constant detection of NiO however low has been observed by the author in several samples of $LaNiO_3$ prepared by different routes. This has also been reported by Matsumoto et al.[36] and Koehler et al.[13]

Goodenough and Longo[8] suggest that nowadays the $R\bar{3}c$ structure can be assumed now that accurate lattice positions can be experimentally observed. This is based on the fact that $LaAlO_3$ has been shown by a whole host of techniques such as NQR to have the $R\bar{3}c$ symmetry. It is worth pointing out that, for all intents and purposes, Al displays only +3 valence and therefore the situation might not be parallel with the transition metal perovskites as a consequence of the variable valence.

1.1.2 Bonding :-

The bonding in ABO_3 perovskites have been treated excellently by a qualitative scheme pioneered by Goodenough and co-workers.[8,9,11.12] The ABO_3 lattice (Figure 3) to first approximation can be treated like the BO_3 lattice (ReO_3 type - Pm3m -) since B-B, B-A-B and A-O-A interactions are feeble (large atomic distances). Only B-O-B interactions are significant.

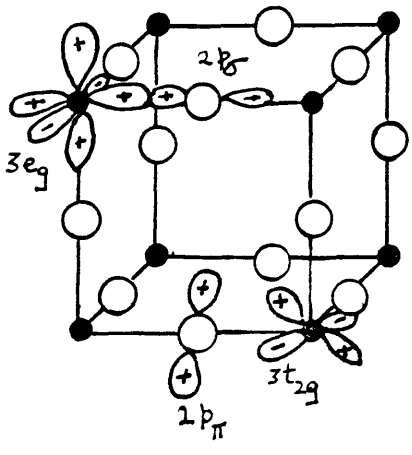

Figure 3 - B-O-B bonding in ABO_3 (Pm3m)

The essentials of the bonding scheme (Figure 4) are summarised below:-

(i) We start with a) 4s, 4p and 3d levels of B - column 1

b) 2s and 2p levels of oxygen - column 5

(ii) Degenerate 4p levels are unaffected by the O_h field of oxygen (the ligand field) but the 3d are split into the $3t_{2g}$ (d_{xy}, d_{yz} and d_{zx}) and the $3e_g$ ($d_{x^2-y^2}$ and d_{z^2}) - column 2

(iii) The Pm3m field (Figure 3) splits the degenerate 2p levels of oxygen into (a) $2p_\sigma$ which point towards nearest neighbour B and are lower in energy than (b) $2p_\pi$ which point away from nearest neighbour B and lies in empty space.

The $3e_g$ levels point towards nearest neighbour O and the $3t_{2g}$ point away from nearest neighbour O into empty space - column 4.

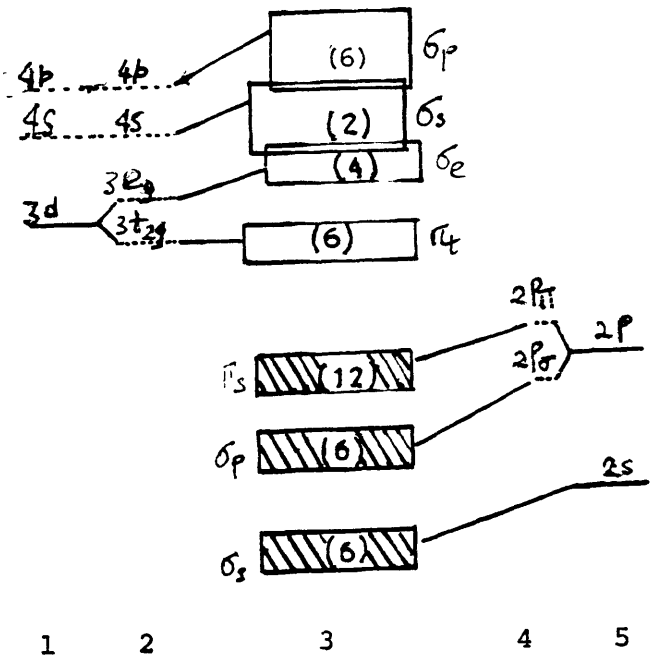

Figure 4 - Energy Level Diagram of BO_3 Perovskite Lattice

(iv) From (iii) σ_e type bonding is symmetry allowed and is continuous throughout the crystal. Each is associated with a certain set of wave functions of varying degrees of 4p, 4s, $3e_g$, $2p_\sigma$ and 2s characters. Similarly π_t is allowed between $3t_{2g}$ and $2p_\sigma$ but resulting bands tend to be narrower.

(v) The final positions of all resulting bands are equally governed by the Madelung Energy of the ABO_3 lattice and by the energy of the respective levels in the isolated atoms - column 3.

(vi) The number of states available for electron occupancy is governed by the principle of conservation states. For example a band of primarily t_{2g} character has a maximum capacity of 6 electrons per ABO_3 and the $2p\pi_t$ band derived from 2s and 2p states of O_3 a maximum of 12 (i.e. 3x 2 x 3) and so on - Figure 4 -.

(vii) For the filling of states, to a first approximation only the top bands are affected by the electrons of the A cation which must be added to the pool.

Whether a given perovskite displays metallic conductivity is dependent on :-

(viii) Sufficient B-O overlap (i.e. $3t_{2g}$-$2p_{\pi}$ or $3e_g$-$2p_{\sigma}$).

(ix) Spin - B-O overlap is impaired for high spin cations. The orbitals tend to be contracted about B.

(x) The total number of electrons to be accommodated is such that at least one band must be partially filled - conduction band.

(xi) Alternative to (x) 'Spill Over' of charge carriers from filled bands into otherwise empty bands.

Goodenough[8] makes the point that for $A^{(6-M)}B^{M}O_3$ there is an increase in covalence with M - there are stronger B-O-B interaction and correspondingly wider bands. He defines a critical size of overlap integral b (b_c) for band formation such that :-

a) $b_c < b_{\pi}$ π_t band formation (delocalised electrons)

b) $b_c < b_{\sigma}$ σ_e band formation (delocalised electrons)

c) $b_c > b_{\sigma}$, $b_c > b_{\pi}$; σ_e and π_t collapses into $3t_{2g}$ and $3\ e_g$ states respectively (i.e. localised electrons).

He also defines a critical size for the overlap integral b_m (relative to b_c) below which magnetic ordering takes place at low temperatures. Sophisticated band structure calculations have been carried out on ReO_3 (metallic), $SrTiO_3$ (insulator) and $KTaO_3$ (insulator)[2b,84] and have supported the Goodenough scheme. As known, the majority of M=3 perovskites of the third row do not have the cubic ($Pm3m$) symmetry but a small rhombohedral distortion as is the case for $LaNiO_3$. This does not appear to have impaired electrical properties[4] and so the Goodenough scheme is applicable[11].

1.1.3. Properties :-

The configuration of the isolated 'NiO_3' 'molecule' is $t_{2g}^6 e_g^1$ (i.e. S = ½). According to the above scheme the e_g^1 configuration is delocalised and therefore crystal configuration is $t^6\sigma_e^1$ (neglecting lower energy states). The compound is metallic (ρ, the resistivity

increases with temperature) with a room temperature resistivity of $10^{-4}\Omega$ cm according to Obayashi et al.[4] (for sintered bars of 80% density). The oxide has a negative Seebeck Coefficient increasing linearly with T indicating partially filled bands and conduction by electrons[16]. Thornton et al.[22] have shown that the transition (in the X-ray Photoelectron Spectra) associated with the $3e_g^1$ configuration is broad and diffuse, indicating delocalisation. No magnetic ordering has been observed down to 10K[13] - only weak Pauli Paramagnetism.

Demazeau et al.[6] have carried out a fairly systematic study of the $LnNiO_3$ (Ln = La⟶Lu) compounds, but only $LaNiO_3$ has the perovskite structure and appears to be metallic. Of the others $YNiO_3$ and $LuNiO_3$ show G type magnetic ordering at low temperature.

The compounds $LaBO_3$ (B=Co, Ni and Cu) are directly comparable under the Goodenough scheme since they are isomorphous - Table 2.

TABLE 2 Properties of $LaBO_3$ Compounds

Property	$LaCoO_3$ *Gopalakrishan et al.[14]	Oxide $LaNiO_3$ *This work	$LaCuO_3$ *Goodenough et al.[9]
$a_H/\AA$	5.499	5.453	5.502
$c_H/\AA$	13.089	13.128	13.228
spin S	0.2	½	1
b	$b \approx b_c$	$b > b_c$	$b > b_c$
elect. conf.	$t^6 \leftrightarrow t^4\sigma_e^2$	$t^6\sigma_e^1$	$t^6\sigma_e^2$
elect. cond.	Sc ↔ m	metal	metal

* Source of lattice parameter data.

In the borderline case ($LaCoO_3$) at 300K there is a 70:30 $Co^{III}:Co^{3+}$ ratio[14] where it is a semiconductor. At 1270K when it becomes a metal, this ratio changes to almost 50:50. There is a clearer analogy

between $LaNiO_3$ and $LaCuO_3$ as they are both metals. In the latter compound (prepared by Demazeau et al.[15] and Arjomand et al.[16b]) the conduction band (from the $3e_g^2$ configuration) is half filled while it is only quarter filled for $LaNiO_3$.

The electrocatalytic effect of $LaNiO_3$ has been extensively studied by Matsumoto et al.[2,17,18] This school has attempted to explain the exceptionally high activity as being due to the σ_e^n configuration. Presumably the Fermi level E_F for such configurations lie close to the O_2 $2\pi^*$ for charge transfer. By analogy $LaCuO_3$ should be catalytically active.

1.2. A Possible Nomenclature for Refractory Phases

Because of the relative underdevelopment of Refractory Inorganic Chemistry and in contradiction the potential enormity of the field there is tremendous ambiguity concerning the name of a compound in this 'line of work'. For example in the literature both $LaNiO_3$ and La_2NiO_4 are both individually and collectively called nickel lanthanum oxide and lanthanum nickel oxide respectively. The author uses the following notation throughout this text which is open to discussion, change or development.

(1) The A site substitution is always named first as in the periodic table.

(2) The B site substitution is named last ending in 'ate'.

(3) A Roman numeral follows (2) to indicate the oxidation state of B (I precedes II).

(4) The prescript chloro, fluoro, oxo etc precedes (2) to indicate the ligand.

(5) The word di, tri, tetra etc. (to indicate the 'formula co-ordination') precedes (4).

(6) A dash then an integer succeeds (1) to indicate the number of A cations.

(7) A dash then an integer followed by a comma before (4) to indicate the number of B cations.

Thus for a system A-B-O where A = Author and B = Beryl :-

$A^{3+}B^{3+}O_3$ = Author trioxoberylate III

$A_5^{3+}B_4^{3+}O_{10}$ = Author 5-4, decoxoberylate III

Subrules :-

(i) Ternary systems where B = B' but differing only in oxidation state is treated like a quarternary system and rule (3) applies.

(ii) Quarternary systems :-

(a) Fractional stoichiometries must be corrected so that only integers appear in the formula.

(b) The reciprocal of the fractional correction (in (a)) precedes all corrected formulae.

(c) A site substitution follows from rule (1)

(d) B site substitution follows from rule (2).

Thus for a system E-A-B-O where E = Edwin

$EA_2B^{III}O_7$ = Edwin Author -2-heptoxoberylate III

And for a system A-B-F-O where F = Florence :-

$AB_3^{III}F_{0.6}O_7$ = 2' Author-4-1,6 heptoxoflorencateberylate II, III

While $AB_{0.4}^{3+}B_{0.6}^{4+}O4$ = 5' Author-5-2,3 tetroxoberylate III,IV

1.3 La_2NiO_4 - Lanthanum-2-tetroxonickelate II

1.3 .1 Structure :-

The oxide crystallize with the tetragonal K_2NiF_4(I4mmm) structure (Figure 5). The structure is a layer structure derived from perovskite in which each of the perovskite layers are displaced half way along the diagonal [110] axis. Examination of Figure 5 will show that the structure is comprised of alternate Pm3m (perovskite) and Fm3m (rock salt) unit cells.

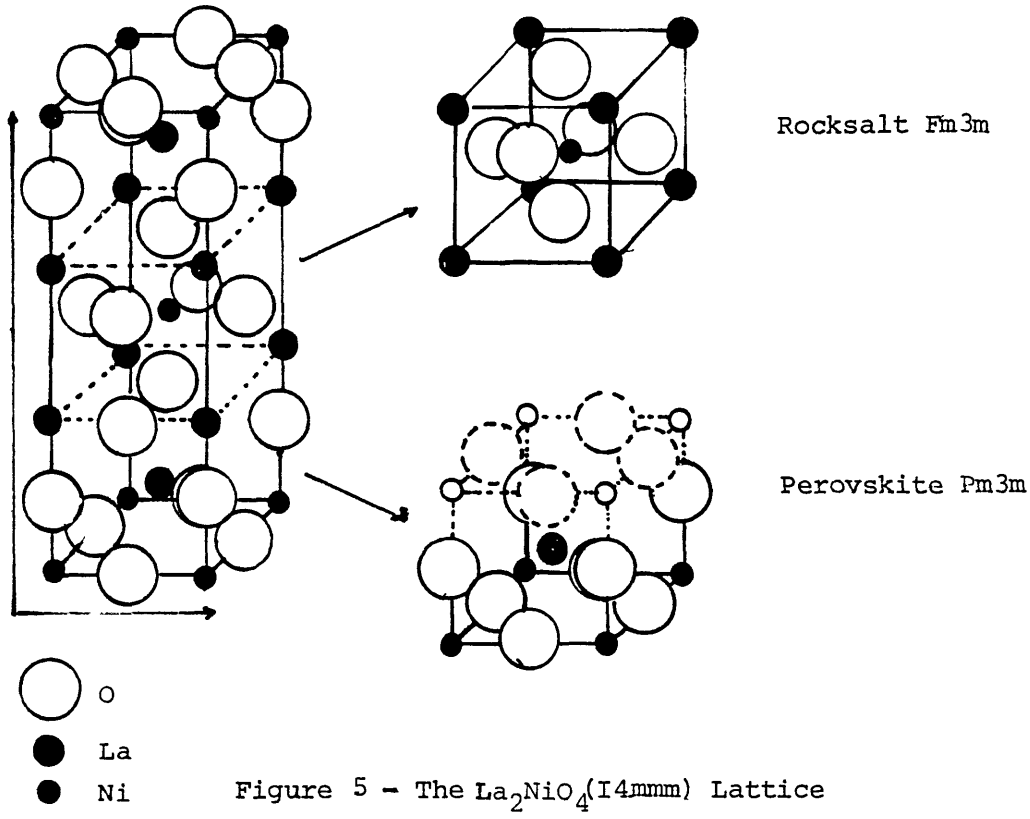

Figure 5 - The La_2NiO_4(I4mmm) Lattice

Results from the X-ray powder diffraction pattern (Plate 1 A (i)) obtained in this work agree well with the results of Rabenau et al.[19] Details are summarised in Table 3.

From geometric considerations it can be shown that $c \sim 3a$; thus the tetragonality ratio is a characteristic property for this class of compounds. The [010] single crystal electron diffraction pattern (Plate 2(b)) confirms that $\frac{c}{a} \sim 3$.

Many of the electron diffraction patterns of La_2NiO_4 contain weak (non allowed) superlattice spots (e.g. x in the $[1\bar{1}0]$ picture - Plate 2(a)). The author has not analysed these in detail but believes that these may be as a result of intergrowth of other La-Ni-O phases sharing the common perovskite sublattice and/or intergrown NiO which is probably just compatible. The author has, during this project, experimented with both A site (with Sr^{2+}) and B site (with Li^{+}) substitution in La_2NiO_4, both of which incorporates Ni^{III} in the A_2BO_4 lattice.

Single crystal E.M. diffraction pattern of N = 1
(La_2NiO_4) Fmmm

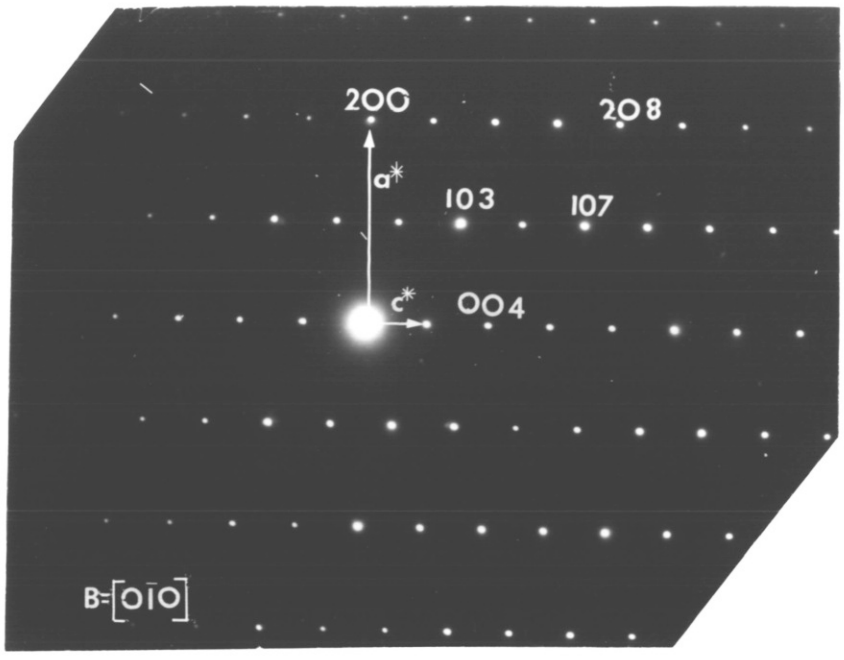

λ = 0.037 Å L = 144 cm

$\frac{c}{a} \simeq 3$ a = 3.85 Å c = 12.65 Å

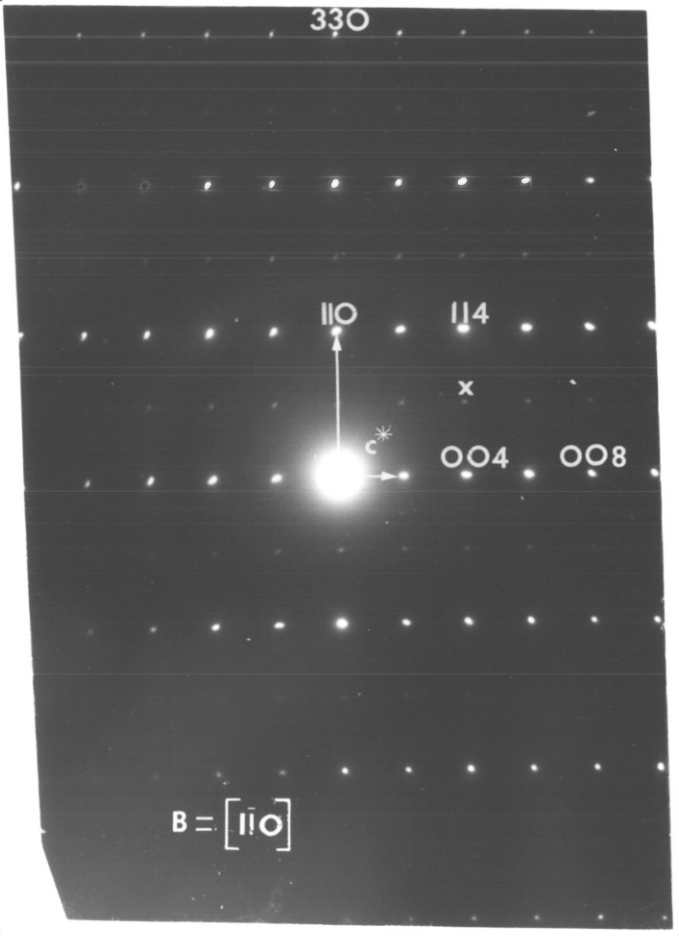

X may be (i) hexagonal perovskite superlattice reflections. (ii) Intergrown NiO along 100 - Chapter 6.

(i) A site :- The compound $SrLaNiO_4$ (Strontium lanthanum tetroxonickelate III) has an X-ray diffraction pattern (Plate 1 A(ii) almost identical to that of La_2NiO_4 and accordingly a $\frac{c}{a}$ ratio close to that of La_2NiO_4 and by inference the d^7 (Ni^{III}) configuration does not appear to have led to a tetragonal (Jahn-Tellar) distortion. Gopalakrishnan et al.[27] in a nicely reported study showed that the $\frac{c}{a}$ ratio in the system $Sr_xLa_{2-x}NiO_4$ reaches a maximum at x=0.5. This was attributed to a tetragonal distortion due to the d^7 configuration.

(ii) B site :- The compound $La_2Ni_{.5}Li_{.5}O_4$ (2'lanthanum-4-1,1, tetroxolithiatenickelate I,III) as reported by Blasse[21] has an enormous tetragonal distortion. The X-ray diffraction pattern (Plate 1A)(iii)) is very different from La_2NiO_4 and $SrLaNiO_4$. The compound is also different visually. The latter two are black like $LaNiO_3$ indicating possible delocalised electron behaviour while $La_2Li_{.5}Ni_{.5}O_4$ is greyish brown.

TABLE 3 Crystallographic Data of A_2BO_4 Compounds of La and Ni

Author	Compound	a/Å	c/Å	$\frac{c}{a}$
Rabenau[19]	La_2NiO_4	3.855±0.001	12.652±0.003	3.28
This work	La_2NiO_4	3.851±0.001	12.650±0.005	3.28
Demazeau[20]	$SrLaNiO_4$	3.826±0.005	12.450±0.02	3.25
Blasse[21]	$SrLaNiO_4$	3.80	12.69	3.29
This work	$SrLaNiO_4$	3.817±0.002	12.462±0.005	3.27
Blasse[21]	$La_2Li_{.5}Ni_{.5}O_4$	3.77	12.89	3.44
This work	$La_2Li_{.5}Ni_{.5}O_4$	3.768±0.003	12.864±0.02	3.41
Gopalak-rishnan[27]	$Sr_{.5}La_{1.5}NiO_4$	3.817	12.766	3.35

1.3.2. Bonding :-

This is a relatively underdeveloped field due in part to the lower symmetry and in part to the danger of making invalid

assumptions concerning A-O bonding. It is known from Crystal Field Theory that for tetragonal field splittings the relative position of levels are dependent on the magnitude of the splitting Δ[53] and the $\frac{c}{a}$ ratio.[54] In Figure 6(b) the author has put together from sparsely available literature a picture of likely orbital energy splittings and consequently bonding after the effect of the I4mmm field.

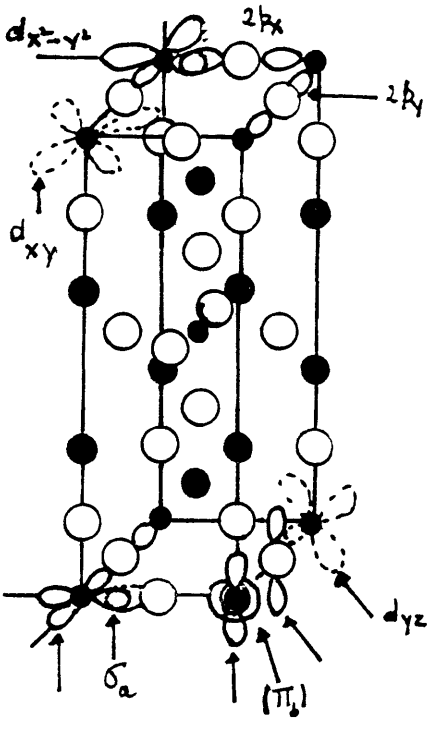

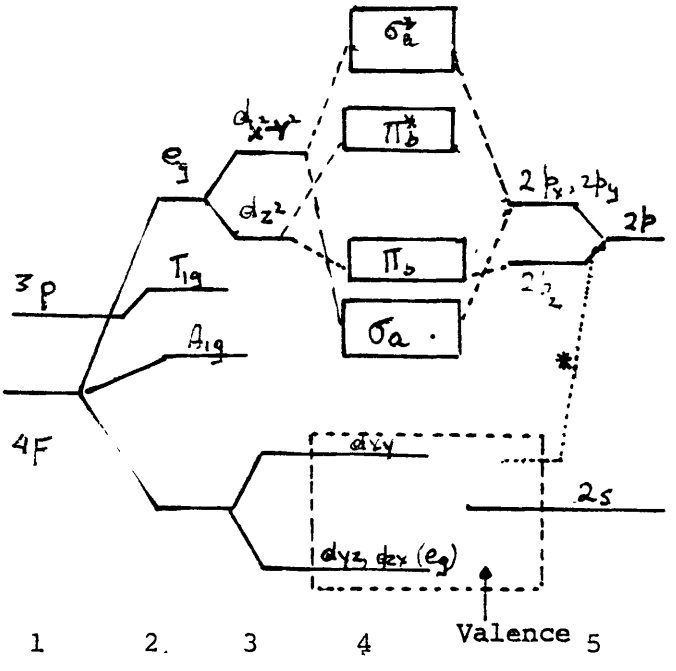

(a) Orbitals available for bonding
(b) Schematic Energy level Diagram of d^8 in the I4mmm Lattice

Figure 6 - Bonding in La_2NiO_4

Ganguly et al.[10] have suggested that La_2NiO_4 is an n type semiconductor at 300K transforming to a metal at (500-600)K. The explanation of this in terms of a bonding scheme has been treated by Goodenough[23]. However neither school[10,23] have said whether the conduction is two dimensional and how the tetragonal field affects the relative positions of the d orbitals.

From purely pictorial considerations, Figure 6a shows that π type overlap is possible between d_z2 and $2p_z$ and σ type overlap between $d_{x^2-y^2}$ and $2p_x$ and $2p_y$. The criterion for the formation of band states according to Goodenough[23] is the magnitude of the Ni-O-Ni

separation. This is 3.855Å in La_2NiO_4 (4.177Å in NiO). Goodenough[23] and Ganguly[10] suggested that since there is a strong tendency to collective electron behaviour in NiO; in La_2NiO_4 the tendency is greater. For the d^8 system Figure 6b should apply; the following are the two possibilities :-

(i) $2p_z$, d_z2 $\longrightarrow$ π_b, max. of 4 electrons per La_2NiO_4

(ii) $2p_x$, $2p_y$, d_x2 $\longrightarrow$ σ_a, max. of 6 electrons per La_2NiO_4.

Goodenough[23] suggests that the latter case is operative and the configuration of La_2NiO_4 is $\sigma_a^1 d_z^1 2$ i.e. the d_z^2 electron remains localized. The d_{z2}^1 configuration posseses a magnetic moment of 1 BM and below 500K it splits the σ_a band (presumably through spin orbit coupling). At (500-600)K the thermal motion of the ions destroys the short range antiferromagnetic coupling and the σ_a band becomes continuous. The semiconductor $\longleftrightarrow$ metal transition is therefore not a sharp one.

Any tendency of σ_a band formation in La_2NiO_4 should be enhanced in $SrLaNiO_4$ (d^7) ($d_{Ni-O-Ni}$ = 3.82Å). Demazeau et al.[20] have confirmed the metallic behaviour of $SrLaNiO_4$. The situation in $La_2Li_{.5}Ni_{.5}O_4$ (d^7) might not be parallel as there are perturbations in the important lattice site (B) along every lattice translation. In other words the Li^+ 2s might be too small for sufficient overlap and the Ni^{III}(d^7) electrons remain localized.

1.3.3 Properties

The compound is an n-type intrinsic semiconductor at room temperature[10] transforming to a metal 500K $<$ T $<$600K as discussed previously. Samples prepared by Ganguly et al.[10] appear to have a room temperature resistivity of about 0.5 Ω cm. There is some indication that properties are variable with conditions of synthesis. For instance Gopalakrishnan et al.[27] reported that samples prepared in air

are black and contain about 15% Ni^{III} and a room temperature resistivity (ρ_{300K}) of 0.3Ω cm while samples prepared under nitrogen were green containing 3-5% Ni^{III} having ρ_{300K} = 2Ω cm. The author has also observed (unpublished work) differences in the lattice parameter of samples prepared in air and oxygen respectively although both have the I4mmm powder diffraction pattern. These indirectly support the explanation given for superlattice reflections in Plate 2(b). Timofeeva et al.[26b] have established that the tetragonal structure of La_2NiO_4 is retained up to 2023K where it melts.

Because of the layer structure this class of compounds have been studied as possible examples of 2-dimensional antiferromagnetism - Figure 7. In A_2BO_4 compounds provided that A has no magnetic moment and B has, 180° exchange is possible along [100] and [010].

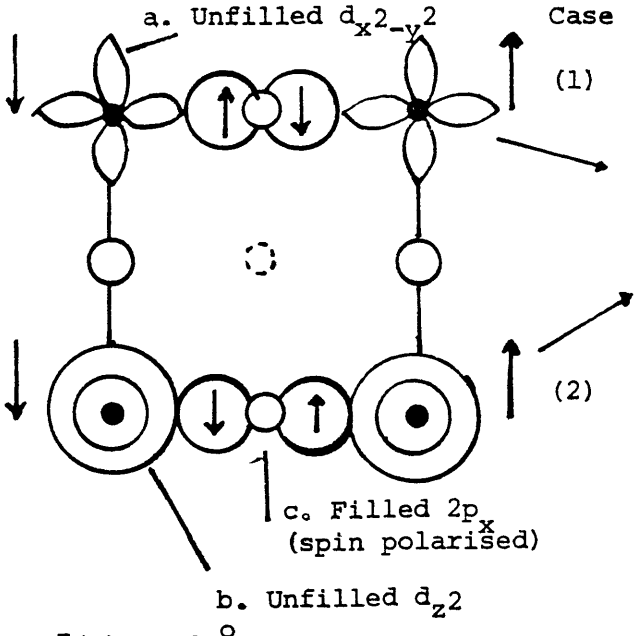

Figure 7(a) - 180° Exchange interaction
Case (1) Strong interaction
Case (2) Weak interaction

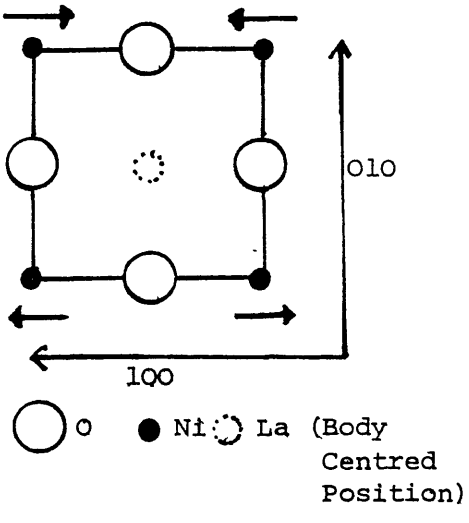

Figure 7(b)- 2 Dimensional Antiferromagnetism in A_2BO_4 Compounds

According to Smolenskii et al.[24] Ni^{2+} in La_2NiO_4 has an effective magnetic moment (μ) of 1BM. They reported departure from Curie-Weiss Law at 200K and a negative Weiss constant θ = -300K and the Neel temperature T_N below 77K. They concluded that the negative Weiss

constant indicated antiferromagnetic ordering. Legrand et al.[25] in a Neutron Diffraction Study did not observe antiferromagnetic ordering. Klienschmager et al.[26a] have studied La_2NiO_4 as interconnection material for the high temperature H_2/O_2 fuel cell.

1.4. Layer Structures Derivable from Perovskite (Geometric Considerations)

Elimination of BO_6 octahedra from ABO_3 (perovskite Pm3m) and translation of half of the structure along [110] produces layer structures of varying layer thickness. Structures with N perovskite layers have a composition $A_{N+1}B_NO_{3N+1}$ and possess ideally I4mmm symmetry (Z=2) Fig.8 after Tilley[3] and Carpy et al.[88] shows the N=1→N=4 structures and their relation to perovskite (N=∞). Clearly phase distinguishability by X-ray will become impossible for large values of N as X-ray wave lengths are of the order of the B-O-B separation. The building blocks of these structures can be considered as Pm3m (perovskite) and Fm3m (rock salt). It is easily seen that if these building blocks do not change (i.e. the I4mmm symmetry is retained) then the unit cell parameters obey the rule $c_T \sim (2N+1)a_c$ where a_c is the lattice constant of the Pm3m) lattice (i.e. the B-O-B separation) and is normally about 3.85 Å. The tetragonality ratio is therefore a characteristic property of this class of compounds. This has been previously outlined for the N = 1 case in the La-Ni-O system (i.e. La_2NiO_4). Table 4 summarises the unit cell properties of $A_{N+1}B_NO_{3N+1}$ compounds.

If the building blocks of these structures change from Pm3m and Fm3m then the compounds will not have I4mmm symmetry. This condition is satisfied if there is a distortion in the perovskite subcell from Pm3m symmetry.

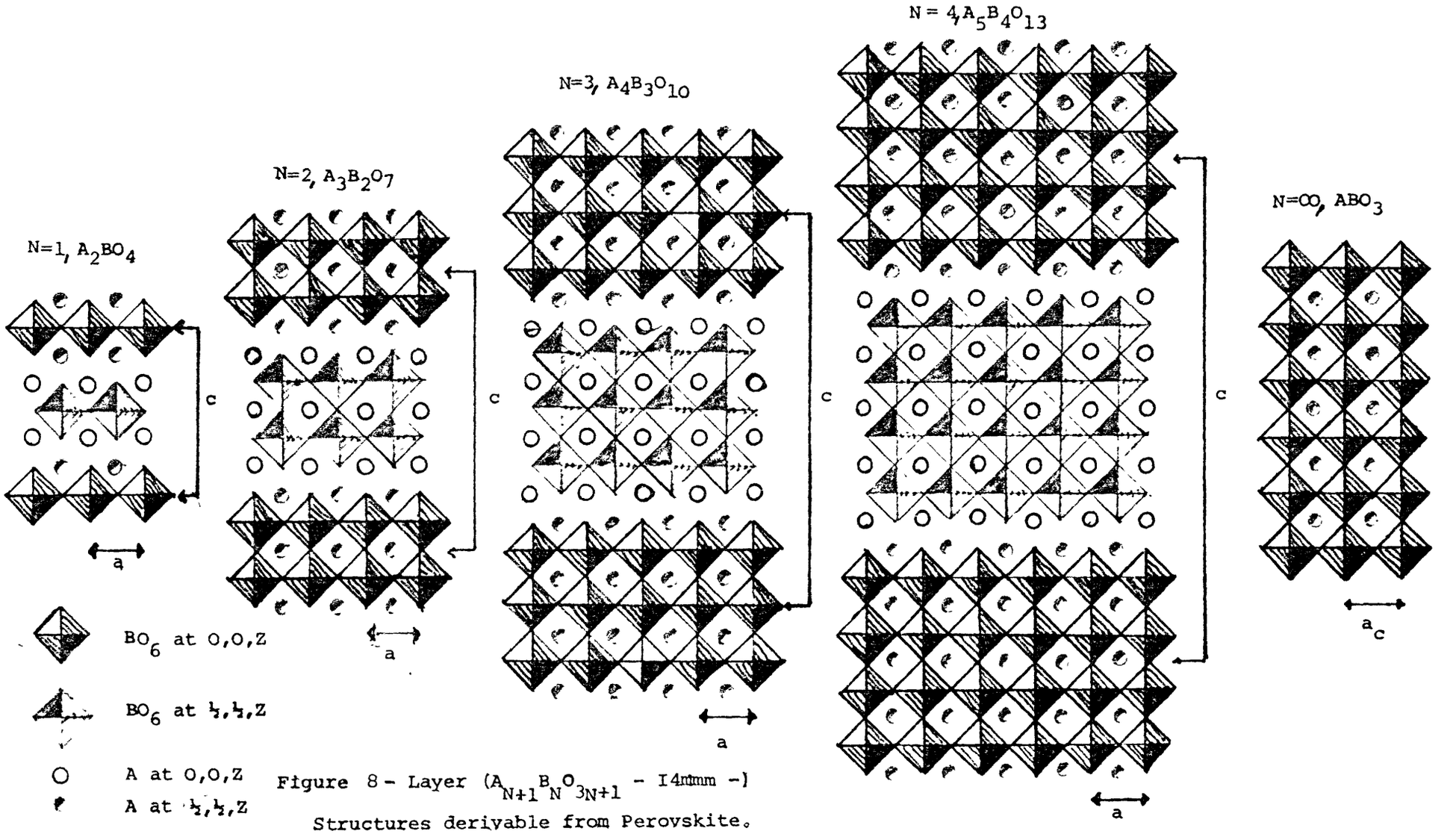

Figure 8 - Layer ($A_{N+1}B_NO_{3N+1}$ - I4mmm -)
Structures derivable from Perovskite.

TABLE 4 Idealized Unit Cell Properties of $A_{N+1}B_NO_{3N+1}$ Phases

N	Formula	Space Group (Ideal)	Approx $\frac{c}{a}$	Approx $\frac{c(N=i)}{c(N=1)}$	Fig. 8
1	A_2BO_4	I4mmm	3	1	a
2	$A_3B_2O_7$	I4mmm	5	5/3	b
3	$A_4B_3O_{10}$	I4mmm	7	7/3	c
4	$A_5B_4O_{13}$	I4mmm	9	9/3	d
5	$A_6B_5O_{16}$	I4mmm	11	11/3	
(∞	ABO_3	Pm3m	1	1/3	e)

If the perovskite possess a rhombohedral distortion and in consequence $R\bar{3}m$ or $R\bar{3}c$ symmetry as does $LaNiO_3$, then the new building blocks will be based on $R\bar{3}m/R\bar{3}c$ and R3 and the symmetry lowers from I4mmm to Fmmm. Under these conditions :-

$a_o = \sqrt{2}\, a_T$ ....(1)

so that $c_T = \frac{(2N+1)a_o}{\sqrt{2}}$ ....(2)

where $b_o \sim a_o$ ....(3)

The remainder of this Chapter will be devoted to phases in the La-Ni-O system possessing the Fmmm symmetry. Some of these phases are new prior to this, work others are sparsely reported.

1.5. (N=2) $La_3Ni_2O_7$ Lanthanum-3-1,1,heptoxonickelate II,III

1.5.1. Structure :-

The compound crystallizes with the Fmmm structure as discussed above. The author has attempted to draw the unit cell - Figure 9. Electron diffraction (Plate 2(c), B = [00$\bar{1}$]) confirms the small distortion along [110]. Zero layer reflections in the B = [1$\bar{1}$0] picture and reflections in the B = [00$\bar{1}$] show that the tetragonality ratio $c_o/a_T \sim 5$. If the zero layer reflections in Plate 2(c) B = [1$\bar{1}$0] are compared with those in Plate 2 (b), B = [100], the

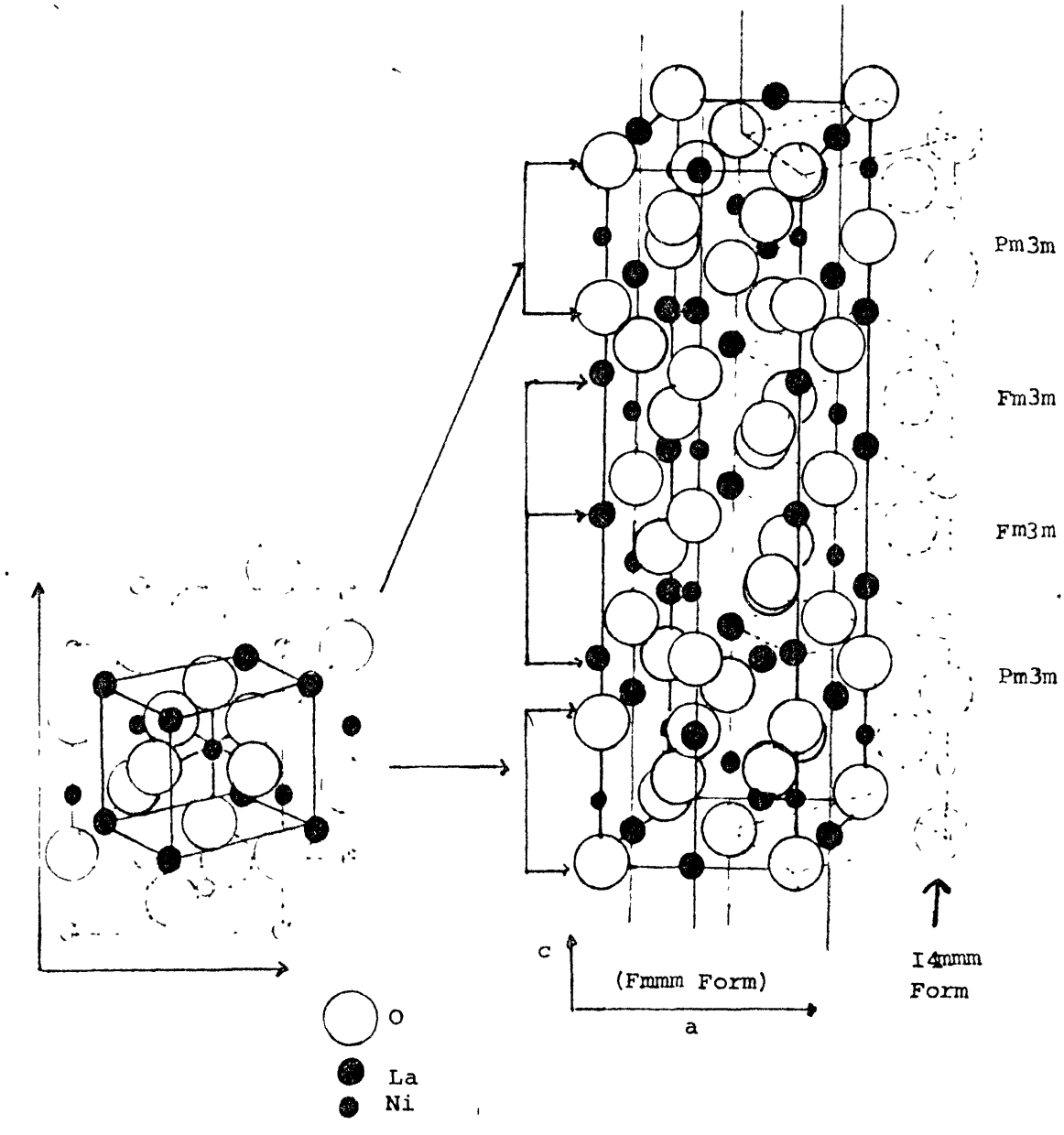

Figure 9 - Unit Cell of $La_3Ni_2O_7$

relationship $c_{N=2}/c_{N=1} \sim$ 5/3 (Table 4) is vindicated. The [001] zone of $La_3Ni_2O_7$ is almost identical to the [001] ($R\bar{3}m$) zone of $LaNiO_3$ (Plate 2(a)). This supports the view that there is some Ni^{2+} 'normally prepared' $LaNiO_3$ as was outlined in Section 1.1.

The indexing of the X-ray powder diffraction pattern of $La_3Ni_2O_7$ (Plate 1 B (iv)) is listed in Table 5.

Plate 2c

Single crystal E.M. diffraction pattern of N = 2 ($La_3Ni_2O_7$) Fmmm

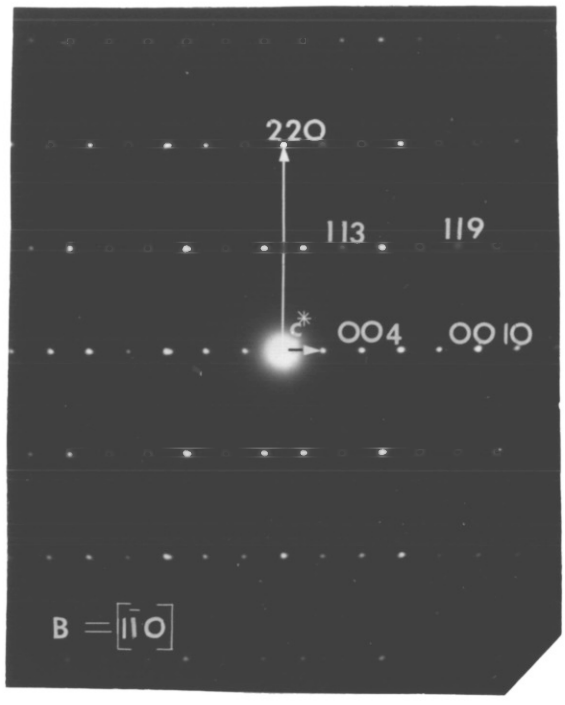

$\lambda = 0.037$ Å L = 144 cm

$\frac{c}{a_T} \simeq 5$ where $a_T = \frac{a_0}{\sqrt{2}}$

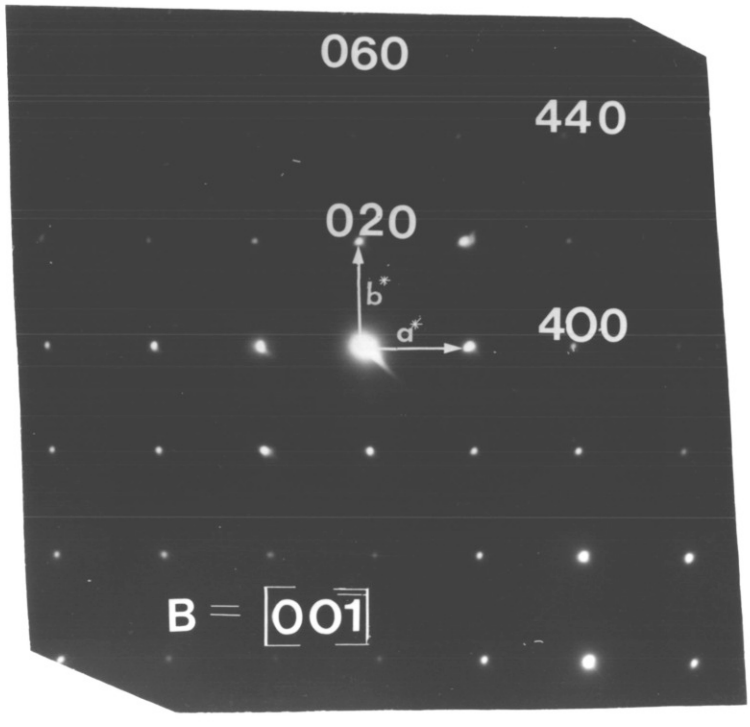

$a_o = 5.397$ Å $b_o = 5.448$ Å $c_o = 20.509$ Å

TABLE 5 X-ray Powder Diffraction Pattern of $La_3Ni_2O_7$

$d_{obs}/\AA$	$d_{cal}/\AA$	I/I_o	hkl	$d_{obs}/\AA$	$d_{cal}/\AA$	I/I_o	hkl
3.770	3.776	16	111	1.6710	1.6721	24	226
3.420	3.418	8	006	1.6347	1.6318	8	2010
3.347	3.342	4	113		1.6384		0210
2.797	2.799	100	115	1.5869	1.5861	28	135
2.724	2.724	47	020	1.5746	1.5750	30	315
2.694	2.698	51	200	1.4480	1.4477	7	0212
2.327	2.323	8	117		1.4431		2012
2.132	2.130	26	026	1.3620	1.3627	10	040
2.115	2.115	23	206	1.3494	1.3496	9	400
2.0595	2.0595	10	0010	1.2887	1.2902	6	0214
1.9585	1.9564	18	119		1.2875		2014
1.9159	1.9155	72	220	1.2657	1.2652	9	046
1.7119	1.7152	5	131	1.2586	1.2559	11	406
1.7095	1.7025	13	311	1.2171	1.2159	12	240
	1.7091		0012				
1.6777	1.6764	3	1111	1.2081	1.2091	8	420

The pattern was indexed using the programmes EGUIN and LSUCRE[34] and KCl as an internal standard. Data was collected on a Guinier focussing camera employing monochromatic CoK_α ($\lambda = 1.7902\AA$) X-radiation. Intensity measurements were collected on a Phillips automatic diffractometer. The lattice dimensions are summarised below :-

$$a = 5.397 \pm 0.001\AA,\ b = 5.448 \pm 0.001\AA \text{ and } c = 20.509 \pm 0.004\AA$$

$$\frac{b}{a} = 1.0088,\ \frac{c_o}{a_T} = 5.37 \text{ and } c_{N=2}/c_{N=1} \sim 1.62 \text{ (cf Table 4)}$$

The existence of $La_3Ni_2O_7$ especially at high temperature has been discounted by Seppanen.[29]

The author is aware of only one other $A_3B_2O_7$ phase having a 50:50 $B^{II}:B^{III}$ ratio. This is the compound $Eu_3Ti_2O_7$ - McCarthy et al.[28] - which could also be written as $Eu^{2+}Eu^{3+}_2Ti^{3+}O_7$ as the rare

earth displays variable valence. Other $A_3B_2O_7$ type phases have been reported but only for the 2:4 A-B-O systems[92].

1.5.2. Bonding :-

The bonding scheme to describe this compound must be more complex than for La_2NiO_4 (N=1) because of the lower symmetry. However following on from the arguments developed by Goodenough[8,11] concerning cationic spin contracting d like atomic orbitals and so impairing B-O bonding, it might be tentatively assumed that in $La_3Ni_2O_7$ there are two principal reasons why $d_{Ni-O-Ni} = d'_{Ni-O-Ni}$ (i.e. Fmmm and not I4mmm symmetry) :-

(i) Size of cation[38] $r_{Ni}2+ = 0.70\text{Å}$ $r_{Ni}3+ = 0.56\text{Å}$

(ii) If there are low spin trivalent Nickel - Ni^{III} ($t_{2g}^6 e_g^1$ S=½) - and Ni^{2+} ($t_{2g}^6 e_g^2$ S = 1) there might be unequal spin orbit coupling interactions such that $d(Ni^{III}\text{---}O) \neq d(Ni^{2+}\text{---}O)$.

In this project the author has attempted the synthesis of $SrLa_2Ni_2O_7$ and $La_3Li_{.5}Ni_{.5}O_7$ (unpublished work). Both sets of experiments gave diphasic mixtures of A_2BO_4 and $A_3B_2O_7$. In the case of the Sr-La-Ni-O system the compound appears to have I4mmm symmetry - no splitting of the 110 reflection - whilst the lithium analogue was Fmmm (splitting of 110 into the 020 and 200 reflections) like $La_3Ni_2O_7$. This, although a preliminary study, suggest spin and ionic size play a role in symmetry as in the former compound all are Ni^{III} and all Ni-O-Ni distances are equal while for the latter there are unequal Li-O- (Li^+ S = 1) and Ni-O distances (Ni^{3+} or Ni^{III} S = $\frac{3}{2}$ or $\frac{1}{2}$ respectively).

1.5.3 Properties :-

No properties of $La_3Ni_2O_7$ have been measured but the existence of the 1:1 Ni^{2+}:Ni^{III} ratio might lead to unusual magnetic

properties. For example magnetic ordering at temperatures higher than for La_2NiO_4 [24] is a possibility.

1.6. (N=3) $La_4Ni_3O_{10}$ -Lanthanum-4-1,2, decoxonickelate II,III

1.6.1. Structure :-

The compound crystallizes with the Fmmm structure as does $La_3Ni_2O_7$. There has been one report of its existence (prior to the writing of this script) by Sappenen[29]. Data from the X-ray powder diffraction pattern, Plate 1 B)(iii), is listed in Table 6 below.

TABLE 6 X-ray Powder Diffraction Data of $La_4Ni_3O_{10}$

$d_{obs}/\AA$	$d_{cal}/\AA$	I/I_o	hkl	$d_{obs}/\AA$	$d_{cal}/\AA$	I/I_o	hkl
3.796	3.793	18	111				
				1.7030	1.7035	1	311
3.540	3.541	5	113				
				1.6777	1.6779	15	228
3.484	3.481	8	008				
				1.6716	1.6717	6	11,15
3.156	3.156	4	115				
				1.6060	1.6063	11	02,14
2.765	2.760	100	117				
				1.6022	1.6016	12	20,14
2.717	2.719	48	020				
				1.5780	1.5781	35	22,10
2.697	2.696	47	200		1.5776		137
2.404	2.408	4	119				
				1.5680	1.5687	28	137
2.143	2.141	21	028				
				1.4768	1.4774	6	22,12
2.132	2.132	20	208				
				1.4660	1.4668	6	02,16
2.111	2.113	8	11,11				
				1.4629	1.4632	5	20,16
1.9920	1.9909	11	00,14				
				1.4250	1.4221	1	13,11
1.9160	1.9146	60	220				
				1.4147	1.4155	1	31,11
1.8712	1.8707	1	11,13				
				1.3809	1.3800	11	22,14
1.7160	1.7149	1	131				

The indexing was performed by the programmes EGUIN and LSUCRE[34] and using KCl as an internal standard - same apparatus and procedure as

Single crystal E.M. diffraction pattern of N = 3
($La_4Ni_3O_{10}$) Fmmm

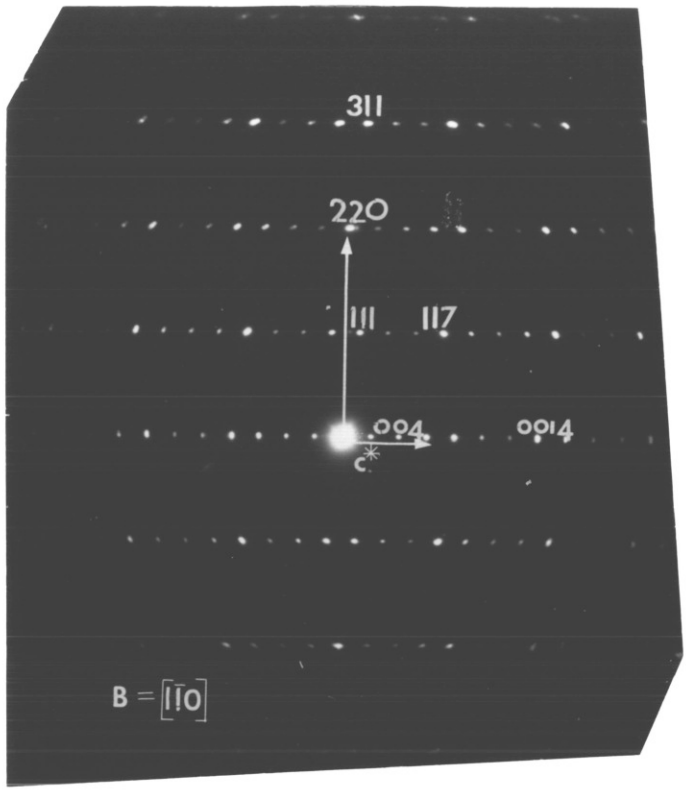

$\lambda = 0.037$ Å L = 144 cm

$\frac{c}{a} \simeq 7$

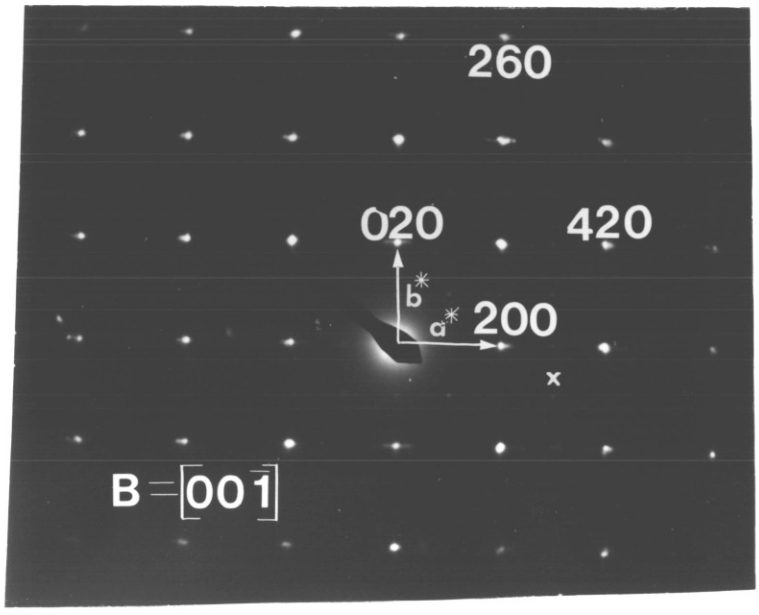

$a_o = 5.396$ Å $b_o = 5.438$ Å $c_o = 27.872$ Å

$a = \frac{a_o}{\sqrt{2}}$

The weak superlattice reflections (X) will be explained in Chapter 6.

for $La_3Ni_2O_7$. The lattice parameter obtained in this study, Seppanen's work[29] together with data from the only other reported oxide of this type,- $La_4Co_3O_{10}$ - are summarised below in Table 7.

TABLE 7 Lattice Parameter of $La_4B_3O_{10}$ Compounds (B = Ni and Co)

Author	Seppanen[29]	This Work	Seppanen[31]	Janeck et al.[30]
oxide	$La_4Ni_3O_{10}$	$La_4Ni_3O_{10}$	$La_4Co_3O_{10}$	$La_4Co_3O_{10}$
$a_o/\AA$	5.413±0.001	5.396±0.001	5.42	5.414
$b_o/\AA$	5.465±0.001	5.438±0.001	5.47	5.471
$c_o/\AA$	27.968±0.002	27.872±0.002	27.81	27.810
b/a	1.0096	1.0077.	1.0092	1.105
*c/a_T	7.306	7.304	7.256	7.264
**$\frac{c(N=3)}{c(N=1)}$	-	2.202	-	2.194

* Equation (1) ** Table 4 Column 5.

There is a discrepancy between findings in this work and Seppanen's work[29]. However data in this study is from a Guiner focussing camera while Seppanen's data was from a diffractometer.

Electron diffraction, Plate 2(d)(i)-B = $[1\bar{1}0]_I$, confirms the tetragonality ratio (c/a_T) of about 7. Comparing zero layer reflections of Plate 2(b)(i) and Plate 2(d)(i) shows that c(N=3)/c(N=1) is about 7/3. Plate 2(d)(ii)-B = $[0\bar{1}0]$ shows the small distortion along $[1\bar{1}0]$. The picture is very similar to the $[1\bar{2}\bar{1}]$ zone of $LaNiO_3$ (Plate 2(a)) as was Plate 2(c)(N=2).

1.6.2 Bonding :

Following on with the arguments (developed for $La_3Ni_2O_7$) concerning cationic spin and the Fmmm symmetry, if these assumptions are correct then the ratio b_o/a_o should decrease as the

population of Ni^{III} increases (i.e. N$\longrightarrow\infty$). We see that for $La_3Ni_2O_7$, b_o/a_o = 1.0094, whilst for $La_4Ni_3O_{10}$ b_o/a_o = 1.0077. In other words the splitting of hkO reflections should decrease as the B-O bonding interaction becomes less and less unequally spin impaired.

1.6.3. Properties :-

As with $La_3Ni_2O_7$ only assumptions can be made. It is plausible that properties will show more and more collective electron behaviour as the perovskite building blocks become larger - Figure 8.

1.7. (N=4) $La_5Ni_4O_{13}$-Lanthanum-5-1,3, tridecoxonickelate II,III

1.7.1. Structure :

The structural evidence for $La_5Ni_4O_{13}$ (N=4) is not as strong as the evidence for $La_3Ni_2O_7$ (N=2) and $La_4Ni_3O_{10}$ (N=3). However the compound, like its other relatives, appears to have the Fmmm symmetry. The X-ray powder pattern shows that by now the splitting between reflections 020 and 11(2N+1) (i.e. h=1, k=1 and l=(2N+1)) appears to be zero - Plate 1 B)(ii). In other words the 119 and 020 reflections overlap and in consequence the extinction around 200 and 020 are different from N=2 and N=3 (Plate 1 B)(iii) and (iv)). The X-ray diffraction pattern of (as prepared) $La_5Ni_4O_{13}$ is indexed as shown in Table 8.

Samples prepared had a small amount of $La_4Ni_3O_{10}$ (N=3) - Plate 1 B)(ii). However only few reflections could be detected, for example the 117 which is the strongest reflection in the N=3 diffraction pattern.

There was insufficient time to get a comprehensive set of electron micrographs. Nevertheless Plate 2(e)(i) appears to be a $[1\bar{1}0]$ or $[100]$ zone slightly off axis showing very small reciprocal distances along c* and Plate 2(ii) is a $[00\bar{1}]$ zone which is similar to the $[\bar{1}2\bar{1}1]$ zone of $LaNiO_3$ (Plate 2(a)(i)).

Plate 2e

Single crystal E.M. diffraction pattern of N = 4 ($La_5Ni_4O_{13}$).

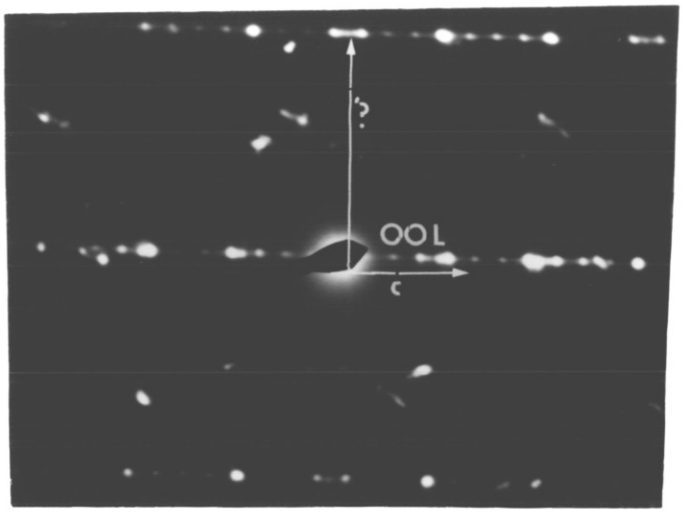

A poor picture in part due to the very small grain size of the crystals.

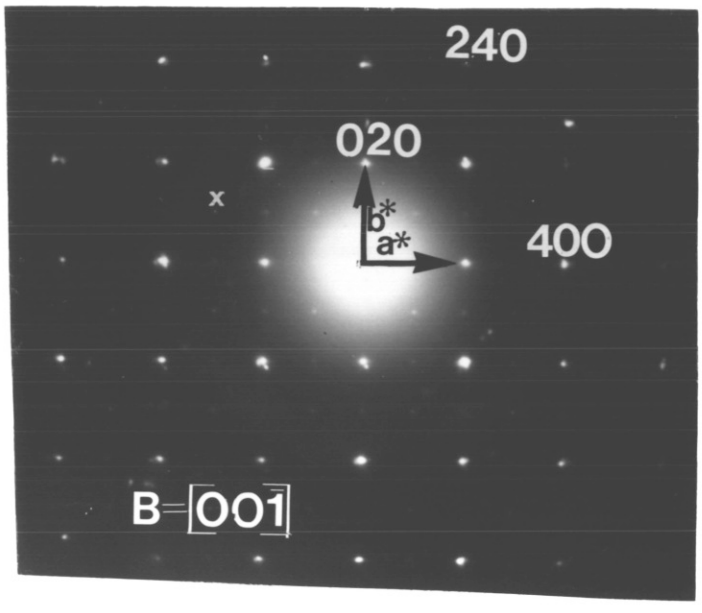

$a_o = 5.415\ \text{Å}$ $b_o = 5.456\ \text{Å}$ $c_o = 34.99\ \text{Å}$

$\frac{c}{a_T} \backsim 9$ $a_T = \frac{a_o}{\sqrt{2}}$

Weak non allowed reflections (X) may be from the hexagonal perovskite sublattice as is seen in Plate 2a(b) and Plate 2b(b).

TABLE 8 X-ray Diffraction Pattern of $La_5Ni_4O_{13}$

$d_{obs}/\AA$	$d_{cal}/\AA$	I/I	hkl	$d_{obs}/\AA$	$d_{cal}/\AA$	I/	hkl
3.280	3.281	m	111				
				1.921	1.922	s	220
3.658	3.648	w	113				
				1.722	1.723	w	131
3.495	3.500	vw	0010				
				1.711	1.7109	w	311
3.041	3.047	vvw	117				
				1.6833	1.6847	m	2210
2.732	2.733	vvs	119				
			020				
				1.6754	1.6766	w	135
2.705	2.705	s	200				
				1.5849	1.5840	w	0218
2.282	2.301	vw	208				
				1.5803	1.5796	m	2018
2.219	2.205	vw	1113				
				1.5674	1.5772	vs	139
2.186	2.187	vw	0016				
				1.5688	1.5674	vs	319
2.151	2.153	w/m	0210				
				1.3647	1.3654	m	040
2.136	2.140	w/m	2010				
1.989	1.993	w/m	0212				
	1.983		2012				

Thus a = 5.415$\AA$ b = 5.456$\AA$ and c = 34.99$\AA$

so b_o/a_o = 1.0075 and c_o/a_T = 9.146 (cf Table 4).

The indexing was performed by the programmes EGUIN and LSUCRE[34] using KCl as an internal standard. Data was obtained on the same equipment as previously described.

As stated previously the N = 4 phase appears to be the limit where X-rays are able to distinguish $La_{N+1}Ni_NO_{3N+1}$ compounds. For example the X-ray powder pattern of $La_6Ni_5O_{16}$ (N = 5) - not represented here - is identical to the diffraction pattern of $LaNiO_3$. Other $A_5B_4O_{13}$ phases have been isolated but in pseudo ternary systems. Carpy et al,[88] have synthesised $A_5B_4O_{13}$ and $A_6B_5O_{16}$ type phases in the pseudoternary. CaO $NaNbO_3$ system.

1.8. Other Phases in the La-Ni-O system

1.8.1. $LaNi_2O_4$ - Lanthanum-1,1,tetroxonickelate II,III

Von J. Sieler et al.[32] reported that the compound $LaNi_2O_4$ ($CaFe_2O_4$ type structure) can be prepared by reacting $LaNiO_3$ and NiO under Argon at 800°C. This has been tried several times without success. Thermodynamic measurements - Chapter 4 - on these samples confirmed that they had a stoichiometry close to $La_6Ni_5O_{16}$ (N = 5) although the diffraction pattern was that of $LaNiO_3$. At higher temperatures the same reaction mixture gave equilibrium mixtures of N = 2,3 or 4.

1.8.2. 'Compound X'

A number of workers, notably Nakamura et al.[33a] and A. Wold et al.[33b] reported the existence of a phase - compound X - in the La-Ni-O system lying between $LaNiO_3$ and La_2NiO_4 and formed at (1000-1100)°C. The author believes that this is probably a compound $La_{N+1}Ni_NO_{3N+1}$ having N = 2,3 or 4 or an equilibrium mixture of these.

1.9. Experimental

(i) X-ray powder diffraction data obtained on -

(a) Guinier focussing camera employing monochromatic Co K_{α_1} (λ = 1.78892Å).

(b) Phillips automatic diffractometer employing monochromatic Cu K_{α} (λ = 1.5418Å)

(ii) Indexing of powder diffraction pattern was performed by the programmes EGUIN[34a] and LSUCRE[34b] :-

(a) EGUIN corrects Guiner film measurements. The programme determines the slope of the straight lines between successive Standard reflections. Corrections are then applied to data points lying between Standard reflections using this calculated slope. The Standard used in this work is KCl - a_o = Fm3m; a_c = 6.2931Å.

Output is in the form $4\theta, 2\theta$ and $\sin^2\theta$.

(b) LSUCRE requires these output values, trial cell parameters, symmetry information, λ and a range of experimental error over which matching can be accepted in the refinement. If more than one calculated value of 2θ agrees, the reflection is not used in refinement.

LSUCRE output is of the form hkl, d_{obs}, d_{cal}, $2\theta_{cal}$, $2\theta_{obs}$, $2\theta_{cal} - 2\theta_{obs}$, refined lattice parameter and corresponding standard deviation.

(iii) Samples suitable for electron diffraction were obtained by grinding the powders under butan-1-ol or liquid nitrogen in an agate mortar. These were then suspended on holey carbon films.

Electron diffraction was performed on a JEOL 120CX Electron Microscope with double tilt stage ($\alpha = \pm 60^\circ$) operating at 100 kV ($\lambda = 0.037$Å).

CHAPTER 2

Synthesis of La-Ni-O Compounds

A good preparative route is the key to obtaining reproducible measurements. It can also be optimized for yield, purity and above all cost. In preparative Solid State Chemistry synthesis is usually at elevated temperatures because refractory materials such as oxides are commonly used as starting materials and diffusion times are long at lower temperatures. In appropriate cases however heating, time and temperature can be considerably lowered by :-

(i) The use of suitable precursors (eg Gallagher on the preparation of $LnCoO_3$ [37b])

(ii) Electrochemical synthesis.

2.1. $LaNiO_3$ - Lanthanum trioxonickelate III

According to Mekhandzhiev[35] above 573K Ni_2O_3 is thermodynamically unstable - a temperature often considered too low for perovskite formation - and therefore NiO, which is also much cheaper, is a traditional starting material for the synthesis of the trioxonickelate III's - equation (4).

$$\tfrac{1}{2}Ln_2O_3 + NiO + \tfrac{1}{2}O_2 \longrightarrow LnNiO_3 \quad \ldots\ldots\ldots\ldots\ldots\ldots\ldots\ldots (4)$$

There is also ample evidence of the instability of the trioxonickelate III's at high temperature (Chapter 4); thus ceramic synthetic techniques involve serious technical difficulties primarily the maintenance of high oxygen pressures.

The majority of workers have used the 'flux method' as developed by Wold et al.[5] over 22 years ago for the synthesis of $LaNiO_3$. This involves using La_2O_3 and NiO in a Na_2CO_3 flux. Great care is needed to produce reasonably pure - NiO free - $LaNiO_3$[13,15] and of course the method has certain restrictions if large scale application was desired :-

(i) The standard 'removal and grinding' procedure.

(ii) The long heating time - 72 hours at 800°C.

(iii) The corrosive nature of the Na_2CO_3 flux - gold apparatus has to be used.

Goodenough et al.[11] heated coprecipitated oxalates at 800°C (in pure oxygen) for 3 days; Matsumoto et al.[17] heated nitrates at 850°C for 2 days. Demazeau et al.[6] prepared $LaNiO_3$ at 950°C (from a mixture La_2O_3:NiO:$KClO_3$ 1:2:1.5) in a platinum capsule at 60kBars in only 12 minutes. This was followed by residence at 500°C for 48 hours at a pressure of 4kBars. Golub et al.[37a] developed the precursor $2La_2O_3.4NiO.3CO_2.nH_2O$ (n = 18 — 22) by coprecipitation of carbonates from nitrate solution. They concluded that perovskite formation began at 700°C but was not complete until 900°C.

All the above methods, to varying degrees, involve synthesis at temperatures T ~ (800 - 950)°C and heating times in excess of 48 hours. The author has used the precursor $NH_4La[Ni(NO_2)_6] \times H_2O$ to prepare $LaNiO_3$ at 650°C-700°C in only 12 hours without the need for removal and grinding.

2.1.1. The Precursor $NH_4La[Ni(NO_2)_6] \times H_2O$

Goodgame et al.[39] have undertaken a systematic spectroscopic study of the Ni-NiO_2 and the Ni-ONO bonding in such compounds. However most of the work on the hexanitronickelate II's seems to be on $M_1^{II}M_2^{I}[Ni(NO_2)_6] \times H_2O$ (where x = 1 or 2) and $M_4^{I}[Ni(NO_2)_6] \times H_2O$. Only one example has been observed in the literature of $M_2^{II}[Ni(NO_2)_6]$, that when M = Sr[41], and no examples of $M^{III}M^{I}[Ni(NO_2)_6]$ have been observed.

It is generally believed that stability of these complexes increase as ionic radius r_M increases[41]. Since $r_{La^{3+}} = 1.18\text{Å}$, $r_{Sr^{2+}} = 1.16\text{Å}$ and $r_{NH_4^+} > r_{Na^+} = 0.99\text{Å}$[38] it is likely that the formation of $NH_4La[Ni(NO_2)_6]$ is favourable from a solution containing NH_4^+ (aq), La^{3+}(aq) and Na^+(aq).

It also follows that $NH_4La[Ni(NO_2)_6]$ and $Sr_2[Ni(NO_2)_6]$ might be isomorphous distinguishable only by the N-H stretching 'peaks' in the infra-red. The presence of 'lattice water' could be confirmed or refuted by infra-red O-H stretching. The electronic spectra (uv and visible) of the compound(s) should decide whether the co-ordinating atom is N(nitro) or O(nitrito) or a mixture. None of these studies were carried out because of lack of time and also because characterisation of the precursor was not the main interest of this study, but rather its decomposition product.

2.1.1. (i) Preparation of $NH_4Ln[Ni(NO_2)_6] \times H_2O$ (Ln = Ca and Ce)

(a) A 1:1:1 aqueous solution of NH_4NO_3:$Ni(NO_3)$:$Ln(NO_3)$ was prepared and cooled on ice.

(b) To (a) was added an ice cold concentrated aqueous solution of $NaNO_2$ containing (relative to (a)) 6-7 moles of $NaNO_2$.

(c) The mixture was stirred vigorously until a beige precipitate formed - $NH_4^+(aq) + Ln^{3+}(aq) + 6Na^+(aq) + 6NO_2^-(aq) + Ni^{2+}(aq) \longrightarrow$

$NH_4Ln[Ni(NO_2)_6] + 6Na^+(aq)$ .....(5)

(d) The precipitate formed was washed with ethanol and then ether and air dried.

(e) X-ray diffraction showed that $NH_4Ce[Ni(NO_2)_6]$ and $NH_4La[Ni(NO_2)_6]$ were isomorphous.

2.1.1. (ii) The T.G.A. of $NH_4La[Ni(NO_2)_6] \times H_2O$

In order to determine x (the number of moles of lattice water) and the decomposition temperature of the complex, the T.G.A. of the complex was studied. Figure 10 shows the profile obtained at 2^{o} minute^{-1}. If we assume that equation (6) is valid :-

$$NH_4La\ Ni(NO_2)_6 xH_2O \longrightarrow \tfrac{1}{2}La_2O_3.NiO + (x+1)H_2O + 3NO_2 + 3NO + NH_3 \quad (6)$$

The 'calculated' percentage weight loss at the 'final decomposition' is 52% , putting x as 2, which is normally the case for other hexanitronickelates[39,41]. Figure 10 shows nearly 80% weight loss at 600°C and 26%-27% at 100°C-150°C.

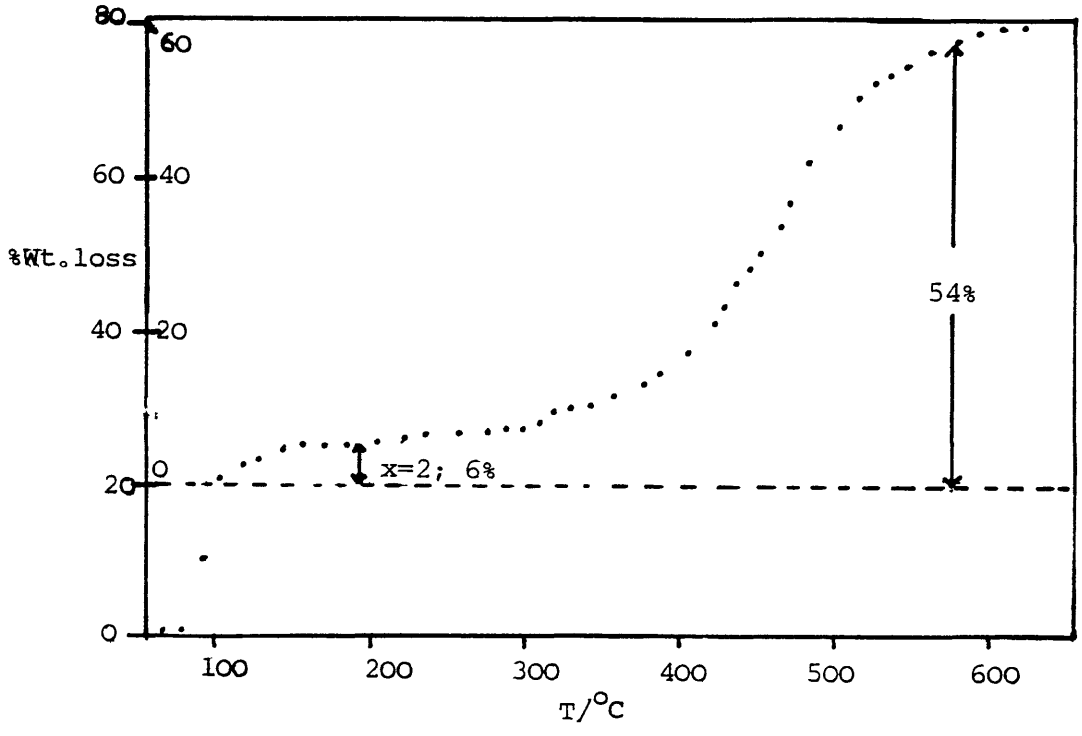

Figure 10- T.G.A. Curve of $NH_4La[Ni(NO_2)_6]\ xH_2O$

These findings disagree with the assumptions discussed above because, it seems, the sample was wet. If the first 20% weight loss, which occurs at 100°C, is offset (dotted line in Fig. 10) then the (6-7)% (T = (100-150)°C) is in agreement with x = 2 and the 54% (T = 600°C) is in accordance with equation (6).

A more detailed study is needed to determine x and therefore final decomposition products. Nonetheless Figure 10 shows that decomposition seems to be complete at 600°C. This temperature is in the range where Bogwlawska et al.[40] and Davies et al.[42] have observed for other hexanitronickelates. The decomposition mechanism according to both schools[40,42] involves the formation of an M-nitrite ($M(NO_2)$). If this is so it might explain why the oxidation $Ni^{2+} \longrightarrow Ni^{III}$ occurs at

such a relatively moderate temperature. The oxidising power of the $\dot{NO}_2$ (radical) is well known in free radical organic chemistry.

2.1.1. (iii) Decomposition product of $NH_4La\ Ni(NO_2)_6$

Plate 3 A) shows the powder X-ray diffraction pattern of $LaNiO_3$ prepared by :-

(a) Heating $NH_4LaNi(NO_2)_6$ at 680°C for 12 hours without periodic removal and grinding.

(b) The flux method of Wold et al[5] with the latter containing the greater NiO impurity.

(d) and (e) compares results for samples held at 550°C for 12 hours using the precursor technique (a) above, and mixed acetates. The pattern in (d) resembles highly disordered $LaNiO_3$ by its fuzziness and clearly indicating that perovskite formation begins at 550° by this method. It is impossible to draw the same conclusions concerning the acetate mixture.

Matsumoto et al.[2a,17] have claimed the preparation of cubic $LaNiO_3$ but have given no crystallographic evidence to support this claim. The fuzzy pattern shown in Plate 3 A)(d) might have been considered as the "cubic" form of $LaNiO_3$.

Energy dispersive X-ray microanalysis, performed on a JEOL 120 CX TEMSCAN operating in the STEM mode, of samples prepared via the precursor is shown in Figure 11. Only La and Ni peaks (Cu peaks being from the specimen grid) and peaks from small amounts of rare earth impurities are observed.

Re-oxidized Lanthanum trioxonickelate III used in this study was also prepared by firing $LaNiO_3$ (either flux prepared or 'precursor' prepared or samples prepared via the oxalate

PLATE 3

A) Prepn. of $LaNiO_3$:-

a) $NH_4La[Ni(NO_3)_6]$ 680°C 12 h

b) $NiO \mid La_2O_3 - Na_2CO_3$ flux 72h · 800°C

c) NiO - 99.99 % (KOCH LIGHT)

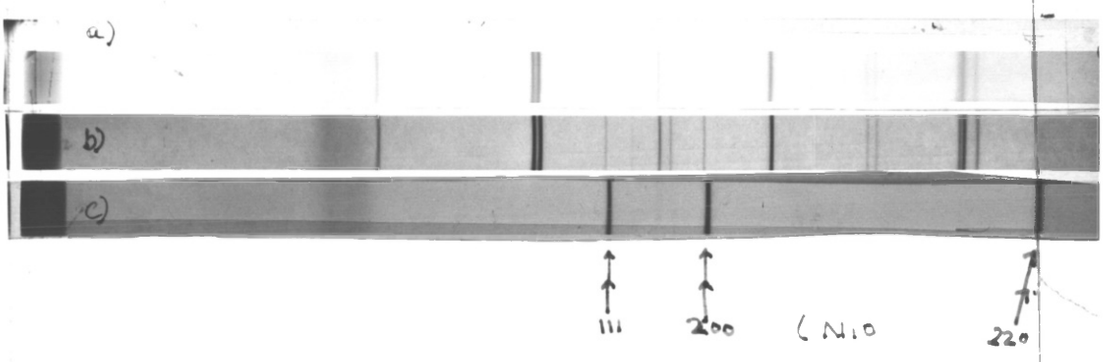

d) $NH_4La[Ni(NO_3)_6]$ 550°C 12 h

e) $Ni(OAc)_2 \mid La(OAc)_3$ 550°C 12 h

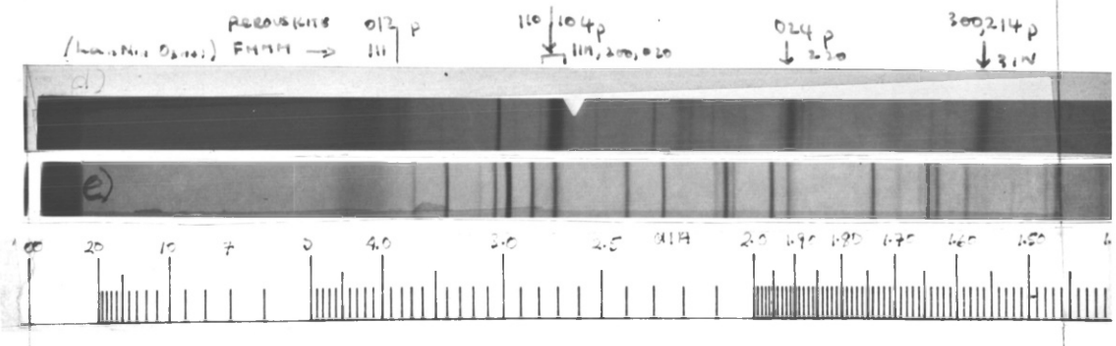

B) Prepn. of $La_5Ni_4O_{13}$:- a) $La_2O_3 \mid Ni(NO_3)_2$ AIR 1050 / 1150 - 12 h

b) $La_2O_3 \mid Ni(NO_3)$ AIR 1150 - 4 h.

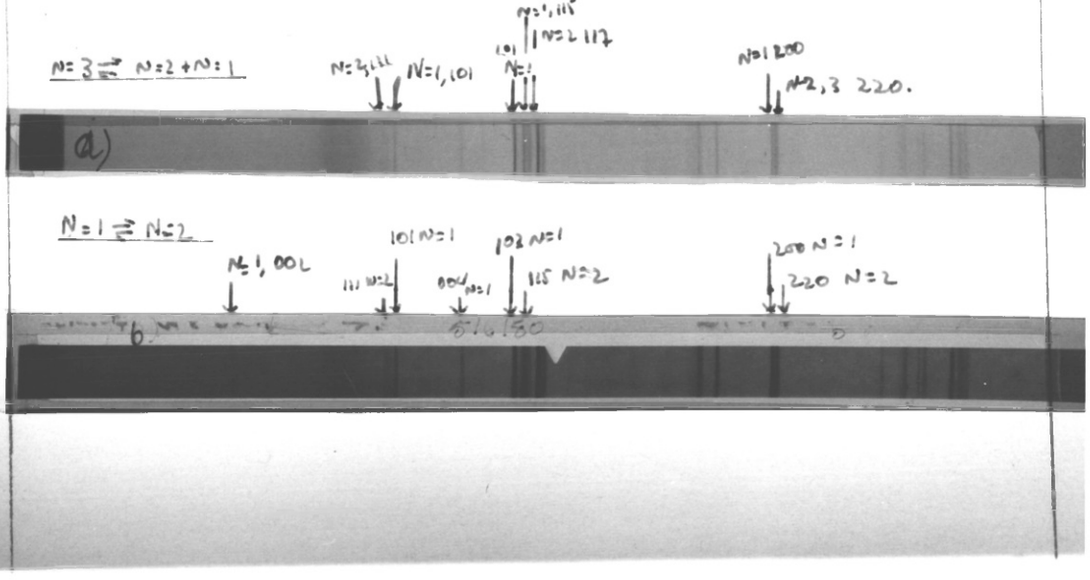

Figure 11 - X-ray Energy Dispersive Microanalysis of $SrLaNiO_4$ & $LaNiO_3$

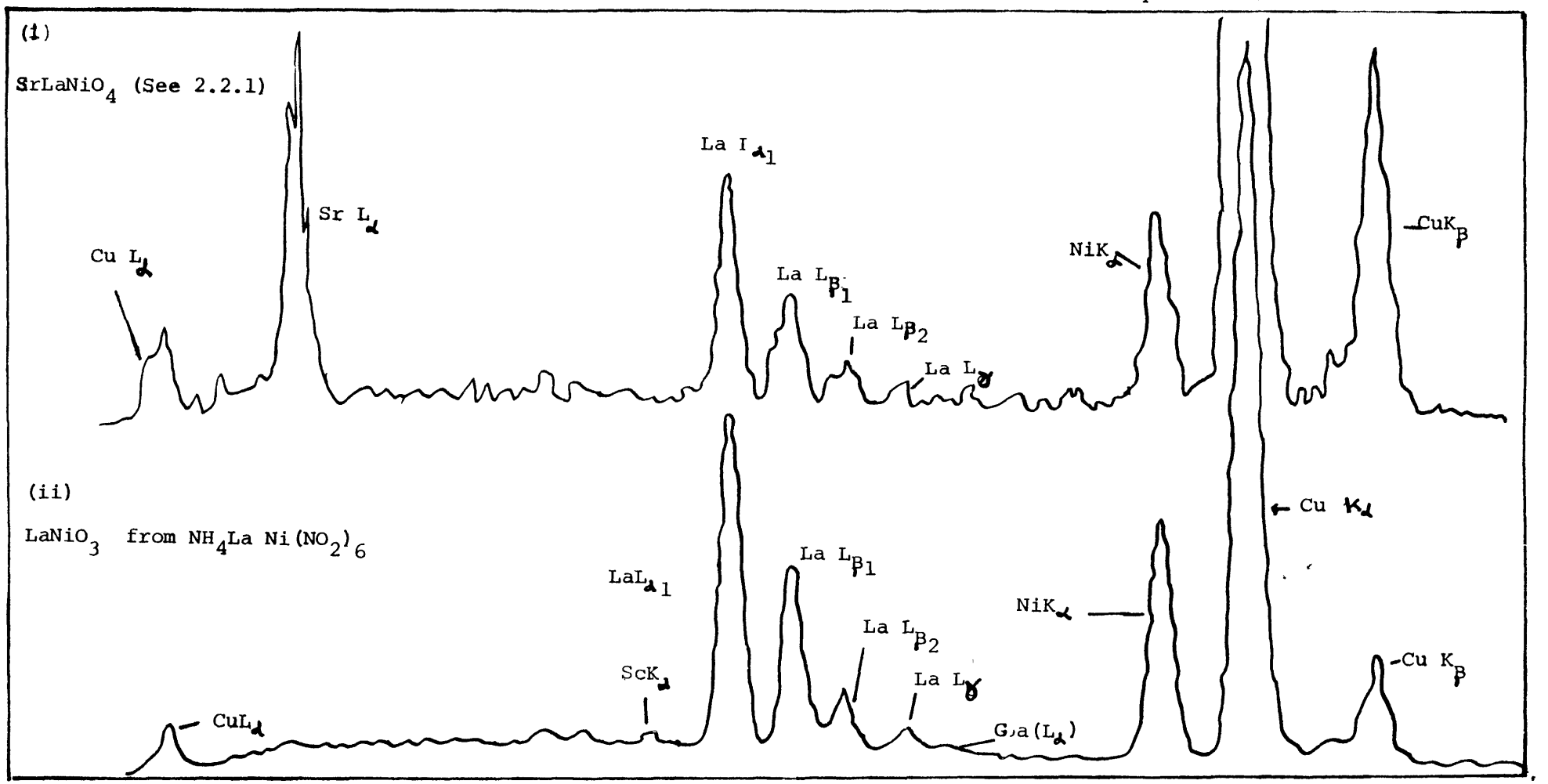

coprecipitation technique) at 850 °C for 12 hours under 240 atmos of oxygen in the apparatus shown in Figure 12.

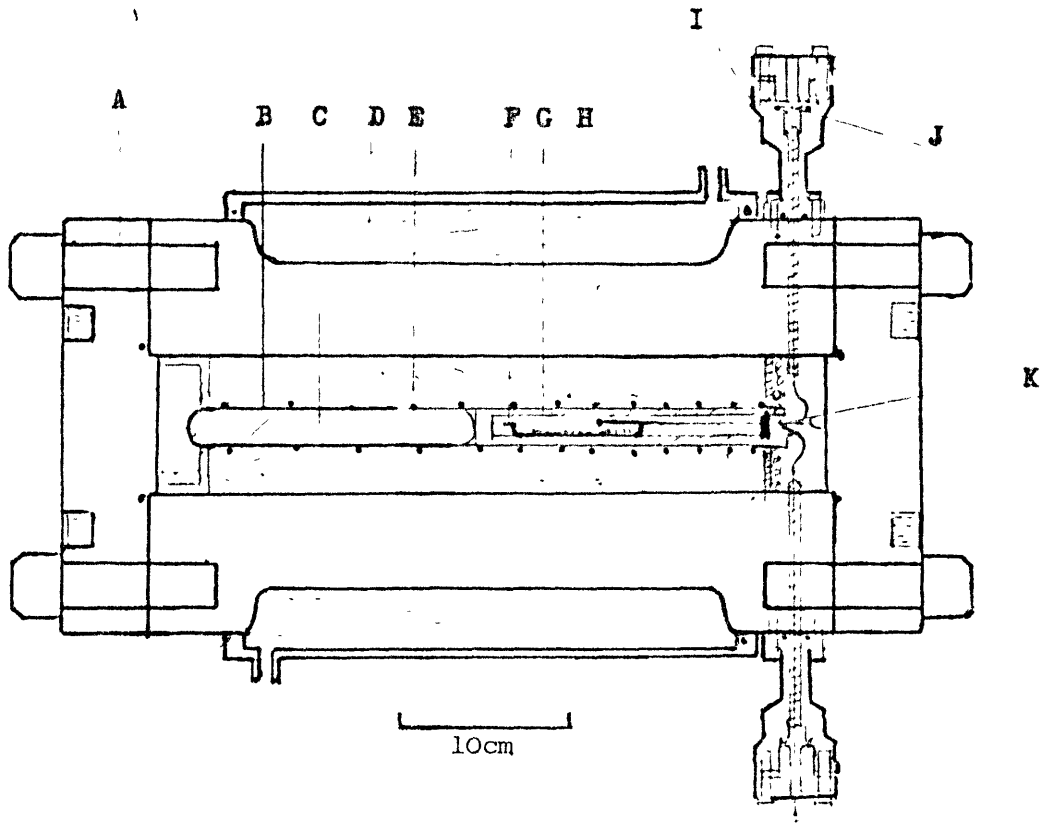

Figure 12 - Internally heated pressure furnace
A-high tenstile bolts; B-nichrome wound furnace;
C-alumina block; D-water cooling; E-alumina powder;
F-alumina boat; G-silica tube; H-samples;
I-phospher bronze assembly for electrical leads
J-metal ceramic seal; K-thermocouple sheath.

2.2. La_2NiO_4 - Lanthanum-2-tetroxonickelate II

This was prepared as described by Rabenau et al.[19], Smolenskii et al.[24] and others[27,80]. The method consists of roasting La_2O_3 and NiO at 1200°C for 4-6 hours with periodic removal and grinding. The author did observe a difference in lattice parameter for samples prepared in air and accidently in oxygen - the a axis seems to be larger in the latter case. There was also a difference in colour, the former is very dark green while the latter is black. Gopalakrishnan et al.[27] have quantified this as explained in Section 1.3.3.

Kniga et al.[43] have studied the kinetics of the formation reaction of La_2NiO_4. They concluded that surface diffusion was the

controlling step. They were also able to obtain single crystals presumably from the melt at 1670°C.

2.2.1. $SrLaNiO_4$ and $La_2Li_{.5}Ni_{.5}O_4$

The $SrLaNiO_4$ - Strontium Lanthanum-textroxonickelate III and $La_2Li_{.5}Ni_{.5}O_4$ - 2'Lanthanum-4-1,1,tetroxolithiatenickelate I,III mentioned in the text were prepared by the method of Blasse[21] with some modifications.

$Sr(NO_3)_2$ and La_2O_3, $Ni(NO_3)_2.4H_2O$ were heated in oxygen at 800°C for 24 hours. The same treatment was applied to the $Li_2CO_3/La_2O_3/NiO$ mixture for the latter compound. The reaction mixture so formed was then heated at 900°C for 24 hours under 240 atmos. of oxygen in the apparatus shown in Figure 12.

For the preparation of the La-Ni-O phases we have dealt with both extreme cases; that in which maximum presence of oxygen is desirable (preparation of $LaNiO_3$) and its converse (preparation of La_2NiO_4). For the phases $La_{N+1}Ni_NO_{3N+1}$ there is an increasing Ni^{III}/Ni^{2+} ratio as $N \longrightarrow \infty$ and thus the oxidizing conditions must be adjusted accordingly - at fixed temperature. Viewed from the other standpoint the decreasing decomposition temperature, at fixed P_{O_2}, must be taken into account.

2.3. $La_3Ni_2O_7$ - Lanthanum-3-1,1, heptoxonickelate II,III

This was prepared by two methods :-

(i) Heating $\frac{3}{2}La_2O_3$: $2Ni(NO_3)_2.4H_2O$ at 1150°C in air for 5 hours with about 5 cycles of the inevitable removal and grinding procedure.

(ii) Heating pellets of $LaNiO_3$: La_2NiO_4 at 1150°C in air for about 12 hours with one removal and grinding.

2.4. $La_4Ni_3O_{10}$ - Lanthanum-4-1,2,decoxonickelate II,III

(i) Heating $2La_2O_3$: $3Ni(NO_3)_2.4H_2O$ at 1080-1100°C in air for 12 hours with about 6 cycles of removal and grinding.

(ii) Heating $4La(NO_3)_3.4H_2O$: $3Ni(OH)_2$ in the same fashion as (i) for about 4 hours at 1100°C.

(iii) Heating pellets of $2LaNiO_3$: La_2NiO_4 overnight at 1100°C as case (ii).

The author was unaware of Seppanen's[25] method of preparation of $La_4Ni_3O_{10}$ when the synthesis was carried out.

2.5. $La_5Ni_4O_{13}$ - Lanthanum-5-1,3,tridecoxonickelate II,III

This proved very difficult to prepare. The majority of mixtures were based on what was learnt from the preparation of $La_3Ni_2O_7$ and $La_4Ni_3O_{10}$. When typical charges of $3Ni(NO_3)_2$: $2La_2O_3$ were made and heated to 1100°C-1150°C in air $La_3Ni_2O_7$ and $La_4Ni_3O_{10}$ and to a lesser extent La_2NiO_4 were obtained. Plate 3 B)(a) and (b) shows this. This Plate is presented also to show that $La_3Ni_2O_7$ and $La_4Ni_3O_{10}$ are clearly distinguishable compounds - identical patterns are also obtained where 'pure' $LaNiO_3$ is heated to these temperatures.

The successful methods developed in this work of preparing $La_5Ni_4O_{13}$ are :-

(i) Heating pellets of $LaNiO_3$: $La_4Ni_3O_{10}$ at 1050°C for 24 hours with about 5 regrinding cycles.

(ii) Heating $5La_2O_3$: $4NiO$ in a K_2CO_3 flux at 1050°C for 48 hours.

2.6. Experimental :-

Starting materials were :-

(1) $LaNiO_3$ (flux method) :- La_2O_3 (99.9% Johnson Matthey)
NiO (99.9% Koch Light)
Na_2CO_3 (AR. Hopkins and Williams)

(2) $LaNiO_3$:- oxalate method - Starting materials were La_2O_3 (as (1)) and $Ni(NO_3)_2.4H_2O$ (AR - Koch Light) using $(COOH)_2.2H_2O$ (AR Hopkins and Williams) as precipitating agent.

(3) $LaNiO_3$ precursor :- $La(NO_3)_3.4H_2O$ (AR Koch Light)
$Ni(NO_3)_2.3H_2O$ (AR Koch Light)
$NH_4(NO_3)$ (AR Hopkins and Williams)
$NaNO_2$ (AR Koch Light)

(4) La_2NiO_4 :- As case (1)

(5) $SrLaNiO_4$:- La_2O_3 (99.9% Johnson Matthey)
$Sr(NO_3)_2$ (AR. Koch Light)
$Ni(NO_3)_2.4H_2O$ (AR Koch Light)

(6) $La_2Li_{.5}Ni_{.5}O_4$:- La_2O_3 (99.9% Johnson Matthey)
Li_2CO_3 (AR Koch Light)
NiO (99.9% Koch Light)

(7) $La_{N+1}Ni_NO_{3N+1}$ phases :-

(i) N=2 La_2O_3 (99.9% Johnson Matthey)
$Ni(NO_3)_2.4H_2O$ (AR Koch Light)

(ii) a) N=3 As case (7)(i).

b) $La(NO_3)_3.4H_2O$ (AR Koch Light)
and $Ni(OH)_2$ (Koch Light)

(iii) As case (1).

Where La_2O_3 was used it was calcined and weighed when hot.

Heating was usually in a horizontal tubular furnace although sometimes (case (4)) a muffle was used.

Grinding was done manually in an agate mortar.

X-ray microanalysis - narrowbeam - was on a JEOL 12CCX on copper and nylon grids - OPERATING IN STEM MODE.

T.G.A. of $NH_4LaNi(NO_2)_6$ was performed on a STANTON 770 MICRO ELECTRONIC BALANCE (at a heating rate of 2 degrees per minute).

CHAPTER 3

Thermodynamic Properties of the $La_{N+1}Ni_NO_{3N+1}$ phases

3.1 Galvanic Cell Application

Because of the singularities in thermodynamic properties of N-phase regions of an N component system (i.e. the activities of all components being fixed at fixed temperature and pressure) the precision obtainable from galvanic cell measurements makes these regions accessible to quantitative study. Galvanic cells can give accurate values of partial pressures and from the temperature dependence of the e.m.f., entropies and enthalpies can be calculated. The e.m.f. must be calculated under open circuit conditions (i.e. equilibrium established between electrodes). For electrocatalytic oxides cell design is simplified by using a solid electrolyte such as Yttria Doped Zirconia (YDZ) without a conventional noble metal electrocatalyst such as Pt on the sample side and in appropriate cases the use of air P_{O_2} = 21.3 kPa as reference electrode.

3.1.1. Cell Voltage of 3 Component Oxide Systems

The cell voltage is a measure of the activity ($p_{O_2}(s)$) according to the Nernst equation :-

$$E = \frac{RT}{ZF} \text{Ln} \frac{p_{O_2}(s)}{p_{O_2}(\text{ref})} \quad \ldots\ldots\ldots\ldots\ldots\ldots\ldots\ldots \quad (7)$$

where Z = no. of moles of electrons involved in the reaction

$R = 8.314 \text{ J mol}^{-1}\text{k}^{-1}$ $F = 96450 \text{ C}$, and T = Temperature in K.

Following the I.U.P.A.C. convention the e.m.f. is positive (+ve) if the right hand electrode is +ve against the left hand electrode. For 3 coexisting solid phases in a system A-B-O this amounts to the following :-

SAMPLE	ELECTROLYTE	REFERENCE say
$A_{\alpha_1} B_{\beta_1} O_{\gamma_1}$		
$A_{\alpha_2} B_{\beta_2} O_{\gamma_2}$	Y D Z	air
$A_{\alpha_3} B_{\beta_3} O_{\gamma_3}$		
p_{O_2} = ? but < 21.3kPa		P_{O_2} = 21.3 kPa
$4e^-$ ⟵	$\leftarrow 2O^{2-} \leftarrow$	⟵ $4e^-$

When p_{O_2} ref = 101.325 kPa according to Chan Li Chuan et al.[44]

$$E = \frac{1}{2Fd} \sum_{i=1}^{3} (-1)^i d_{i,3} \quad G\,(A_{\alpha_i} B_{\beta_i} O_{\gamma_i}) \quad \ldots\ldots\ldots\ldots\ldots\ldots \quad (8)$$

(α & γ are stoichiometric numbers.)

Where d is the determinant formed by the stoichiometric numbers of the 3 coexisting solid phases and $d_{i,3}$ is the minor of d formed by eliminating the third row and the i^{th} line of d - the stoichiometric numbers of oxygen -. For such 3 phase regions it is imperative to study 2 ternary phases which have one side in common with one of the two legs of the Gibbs Triangle (oxygen forming the third leg). In the La-Ni-O system this amounts to :-

(i) $La_{N+1}Ni_NO_{3N+1}$ | NiO | $La_{n+1}Ni_nO_{3n+1}$

and (ii) $La_{N+1}Ni_NO_{3N+1}$ | La_2O_3 | $La_{n+1}Ni_nO_{3n+1}$

accordingly for (i) :-

$$d = \begin{vmatrix} N+1 & N & 3N+1 \\ n+1 & n & 3n+1 \\ 0 & 1 & 1 \end{vmatrix} = N - n$$

$d_{1,3} = n+1$ $\qquad$ $d_{2,3} = -(N+1)$ $\qquad$ and $\qquad$ $d_{3,3} = -(N-n)$.

Thus (i) can be written as :-

$$N\ La_{N+1}Ni_NO_{3N+1} \longrightarrow (N+1)La_{n+1}Ni_nO_{3n+1} + (N-n)NiO + \frac{(N-n)}{2}O_2 \ldots (9)$$

The condition for coexistence is therefore N − n = 1. Under these conditions Z=2 and equation (8) can be written :-

$$E = \frac{-1}{2F}\left\{(N+1)\Delta G_f^{\circ}(La_{n+1}Ni_nO_{3n+1}) + \Delta G_f^{\circ}(NiO) - N\Delta G_f^{\circ}(La_{N+1}Ni_NO_{3N+1})\right\} \ldots (10)$$

and since $\frac{2.303RT}{2} \log_{10} p_{O_2} = \Delta \bar{G}_{O_2}$ .....(10a)

where p_{O_2} / kPa = 21.3 exp $-\frac{4EF}{RT}$ .....(10b)

Equation (10) can be written :-

$$\Delta \bar{G}_{O_2} = (N+1)\Delta G_f^{\circ}[n] + \Delta G_f^{\circ}(NiO) - N\Delta G_f^{\circ}[N] \quad \text{.....(11)}$$

where [n] and [N] are the ternary La-Ni-O phases.

Similarly for (ii)

$$d = \begin{vmatrix} N+1 & N & 3N+1 \\ n+1 & n & 3n+1 \\ 2 & 0 & 3 \end{vmatrix} = -(N-n)$$

$d_{1,3} = -2n$ $\quad d_{2,3} = 2N$ and $d_{3,3} = -(N-n)$

Thus (ii) can be written :-

$$2nLa_{N+1}Ni_NO_{3N+1} + (N-n)La_2O_3 \longrightarrow 2NLa_{n+1}Ni_nO_{3n+1} + \frac{(N-n)}{2} O_2 \quad \text{.....(12)}$$

Accordingly :-

$$\Delta \bar{G}_{O_2} = 2N\Delta G_f^{\circ}[n] - 2n\Delta G_f^{\circ}[N] - \Delta G_f^{\circ}(La_2O_3) \quad \text{.....(13)}$$

as N - n = 1 as case (i).

Often in this text the author refers to a phase by its stoichiometric number as is shown above. For example if 010 = Ni, 001 =O and 100 = La then (203) = La_2O_3 and (011) = NiO. Ternary $La_{N+1}Ni_NO_{3N+1}$ phases are referred to by the value of N. Mixtures are therefore named in accordance e.g. n = 1,2(011) defines a mixture of two ternary phases n = 1 and n = 2 with NiO.

3.2. The Activity Cell and its Calibration

The design of the apparatus and measurement procedure are described in the experimental section of this Chapter. In all cases the reference electrode was air p_{O_2} = 21.3kPa. The cell was calibrated using the Ni/NiO (010,011) equilibrium.

$$Ni + \tfrac{1}{2} O_2 \longrightarrow NiO \quad \text{.....(14)}$$

Figure 13a(i) shows plots of e.m.f. vs T(K) and Figure 13b(i) the plot

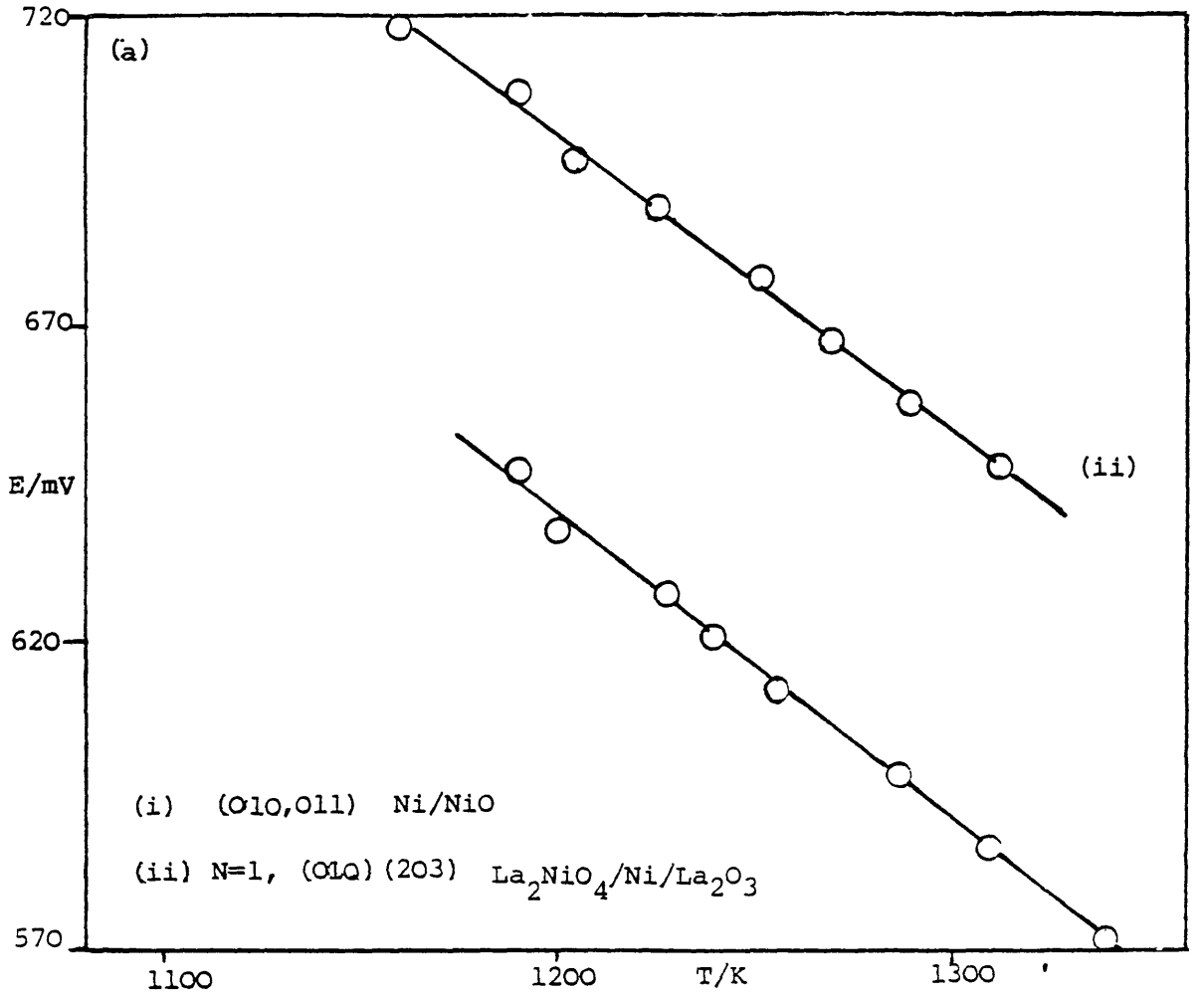

Figure 13 - Galvanic Cell Measurements (a) E(T) (b) $\log_{10} p_{O_2}$ ($^1/_T$)

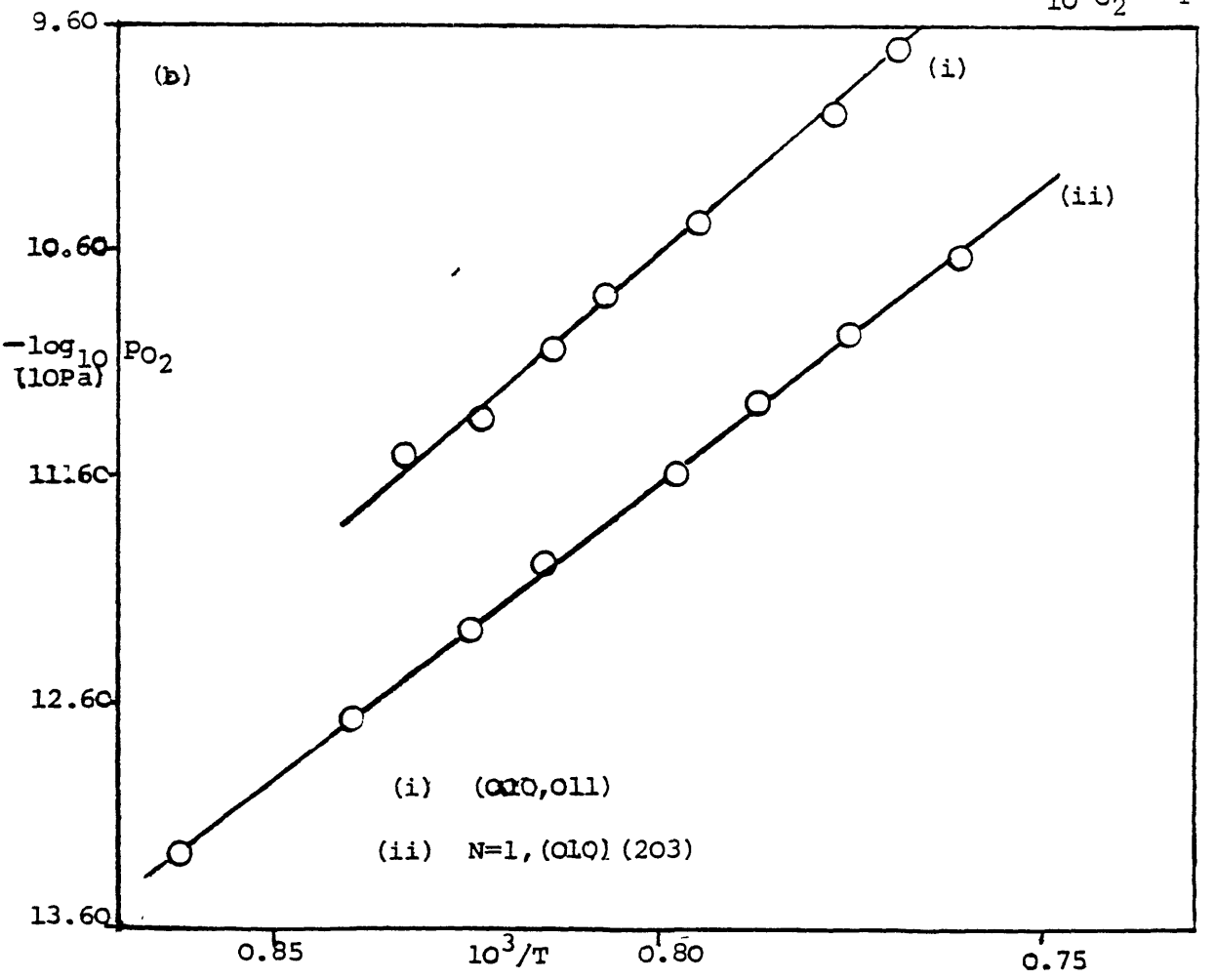

of $\log_{10}P_{O_2}$ vs $10^3/T$. Least squares treatment of the latter gives :-

$$\log_{10}P_{O_2} = -\frac{24.736 \times 10^3}{T} + 9.204 \pm 0.15 \quad \text{.....(15)}$$

$$1150K \leqslant T \leqslant 1350K$$

Putting equation (10a) in equation (15)

$$\Delta \bar{G}_{O_2} = -236.8 + 0.0881T \pm 1.5 kJmol \quad \text{.....(16)}$$

Assuming that Ni and O_2 are in their standard states at 1200K eqn.(16) is the expression for ΔG_f° (NiO) which is in agreement with the data of Steele[45] ($\Delta H_f^\circ = -234.2 \pm 0.9 kJmol^{-1}$, $\Delta S^\circ = 84.89 JK^{-1}mol^{-1}$

$$900K \leqslant T \leqslant 1400K)$$

Remembering that $\Delta G_f^\circ = \Delta H_f^\circ - T\Delta S^\circ$ .....(17)

At 1200K the Third Law Treatment for the entropy S°(NiO) reads :-

$$\Delta S^\circ = S^\circ_{NiO} - \tfrac{1}{2}S^\circ_{O_2} - S^\circ_{Ni} \quad \text{.....(18)}$$

$$S^\circ_{NiO} = 111.5 JK^{-1}mol^{-1}$$

Using ΔS from equation (16) where $S^\circ_{O_2} = 250 JK^{-1}mol$ and $S^\circ_{Ni} = 74.5\ JK^{-1}mol$ as calculated from heat capacity data given in Kubacheweski[46] as outlined in Appendix A 3. The calculated value for NiO is $102.5 JK^{-1}mol^{-1}$ which agrees with equation (18).

3.3. Results of Galvanic Cell measurements on the $La_{N+1}Ni_NO_{3N+1}$ Phases.

Excellent data is available on the thermodynamic properties of NiO as is evident from the previous section of this Chapter. The same is not true for La_2O_3. Examples can be cited in the literature of authors[47,48] using enthalpies and entropies at 1000K-1200K with a variation as large as $86 kJmol^{-1}$ and $29 JK^{-1}mol^{-1}$ respectively. In consequence uncertainties are large in measurements concerning La_2O_3[46,50].

3.3.1. N = 1, La_2NiO_4 - Lanthanum-2-tetroxonickelate II -

The e.m.f. vs T curve for the reaction

$$La_2O_3 + Ni + \tfrac{1}{2}O_2 \longrightarrow La_2NiO_4 \quad \text{.....(19)}$$

and the corresponding $\log_{10}P_{O_2}$ vs 1/T plot are shown in

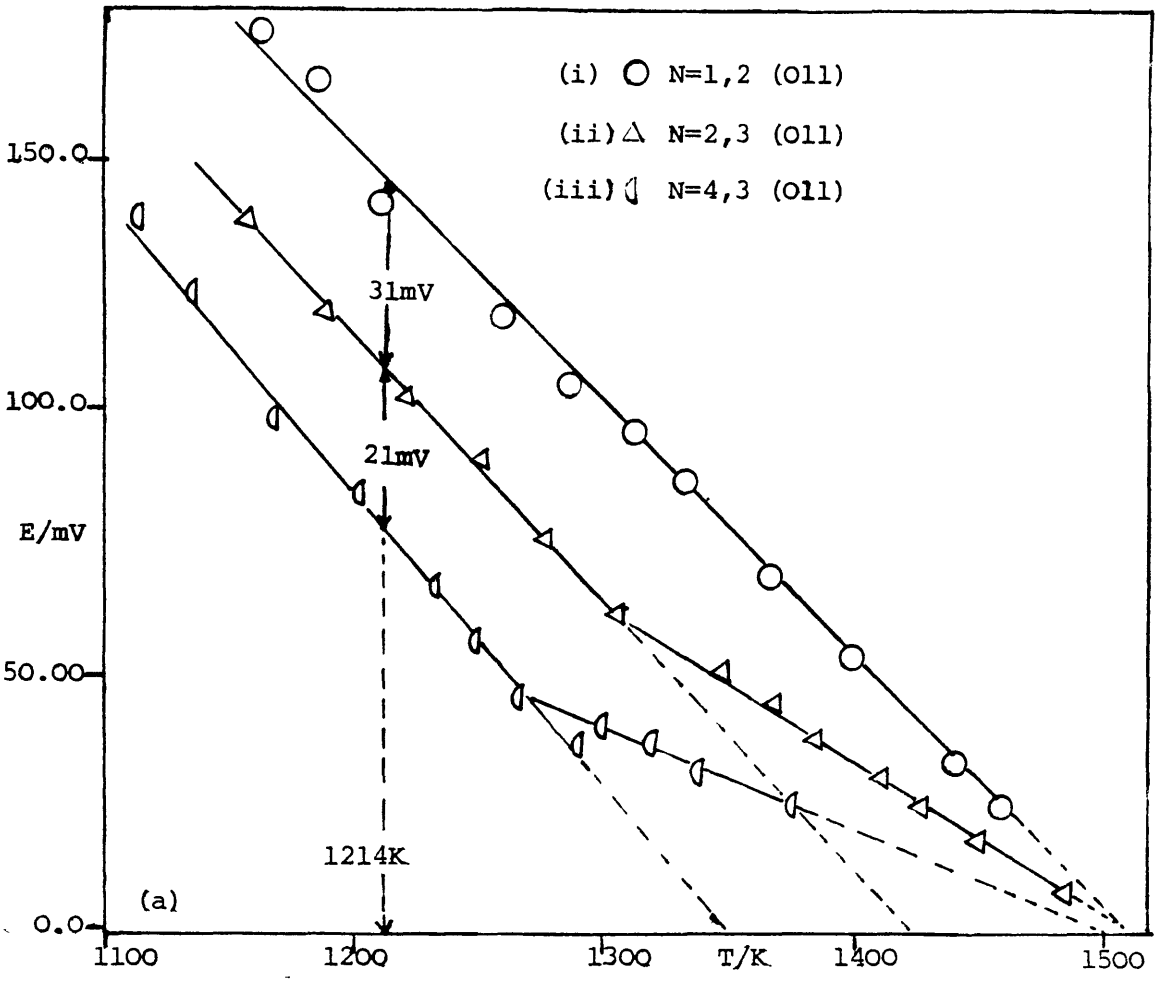

Figure 14 - E(T) plots for [N] [N+1] and (a) NiO (b) La_2O_3

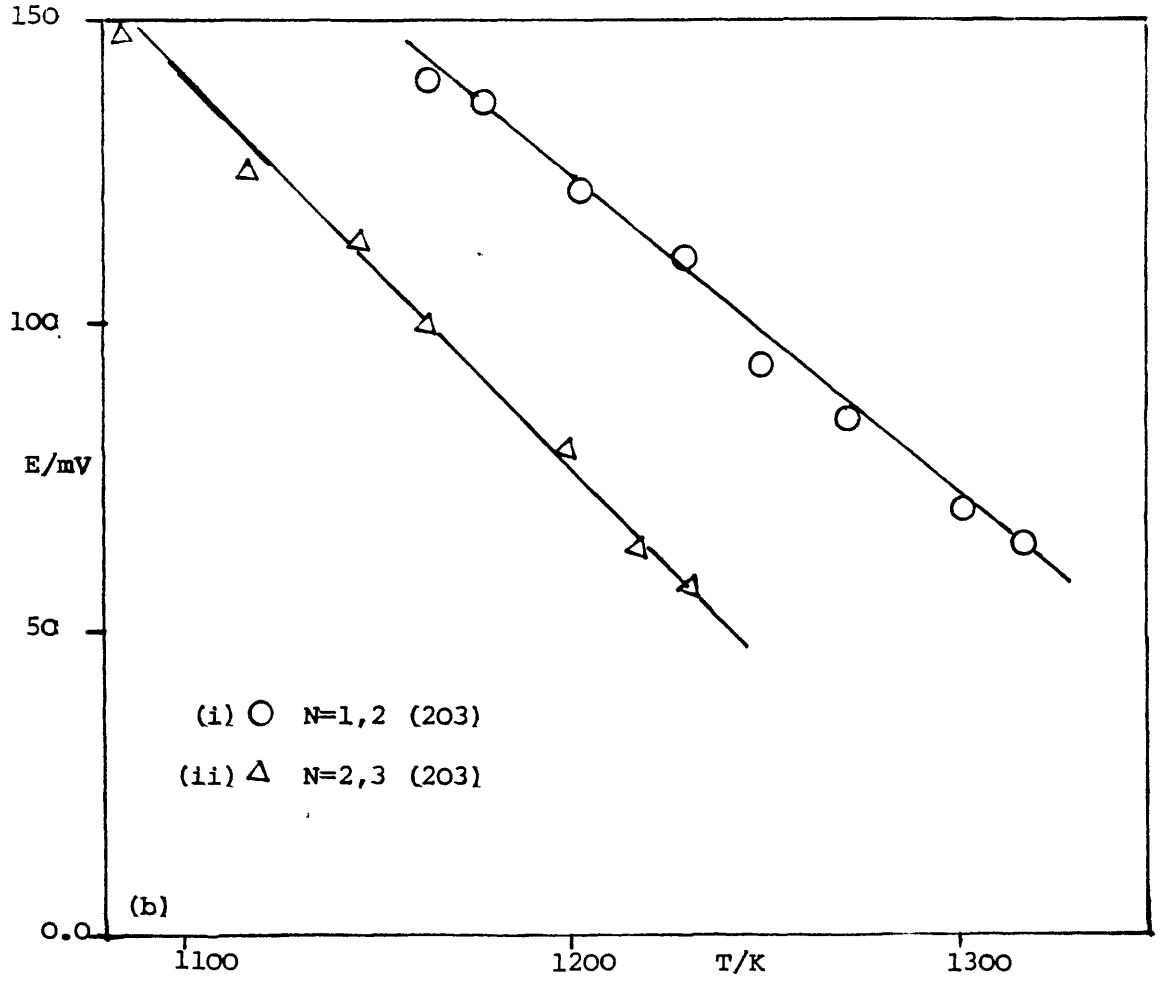

Figures 13(a)(ii) and 13(b)(ii) respectively labelled as N=1,(010)(203). Least mean square treatment of the latter gives :-

$$\log_{10} p_{O_2} = \frac{-26.14 \times 10^3}{T} + 9.285 \pm \frac{0.10}{T}$$

Therefore $\Delta \bar{G}_{O_2} = -250.2 + 0.0889T \pm 1.0$ kJmol^{-1} .....(20)

Assuming Ni and O_2 are in their standard states and using a value of

ΔG_f° (La_2O_3) = -1811 + 0.289T $\pm$ 12kJmol^{-1} gives :-

ΔG_f° (La_2NiO_4) = -2061 + 0.377T $\pm$ 12kJmol^{-1} .....(21)
1150K $\leqslant$ T $\leqslant$ 1340K

ΔG_f° (La_2O_3) is calculated from heat capacity data given in Kubacheweski et al.[46] and Barin et al.[49] and are given in Appendix A2. Sreedharan et al.[48] have measured the thermodynamic properties of La_2NiO_4 using NiO as reference electrode within the same temperature range, and arriving at the value of :-

a) $\Delta G_f^\circ(La_2NiO_4)$ = -2057.1 + 0.322T $\pm$ 17.3 kJmol^{-1}.

For the reaction :- $La_2O_3 + NiO \longrightarrow La_2NiO_4$ they obtained

b) ΔG = -25.568 + 0.03018T $\pm$ 0.19 kJmol^{-1}. When this is combined with the data for NiO and La_2O_3 as is used in this work the final result reads :-

c) ΔG_f° (La_2NiO_4) = -2070 + 0.351T $\pm$ 0.19 kJmol^{-1}.

In other words the calculated value is more in agreement with equation (21). From the data of Sreedharan (b) above it is implicit that $T_{\Delta G=0}$ = 847K i.e. the decomposition temperature of La_2NiO_4. Timofeeva et al.[26b] reported that La_2NiO_4 melts congruently at 2023K. Under these circumstances the author thinks it best to use an average between data obtained in this work and that derived from Sreedharan et al.[48] for further calculations. The value obtained is :-

d) ΔG_f° (La_2NiO_4) = 2065.5 + 0.364T $\pm$ 13kJmol^{-1} .....(22)

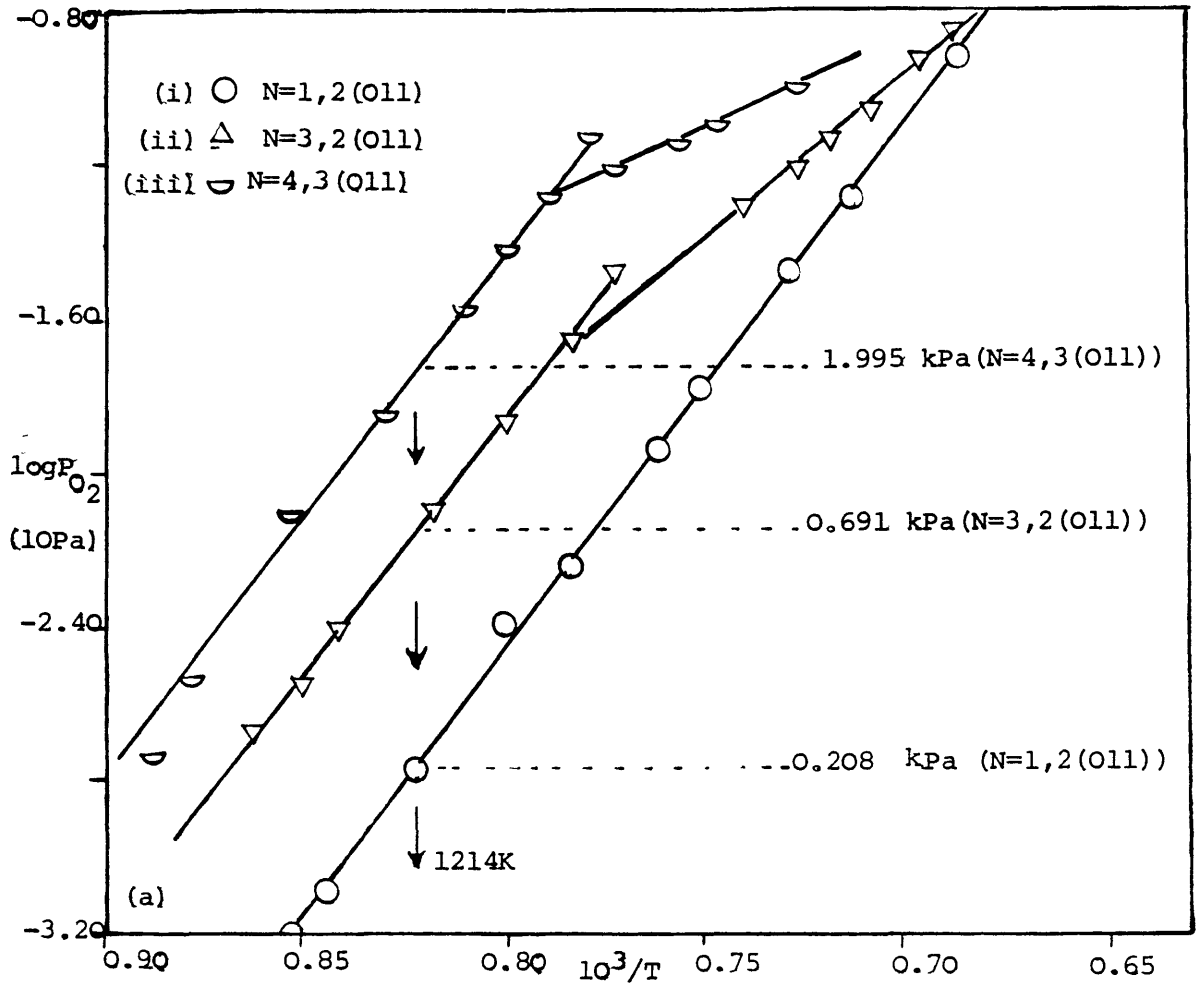

Figure 15 - $\log_{10}Po_2 (^1/_T)$ for [N] [N+1] with (a) NiO (b) La_2O_3

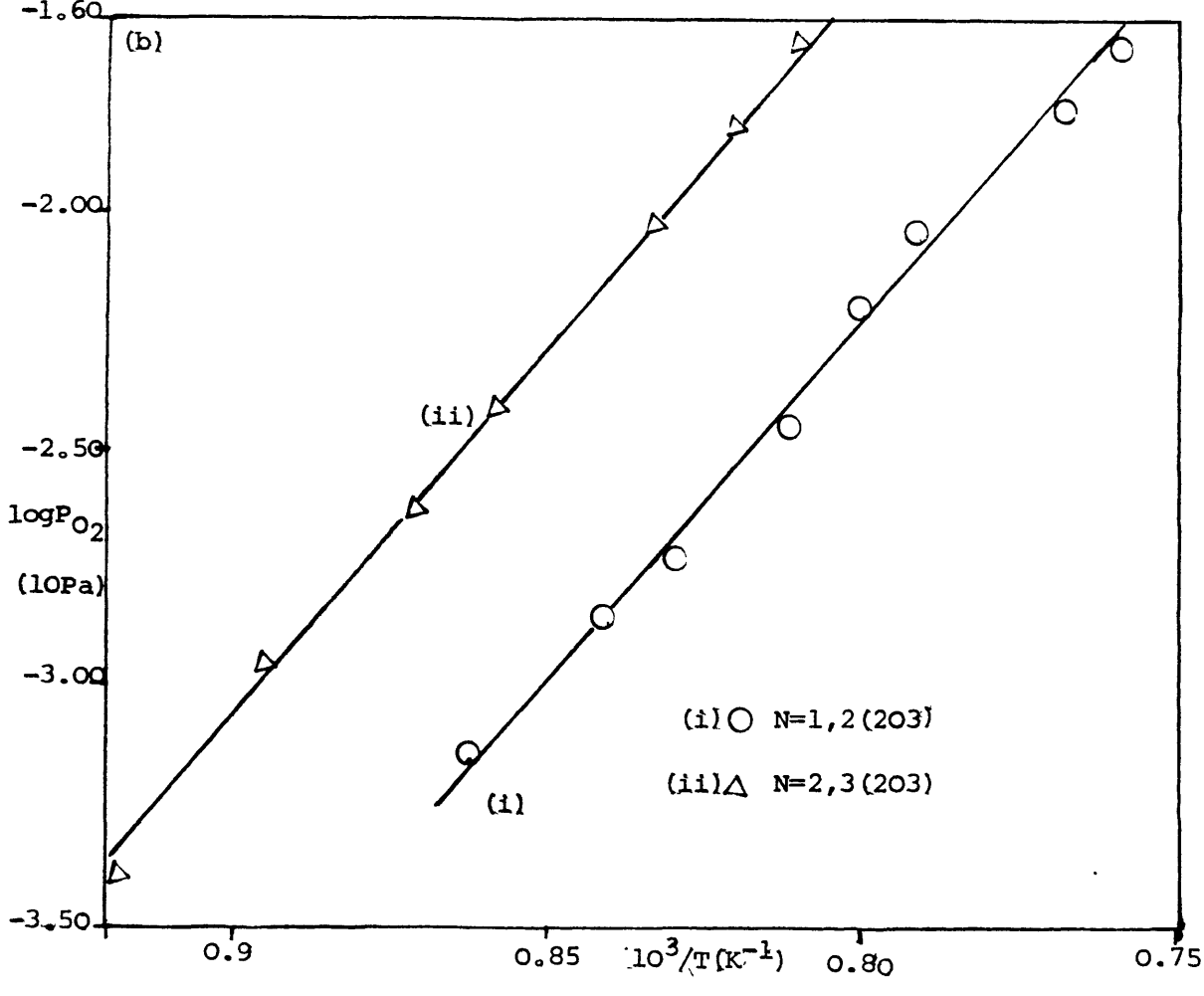

3.3.2. N = 2, $La_3Ni_2O_7$ - Lanthanum -3-1,1,heptoxonickelate II,III -

a) Along the NiO phase boundary :-

Equation (9) applies with N = 2 and the reaction

$$2La_3Ni_2O_7 \longrightarrow 3La_2NiO_4 + NiO + \tfrac{1}{2}O_2 \quad \ldots\ldots\ldots\ldots (23)$$

e.m.f. vs T and $\log_{10}P_{O_2}$ vs 1/T plots labelled as N = 1,2,(011) are shown in Figures 14(a)(i) and 15(a)(i) respectively. Least mean square treatment of the latter gives :-

$$\log_{10}P_{O_2} = \frac{13.528 \times 10^3}{T} + 9.052 \pm 0.1 \quad \ldots\ldots\ldots\ldots\ldots (24)$$

Therefore $\Delta\overline{G}_{O_2} = -129.5 + 0.0866T \pm 1 kJmol^{-1}$ $\ldots\ldots\ldots\ldots\ldots (25)$

Putting equation (25) in equation (11) i.e.

$$\Delta\overline{G}_{O_2} = 3\Delta G_f^{\circ}(N=1) + \Delta G_f^{\circ}(011) - 2\Delta G_f^{\circ}(N=2) \quad \ldots\ldots\ldots\ldots (26)$$

Now using the data of Steele[45] for $\Delta G_f^{\circ}(NiO)$ together with equation (22) in equation (26) :-

$$\Delta G_f^{\circ}(La_3Ni_2O_7) = 3150.5 + 0.5452T \pm 13 kJmol^{-1} \quad \ldots\ldots\ldots (27)$$

$$(1160K \leqslant T \leqslant 1460K)$$

Figure 14(a)(i) also shows the decomposition temperature ($T_{\Delta G=0}$) of $La_3Ni_2O_7$. Graphically this is $\sim$ 1505K while equation (20) gives 1494K. The significance of this will become apparent in the following Chapter.

b) Along the La_2O_3 phase boundary :-

Equation (12) applies with N = 2. The reaction

$$2La_3Ni_2O_7 + La_2O_3 \longrightarrow 4La_2NiO_4 + \tfrac{1}{2}O_2 \quad \ldots\ldots\ldots\ldots\ldots (28)$$

e.m.f. vs T & $\log_{10}P_{O_2}$ vs 1/T plots labelled as N=1,2,(203) are shown in Figures 14(b)(i) and 15(b)(i) respectively. Least squares treatment of the latter gives :-

$$\log_{10}P_{O_2} = \frac{-12.732 \times 10^3}{T} + 9.259 \pm 0.5 \quad \ldots\ldots\ldots\ldots\ldots (29)$$

and therefore $\Delta\overline{G}_{O_2} = -121.8 + 0.08864T \pm 5 kJmol^{-1}$ $\ldots\ldots\ldots\ldots\ldots (30)$

Putting N=2 in equation (13) gives :-

$$2\Delta G_f^{\circ}(N=2) = 4\Delta G_f^{\circ}(N=1) - \Delta G_f^{\circ}(203) - \Delta\overline{G}_{O_2} \quad \ldots\ldots\ldots\ldots (31)$$

Now combining equations (22),(30),(31) and $\Delta G_f^o(La_2O_3)$ gives :-

$$\Delta G_f^o(La_3Ni_2O_7) = -3164.6 + 0.5391T \pm 18 kJmol^{-1} \quad (116OK \leqslant T \leqslant 132OK) \quad \ldots\ldots\ldots\ldots (32)$$

compared with equation (27) determined along the NiO phase boundary.

In this study small amounts of NiO in(as prepared)$La_3Ni_2O_7$ interfered with the equilibration process [48]. In consequence equilibration times were very long indeed, sometimes up to and greater than 12 hours at $1000K < T < 1300K$. There is also quite a larger scatter as is evident in the large uncertainty.

3.3.3. N=3, $La_4Ni_3O_{10}$ — Lanthanum-4-1,2,decoxonickelate II,III -

a) Along the NiO phase boundary :-

Equation (9) is valid for N = 3, i.e.

$$3La_4Ni_3O_{10} \longrightarrow 4La_3Ni_2O_7 + NiO + \tfrac{1}{2}O_2 \quad \ldots\ldots\ldots\ldots (33)$$

The e.m.f. vs T plot for this reaction is shown in Figure 14(a)(ii) labelled as N=3,2(011). The system shows a change of slope at 1310K. From 1150K to 1310K equation (36)is obeyed i.e. the system is univarient. Above this temperature metastable 'nonstoichiometric' phases are formed and the variance changes. This,termed 'subdivision equilibrium' by Anderson[52], is reviewed more fully in Chapter 5. It is primarily as a result of phase broadening making phase distinguishability small or non-existent. The two branches of the E(T) curve are summarised below :

$$E/mV = 589.9 - 0.4182T \pm 1 \quad (1150K < T < 1310K,\ T_{\Delta G=0} = 1432K) \quad \ldots\ldots\ldots\ldots (34)$$

$$E/mV = 451.12 - 0.300T \pm 1 \quad (1310K < T < 1495K,\ T_{\Delta G=0} = 1503K) \quad \ldots\ldots\ldots\ldots (35)$$

The high temperature branch extrapolates to the decomposition temperature of $La_3Ni_2O_7$ (i.e. formation of La_2NiO_4) which indicates some participation of the latter compound (N=1) in the subdivision equilibrium process. The $\log_{10}P_{O_2}$ vs 1/T plot is shown in Figure 15(a)(ii) labelled as N = 3,2 (011). Least squares treatment of the low temperature branch gives :-

$$\log_{10}P_{O_2} = \frac{-12.113}{T} + 8.460 \pm 0.1 \quad \ldots\ldots(36)$$

$$\text{and } \Delta\bar{G}_{O_2} = -115.9 + 0.0810T \pm 1\text{kJmol}^{-1} \quad \ldots\ldots(37)$$

Putting N = 3 in equation (11) gives :

$$3\Delta G_f^{\circ}(N=3) = 4\Delta G_f^{\circ}(N=2) + \Delta G_f^{\circ}(011) - \Delta\bar{G}_{O_2} \quad \ldots\ldots(38)$$

Combining equations (27), (37), ΔG_f°(NiO) [45] and (38) gives :-

$$G_f^{\circ}(La_4Ni_3O_{10}) = 4239.6 + 0.7239T \pm 13\text{kJmol}^{-1} \quad \ldots\ldots(39)$$
$$(1150K < T < 1310K)$$

b) Along the La_2O_3 phase boundary :-

Equation (12) is applicable with N = 3 i.e.

$$4La_4Ni_3O_{10} + La_2O_3 \longrightarrow 6La_3Ni_2O_7 + \tfrac{1}{2}O_2 \quad \ldots\ldots(40)$$

The E(T) and $\log_{10}P_{O_2}$ (1/T) plots labelled as N=2,3(203) are shown in Figures 14(b)(ii) and 15(b)(ii) respectively. Regression analysis of the latter yields :-

$$\log_{10}P_{O_2} = \frac{15.017X10^3}{T} + 10.488 \pm 0.3 \quad \ldots\ldots(41)$$

$$\Delta\bar{G}_{O_2} = -143.8 + 0.1004T \pm 3\text{kJmol}^{-1} \quad \ldots\ldots(42)$$

Putting N = 3 in equation (13) gives :-

$$4\Delta G_f^{\circ}(N=3) = 6\Delta G_f^{\circ}(N=2) - \Delta G_f^{\circ}(203) - \Delta\bar{G}_{O_2} \quad \ldots\ldots(43)$$

Putting $\Delta G_f^{\circ}(La_2O_3)$, equations (27) and (42) in equation (43) gives :-

$$\Delta G_f^{\circ}(La_4Ni_3O_{10}) = -4236.3 + 0.7293T \pm 16\text{kJmol}^{-1} \quad \ldots\ldots(44)$$
$$(1080K < T < 1230K)$$

compared with equation (39) when determined along the NiO phase boundary.

As was the case for N = 2 ($La_3Ni_2O_7$) traces of NiO in (as prepared) $La_4Ni_3O_{10}$ interfered with the equilibration process and times were inordinately long. It was decided to terminate the studies involving La_2O_3.

3.3.4. N = 4, $La_5Ni_4O_{13}$ - Lanthanum-5-1,3,tridecoxonickelate II,III -

Along the NiO phase boundary :-

Equation (9) holds for N = 4 i.e.

$$4La_5Ni_4O_{13} \longrightarrow 5La_4Ni_3O_{10} + NiO + \tfrac{1}{2}O_2 \quad \ldots\ldots\ldots\ldots\ldots (45)$$

As for the previous case the E(T) plot shows a change of slope above a certain temperature, indicating the formation of metastable phases. The details of the E(T) plot, Figure 14(a)(iii), are as follows :-

$$E = 585 - 0.4290T \pm 1.5 \text{ mV} \quad \ldots\ldots\ldots\ldots\ldots\ldots\ldots\ldots (46)$$
$$(1100K < T \leqslant 1270K \quad T_{\Delta G=0} = 1360K)$$

$$E = 254.3 - 0.1698T \pm 1 \text{ mV} \quad \ldots\ldots\ldots\ldots\ldots\ldots\ldots\ldots (47)$$
$$(1270K \leqslant T < 1400K \quad T_{\Delta G=0} = 1500K)$$

As before the latter high temperature branch shows that La_2NiO_4 is involved in the sub-division equilibrium process[52]. The low temperature branch of the $\log_{10}P_{O_2}$ vs 1/T plot shown in Figure 15(a)(iii) as analysed by least squares is shown below :-

$$\log_{10}P_{O_2} = \frac{-11.746 \times 10^3}{T} + 8.648 \pm 0.1 \quad \ldots\ldots\ldots\ldots\ldots (48)$$

$$\Delta G_{O_2} = -112.45 + 0.0831T \pm 1 \text{kJmol}^{-1} \quad \ldots\ldots\ldots\ldots\ldots (49)$$

Putting N = 4 in equation (11) gives :-

$$4\Delta G_f^{\circ}(N=4) = 5\Delta G_f^{\circ}(N=3) + \Delta G_f^{\circ}(011) - \Delta \bar{G}_{O_2} \quad \ldots\ldots\ldots\ldots (50)$$

Combining $G_f^{\circ}(NiO)$[45] with equations (39), (49) and (50) yields :-

$$\Delta G_f^{\circ}(La_5Ni_4O_{13}) = -5330 + 0.9129T \pm 13\text{kJmol}^{-1} \quad \ldots\ldots\ldots\ldots (51)$$
$$(1100K < T < 1270K)$$

The e.m.f. was constant in the regions studied indicating that no other phases exist in this region of the La-Ni-O phase diagram at these temperatures. The 'anomalous' E(T) behaviour observed for some of the oxides constitutes metastable phases which are solutions of the various ternary oxides dissolved in one another. The temperature at which the anomaly begins appears to decrease as the Ni^{III} content increases (i.e. $T_{3\leftarrow 2} = 1310K$, $T_{4\leftarrow 3} = 1270K$, equations (34) and (46), suggesting that compounds with the larger value of N are less

stable and are probably more apt to enter into 'solution'. Data collected for samples of $LaNiO_3$ heavily 'doped' with NiO from 'failed' attempts to prepare Von J. Sieler's[32] $LaNi_2O_4$ - Section 1.5.1 - fitted the data of (as prepared) $La_5Ni_4O_{13}$. This further supports the view that although '$LaNiO_3$' samples might have an X-ray diffraction pattern of $LaNiO_3$ compositionally this might not be the case. Table 9 summarises Free Energy Reaction for the so far known compounds in the La-Ni-O system.

TABLE 9 Free Energy of Transformation of the $La_{N+1}Ni_NO_{3N+1}$ Phases

	Reaction	$\Delta H/kJmol^{-1}$	$\Delta S/JK^{-1}mol^{-1}$	$U/kJmol^{-1}$	Temp.range/K
a)	N=1 ← N=2	129.5	86.6	1	1160-1460
	N=2 ← N=3	115.9	82.0	1	1150-1310
	N=3 ← N=4	112.4	83.1	1	1100-1270
b)	N=1 ← N=2	121.8	88.6	5	1160.1320
	N=2 ← N=3	143.8	100.4	3	1080.1230

a) determined along the NiO phase boundary
b) " " " La_2O_3 " " U = uncertainty

The derived thermodynamic properties (from b) above) of the $La_{N+1}Ni_NO_{3N+1}$ phases are summarised below in Table 10.

TABLE 10 Thermodynamic Properties of $La_{N+1}Ni_NO_{3N+1}$ Compounds :-

N	Formula	$\Delta H_f^\circ/kJmol^{-1}$	$U/kJmol^{-1}$	$\Delta S^\circ/JK^{-1}mol^{-1}$	T_d/K	$S^\circ/MeVK^{-1}$
1	La_2NiO_4	2065.5	13	364	2023*	3.92
2	$La_3Ni_2O_7$	3150	13	542	1505	6.55
3	$La_4Ni_3O_{10}$	4239	13	729	1420	9.25
4	$La_5Ni_4O_{13}$	5330	13	915	1360	11.92

T_d is the decomposition temperature accurate to $\pm 5^\circ$
*Melting point[26b]
$S^\circ/meVK^{-1}$ is the Third Law Entropy (at 1200K) calculated from the relationship - $NS^\circ[N] = (N+1)S^\circ[n] + S^\circ(NiO) + \frac{1}{2}S^\circ_{O_2} - \Delta S^\circ$ ..(52)
Where [N] and [n] are coexisting ternary phases and S° is the reaction entropy shown in Table 9.

Outside the 'anomalous' region in the E(T) plots (Figures 14(a) and 15(a)), the univarient conditions approximate to a set of parallel slopes. For the 3 three-phase regions there is one phase common to two regions, therefore the difference in activity between the 'common' phases at a particular temperature is reflected in the difference in cell voltage ($=f(\Delta\mu_{O_2})$). At 1214K this amounts to the following :

$\Delta E_{N=2/N=3}$ = 31 mV and $\Delta E_{N=3/N=4}$ = 21 mV. One would need to know the activitiy of at least one more component say NiO to be able to calculate absolute activities of the ternary phases.

3.4. The La-Ni-O Phase Diagram

Cassendene[51] reported only two phases in the pseudobinary La_2O_3/NiO phase diagram namely $LaNiO_3$ and La_2NiO_4. We are now in a position to expand on this. We can use two models :-

a) Pseudobinary

We consider the formation of a series of 'solutions' along the line connecting La_2NiO_4 (N=1) and $LaNiO_3$ (N=∞) as shown in equation (53) below.

$$La_2NiO_4 + (N-1)LaNiO_3 \longrightarrow La_{N+1}Ni_NO_{3N+1} \quad \ldots\ldots\ldots\ldots (53)$$

solute (N = 1) solvent (N = ∞) 'matrix'

According to the Gibbs-Duhem relation[83]:-

$$G(N) = X_{N=1}G_{N=1} + X_{N=\infty}\overline{G}_{N=\infty} \quad \ldots\ldots\ldots\ldots\ldots\ldots\ldots\ldots (54)$$

where $\overline{G}_{N_i} = \left(\frac{\partial G}{\partial n_{N_i}}\right)_{N_k,T,P}$

and from equation (53) the mole fraction of La_2NiO_4 is given by :-

$$X_{N=1} = \frac{1}{1+N-1} \quad \ldots\ldots\ldots\ldots\ldots\ldots\ldots\ldots\ldots\ldots\ldots\ldots\ldots\ldots (55)$$

so that $\lim_{N\to\infty} X_{N=1} = 0$.

Combining equations (54) and (55) leads to :-

$$G(N) = NX_{N=1}\left[\overline{G}_{N=1} - N(N-1)\overline{G}_{N=\infty}\right] + N(N-1)\overline{G}_{N=\infty} \quad \ldots\ldots\ldots (56)$$

Both $\overline{G}_{N=1}$ and $\overline{G}_{N=\infty}$ are in principle determinable from the slope and

intercept of the G(X) plot. Arbitrarily we know that as $N \rightarrow \infty$ X_{O_2} and therefore p_{O_2} increases.

Table 11 summarises G(N) calculated from $\Delta G_f^\circ = \Delta H_f^\circ - T\Delta S^\circ$ at 1200K and the corresponding $X_{N=1}$ calculated using equation (55)

TABLE 11 Free Energy of $La_{N+1}Ni_NO_{3N+1}$ 'solutions' as $f(X_{N=1})$ at 1200K

N	Formula	$X_{N=1}$	G(N)/kJmol^{-1}
1	La_2NiO_4	1.00	1628
2	$La_3Ni_2O_7$	0.50	2499
3	$La_4Ni_3O_{10}$	0.33	3361
4	$La_5Ni_4O_{13}$	0.25	4232
5	$La_6Ni_5O_{16}$	0.20	5101*
0	$LaNiO_3$	0.00	?

* determined from coulometric studies on $LaNiO_3$ (Chapter 4)

The data in Table 11 is plotted in Figure 16 below.

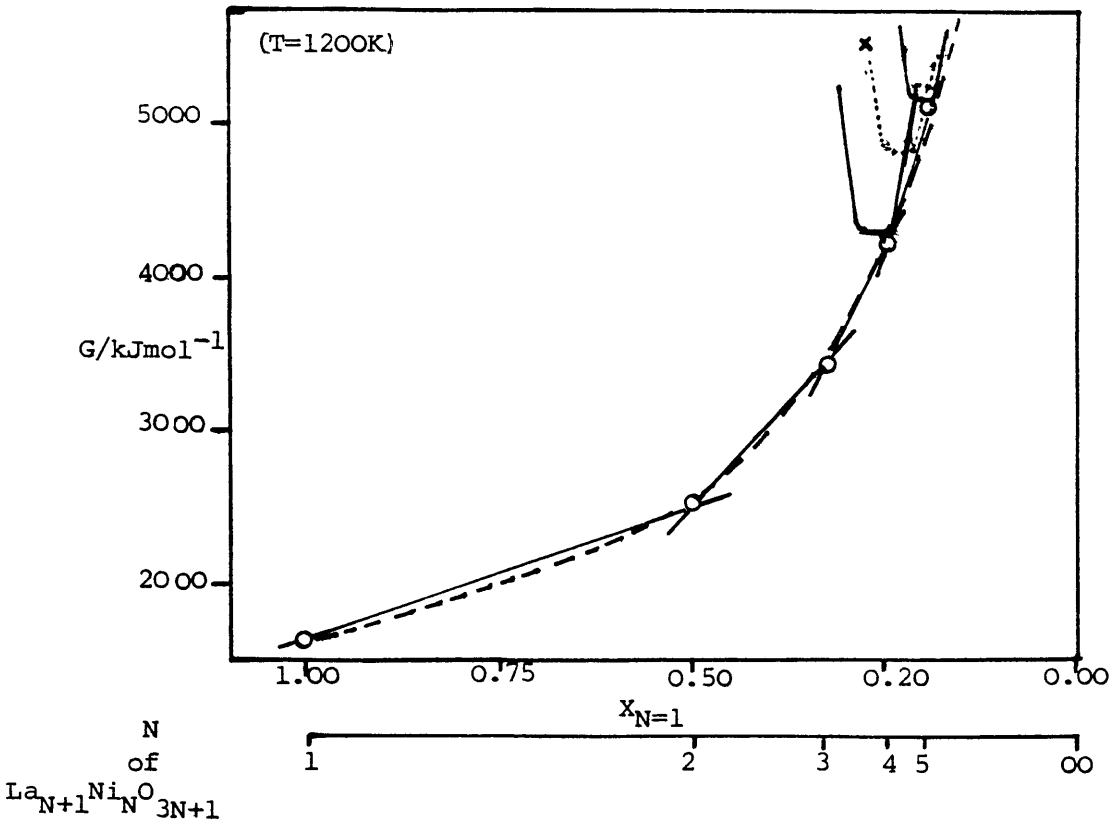

Figure 16 - G-X plot for the pseudobinary $LaNiO_3$ (N=∞) : La_2NiO_4 (N=1) System at 1200K.

The envelope formed by the coexistence tangents approximates to a smooth curve (dotted line). This can easily be mistaken for a smooth bivarient curve if crystallographic data was lacking or if the thermodynamic measurements were too widely spaced. The inability to distinguish phases increases with N (i.e. $X_{N=1}$ decreases). Now if each phase represents the most probable configuration of the atoms at this temperature, the Third Law of Thermodynamics tells us that this is a distribution function of the type :-

$$w = \exp \frac{-G}{kT} \quad \text{Where } w = \text{probability}$$

Fluctuation in the most probable distribution may occur if there is a net gain in free energy according to Anderson[52]. At fixed temperature this will predominantly be dependent on the separation along X. If w is a parabolic function, the 'width' of the parabola should indicate how readily a phase mixes randomly with neighbouring phases. As w becomes narrower this random mixing will increase and fluctuations in w increases. This is indicated as x in Figure 16.

b) Ternary

We consider the formation of a solution of 3 components of the type shown in equation (57) :-

$$\frac{(N+1)}{2}La_2O_3 + N\,NiO + \frac{(N-1)}{2}'O' \longrightarrow La_{N+1}Ni_NO_{3N+1} \quad \ldots\ldots(57)$$

and $$G(N) = X_{La_2O_3}\bar{G}_{La_2O_3} + X_{NiO}\bar{G}_{NiO} + X_O\bar{G}_O$$

Now $X_{La_2O_3} = \frac{N+1}{4N}$ so that $\lim_{N\to\infty} X_{La_2O_3} = \frac{1}{4}$

and $X_O = \frac{N-1}{4N}$ so that $\lim_{N\to\infty} X_O = \frac{1}{4}$

while $X_{NiO} = \frac{N}{2N} = \frac{1}{2} = \text{const.}$

Data from Table 9 is used to calculate Molar Free Energies G(N) using $\Delta G = \Delta H - T\Delta S$ (T = 1200K). These are tabulated with the relevant mole fractions in Table 12.

TABLE 12 Molar Free Energies & relevant Mole Fractions for the $La_{N+1}Ni_NO_{3N+1}$ phases at 1200K

N	$X_{La_2O_3}$	X_O	X_{Ni}	$G(N)/kJmol^{-1}$
1	0.500	0.000	0.500	+10.60*
2	0.375	0.125	"	-25.50
3	0.333	0.166	"	-17.50
4	0.312	0.187	"	-12.80
5	0.300	0.200	"	-11.63**
0	0.250	0.250	"	?

* calculated from the data of Sreedharan et al.[48]

** calculated from P-X profile of $LaNiO_3$ obtained coulometrically (Chapter 4)

Figure 17 shows the Molar Free Energy surface for the La-Ni-O system at 1200K plotted in 2kJ steps approximately

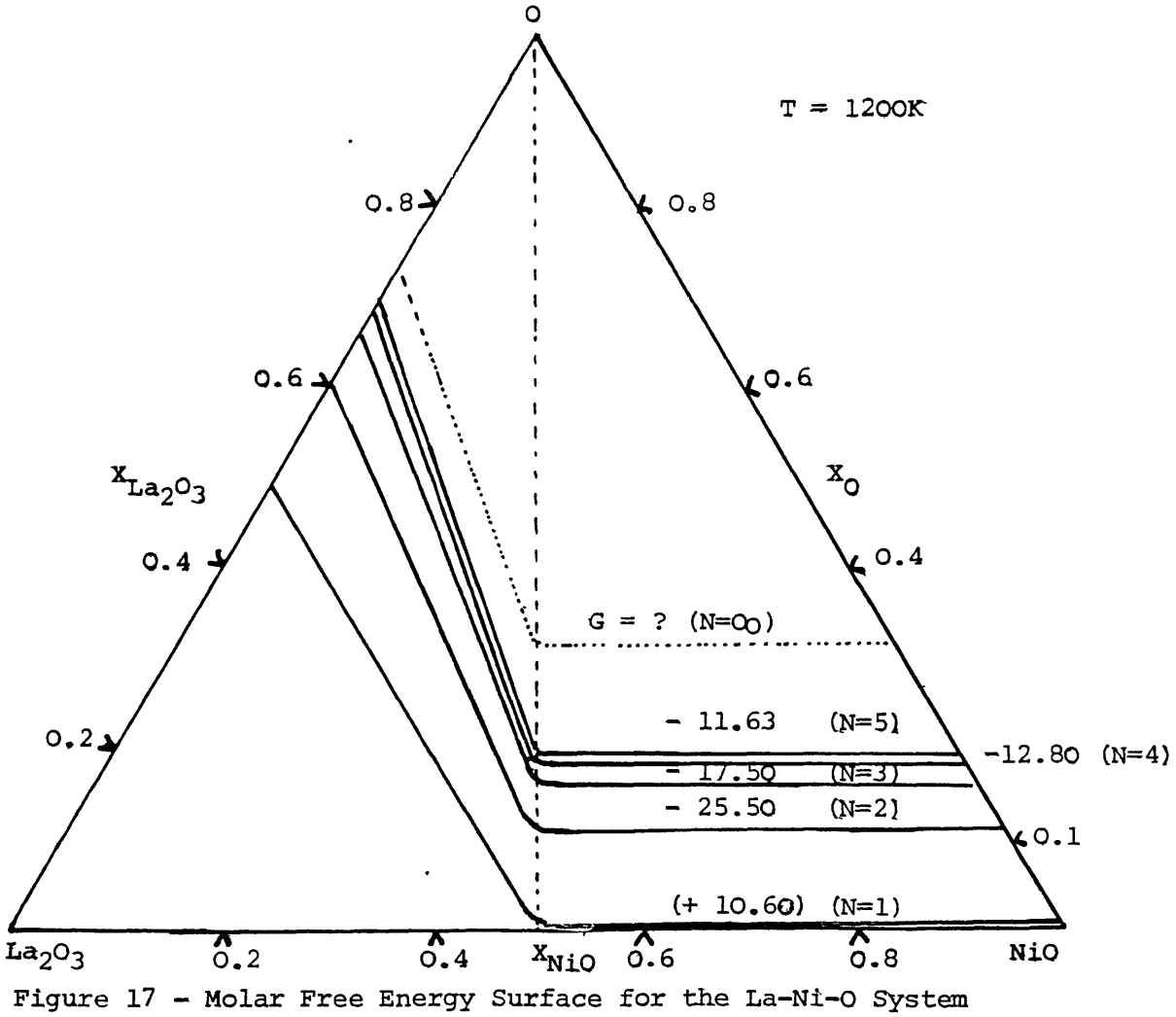

Figure 17 - Molar Free Energy Surface for the La-Ni-O System ($La_{N+1}Ni_NO_{3N+1}$ Phases) at 1200K in approximately 2 kJ steps.

Figure 17 reiterates the small steps in Free Energy (say $\bar{G}_{O_2}$) to change from configuration N to N' at this temperature particularly as N→∞. G(N) for the latter compound (i.e. $LaNiO_3$) is indicated by a dotted line on the Figure as no thermodynamic properties are available. The partial molar free energy for the formation of La_2NiO_4 from La_2O_3 and NiO is +ve at 1200K according to the data of Sreedharan et al.[48] This is out of character with the values for the other oxides (Table 12) and indeed contrary to expectation.

3.5. Experimental

(a) The Activity Cell

A long tubular activity cell design (Figure 18) was adopted. This has several advantages over the conventional 'pellet cell' as was used by Screedharan et al.[48] or small crucible type cells as reviewed by Steele[59]. These advantages include :-

(i) The possible use of a cold seal such as araldite between electrolyte tube and 'sealing off facilities'. For the small crucible type cells a glass ceramic seal is normally used. This seal has to be made at high temperature (1000°C - 1400°C) and is not suitable for application in cells running at T ≲ 1100°C particularly for samples of low oxygen potentials (closed cells).

(ii) The reclycleability of the cell particularly when the compounds to be studied are very soluble in a solvent such as dilute acid in which the electrolyte is only sparingly soluble. This condition is fulfilled for the La-Ni-O compounds when the solvent is dilute HNO_3 and the electrolyte YSZ.

The cell used in this study is shown in Figure 18. The electrolyte tube was manufactured by the Zircoa Corporation

containing about 1% Fe^{2+} impurity and having a nominal thickness of 1mm. The air electrode was made by firing on platinum paste (Englehard Type 6082) as recommended by the manufacturer; contact to the thermocouple leads was made by 'tying on' Johnson Matthey specpure platinum gauze. The D.V.M. was manufactured by Data Precision (series 2000, type 2400) with an input impedance of 10^{10} Ω.

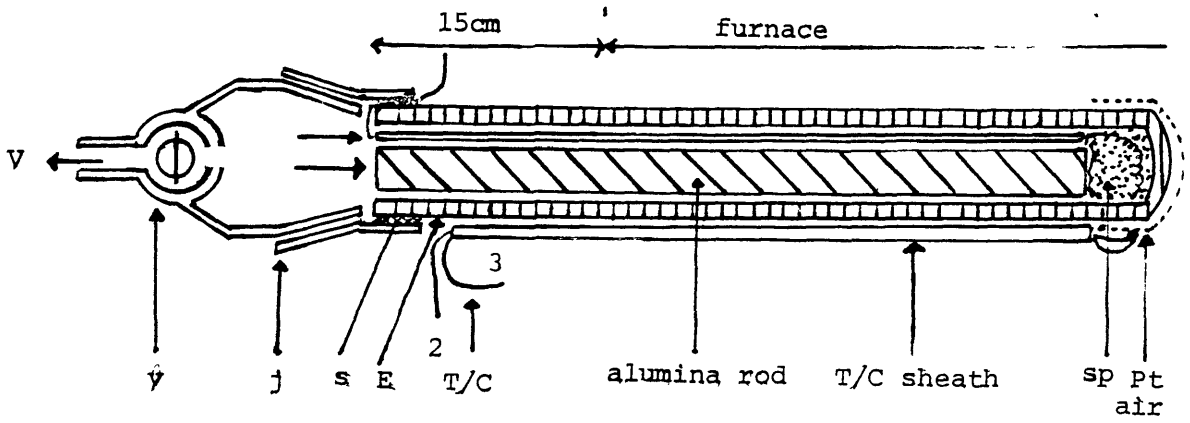

(a) Cell Design :-

s = araldite seal
sp = specimen
e = YSZ tube
j = ground glass joint
v = glass vacuum value

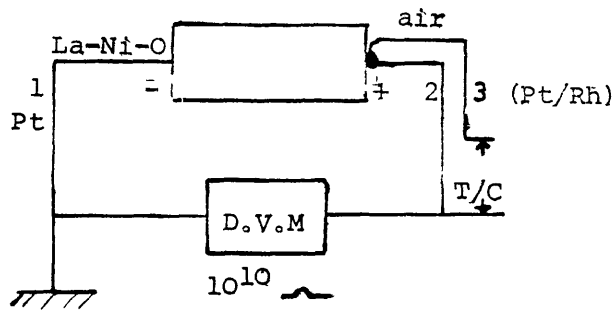

(b) Equivalent circuit for E(T) measurements

Figure 18 - Activity Cell for the Evaluation of Thermodynamic Properties of the La-Ni-O Compounds

(b) Setting Up Procedure

After any one cycle of experiments was completed the cell and the solid alumina rod were washed thoroughly first with dilute HNO_3, then with distilled water and occasionally with diethyl ether. The cell was then left in an oven to dry for 2-3 hours or where a very dry cell was required degassing was performed at 100°C on a silicone oil diffusion pump.

All specimens were in powdered form. These were mixed thoroughly in an agate mortar. The best way for loading the cell was by using a specially made long paper funnel. For good electrical contact, powders were pressed firmly to the bottom of the tube by an alumina rod longer than the one shown in Figure 18.

The internal volume of the system was determined by filling the system, as it is in Figure 18 but without the sample, with water. This was then weighed. The volume was typically (11-13)cm depending on the electrolyte tube. It was calculated that (1-1.5)g samples were more than adequate to 'fill the system' with the p_{O_2} at the triple point.

(c) Specimens

(1) Calibration :

Koch Light NiO(99.9%) and Johnson Matthey Ni (specpure) were used. The powders were thoroughly mixed in an agate motar. The cell was then evacuated down to 10^{-5} Torr on a silicone oil diffusion pump and sealed off via v in Figure 18. E(T) values obtained on both heating and cooling cycles are shown in Figure 13(i). The experiment took about 12 hours.

(2) Test Cases :

(i) $La_2O_3/Ni/La_2NiO_4$ - In a 1:1:1 ratio an evacuated cell was used. Koch Light La_2O_3 (99.9%), Johnson Matthey Ni (specpure) and as prepared, La_2NiO_4 were used. E(T) values obtained on both heating and cooling cycles are shown in Figure 13(ii). The E(T) profile was determined once and took ~18 hours. No phase changes were observed in the region where E(T) was determined. At lower temperatures ($1150K < T < 1220K$) E 'settled down' in about 40 minutes after temperature change, but values were taken as an average over a

(60-90) minute period. At higher temperature 1220K $<$ T $<$ 1300K equilibrium was established in $\sim$ 20 minutes after temperature change but voltages were taken as an average over a (40-60) minute period.

(ii) $La_3Ni_2O_7/La_2NiO_4/NiO$ - In a 2:2:1 ratio the E(T) profile was determined. As prepared, $La_3Ni_2O_7$ together with the previously described La_2NiO_4 and NiO were used. Voltages obtained on both heating and cooling cycles are shown in Figure 14(i). The E(T) profile was studied in the ranges 900K $<$ T $<$ 1100K and 1100K $<$ T $<$ 1469K. Measurements in the low temperature range took up to 120 minutes to reach equilibrium and there was more scatter in the E(T) data obtained in this region. In the high temperature range equilibrium was established in about 30 minutes (for T $>$ 1150K) but readings were averaged over a (40-60) minute period. The E(T) profile was determined 4 times; twice within the low temperature range (data not shown) and twice within the high temperature range over a 10 day period. A typical EMF vs T reads :-

a) High Temperature Range

T/K	E/mV	Time/Mins.
1164	196.3	3
	170.7	37
	168.3	60
	169.0	75
-	168$\pm$1	-
1272	105.9	5
	102.4	20
	102.0	35
	102.5	45
-	102$\pm$0.5	-

b) Low Temperature Range

T/K	E/mV	Time/Mins.
954	220	0
	295	30
	290	60
	293	90
-	292$\pm$1	-
990	252	10
	257	30
	264	60
	266	90
-	265.3$\pm$1	-

High Temperature Range			Low Temperature Range		
T/K	E/mV	Time/Mins.	T/K	E/mV	Time/Mins.
1332	74.8	5	1008	236	10
	74.1	20		244	30
	74	30		247.6	55
	- 74±0.5 -	40		246	75
1369	55.1	5		- 246.6±1 -	
	54.8	20	1029	220	0
	- 54 -	30		238	50
	54±0.5			239	60/60
1399	41.6	10		- 239.9±1 -	
	41.9	20	1079	210	0
	42.2.	30		214	30
	42.2±0.2			215	60
1437	24.7	0		- 214.5±1 -	
	25.3	25	1087	210	10
	25.3±0.1			212	60
1457	13.9	0		- 212.0±1 -	
	14.6	10	1119	187	10
	14.7	20		193	55
	- 14.7±0.1 -			- 192.6±1 -	
			1127	186	6
				189	60
				189.4±1	
			1159	168.0	10
				171.7±1	60

(iii) $La_3Ni_2O_7/La_2NiO_4/La_2O_3$ - in a 2:2:1 ratio were used in an open cell. Materials were as in (ii) but using La_2O_3 (as in (i)) and excluding the NiO. E(T) was determined within the range 900K < T < 1100K and 1100K < T < 1300K. Equilibrium in the latter range (not shown in Figure 14(b)(i)) took up to

18 hours to establish because of small traces of NiO in, as prepared, $La_3Ni_2O_7$ and La_2NiO_4. In the high temperature range (Figure 14(b)(i) equilibrium was still sluggish (e.g t~ 5 hours at ~ 1150K). Overall E(T) was determined 4 times over a 10 day period.

(iv) $La_4Ni_3O_{10}/La_3Ni_2O_7/NiO$ - Determination of E(T) was by using a 2:2:1 mixture. Materials were as in (ii) but replacing La_2NiO_4 with as prepared $La_4Ni_3O_{10}$. Three determinations of E(T) were carried out one within the range $900K < T < 1150K$ (not shown in Figure 14(a)(i))where the voltage was by and large reversible for heating and cooling cycles. The other two were within the range shown in Figure 14(a)(ii) (i.e $1150 < T < 1490K$). Voltages up to 1300K were reversible but at temperatures greater than 1300K (where the variance changes) voltages were not reversible. From 1190K downwards E(T) lay in between the E(T) for the N=1,2 (011) equilibrium and the N=2,3(011) equilibrium - Figure 14. Equilibrium was faster than in (ii). Typically equilibrium was established (with the high temperature range at ~ 1200K) in about 30 minutes but readings were averaged over a 40-60 minute period.

(v) $La_4Ni_3O_{10}/La_3Ni_2O_7/La_2O_3$ - A 2:2:1 ratio was used. Materials were as in (iv) but replacing NiO with La_2O_3 as in (i). E(T) was determined 4 times; twice within $900K < T < 1100K$ (not shown) and twice within $1100K < T < 1250K$ (shown in Figure 14(b)(ii)). Equilibrium times were long because of traces of NiO in $La_4Ni_3O_{10}$ and $La_3Ni_2O_7$ (e.g ~ 24 hours at 1000K), and results showed a large amount of scatter.

Results for studies involving La_2O_3 were not as good as those involving NiO. The author believes a more thorough investigation of the La-Ni-O phase diagram along the La_2O_3 phase boundary is necessary.

(vi) $La_5Ni_4O_{13}/La_4Ni_3O_{10}/NiO$ - E(T) was determined from a 2:2:1 mixture. Materials were as in (iv) but replacing $La_3Ni_2O_7$ with as prepared $La_5Ni_4O_{13}$. E(T) was determined trice; twice within the range shown in Figure 14(a)(iii) $1100K < T < 1400K$ and once within the range $900K < T < 1100K$. Voltages were reversible up to about 1270K where the variance changes. Equilibrium times were relatively short (e.g. at 1200K typically $t \sim 20$ minutes) but readings were averaged over a 40-60 minute period.

CHAPTER 4

Thermogravimetric and Coulometric Studies on Lanthanum Trioxonickelate III ($LaNiO_3$)

4.1 Thermogravimetric

The thermal decomposition of any compound is controlled by kinetic and thermodynamic factors; the former of which is not considered in this work. We can say however that even on purely thermodynamic grounds the decomposition profile should indicate what species are formed and suggest a model for intermediate phase formation and decomposition. For a ternary oxide such as $LaNiO_3$ formation of at least one of the two binary oxides that form two of the legs of the ternary triangle (Figure 18) is possible. In other words at normal oxygen pressures and at $T > 500K$ La_2O_3 or NiO. We know from previous studies that ternary phases of the type $La_{N+1}Ni_NO_{3N+1}$ are formed so it is more than likely that they are involved in the decomposition process.

A number of workers notably Gai and Rao[56] and Obayashi et al.[4] have studied the T.G.A. (or T-X) profile of $LaNiO_3$. Both schools reported that there was evidence of oxygen loss in well defined equilibrium stages. Figure 19 shows that the T.G.A. of $LaNiO_3$ in air (p_{O_2} = 21.3kPa) performed on a Stanton 707 Electro Microbalance. The sample was flux prepared (Chapter 2) then reoxidised at 850°C under 240 atmospheres of oxygen for 24 hours. Since neither La nor Ni form volatile oxides under these conditions, then the following is valid.

Weight loss = oxygen loss

Since mass of 1 mol of $LaNiO_3$ = 245.613g

% oxygen in $LaNiO_3$ = 19.54%

and therefore if x is the % weight loss, n_O the number of moles of oxygen loss per mol of $LaNiO_3$ then

$$n_O = \frac{3x}{19.54}$$

Both x and n_O are plotted vs T in Figure 19.

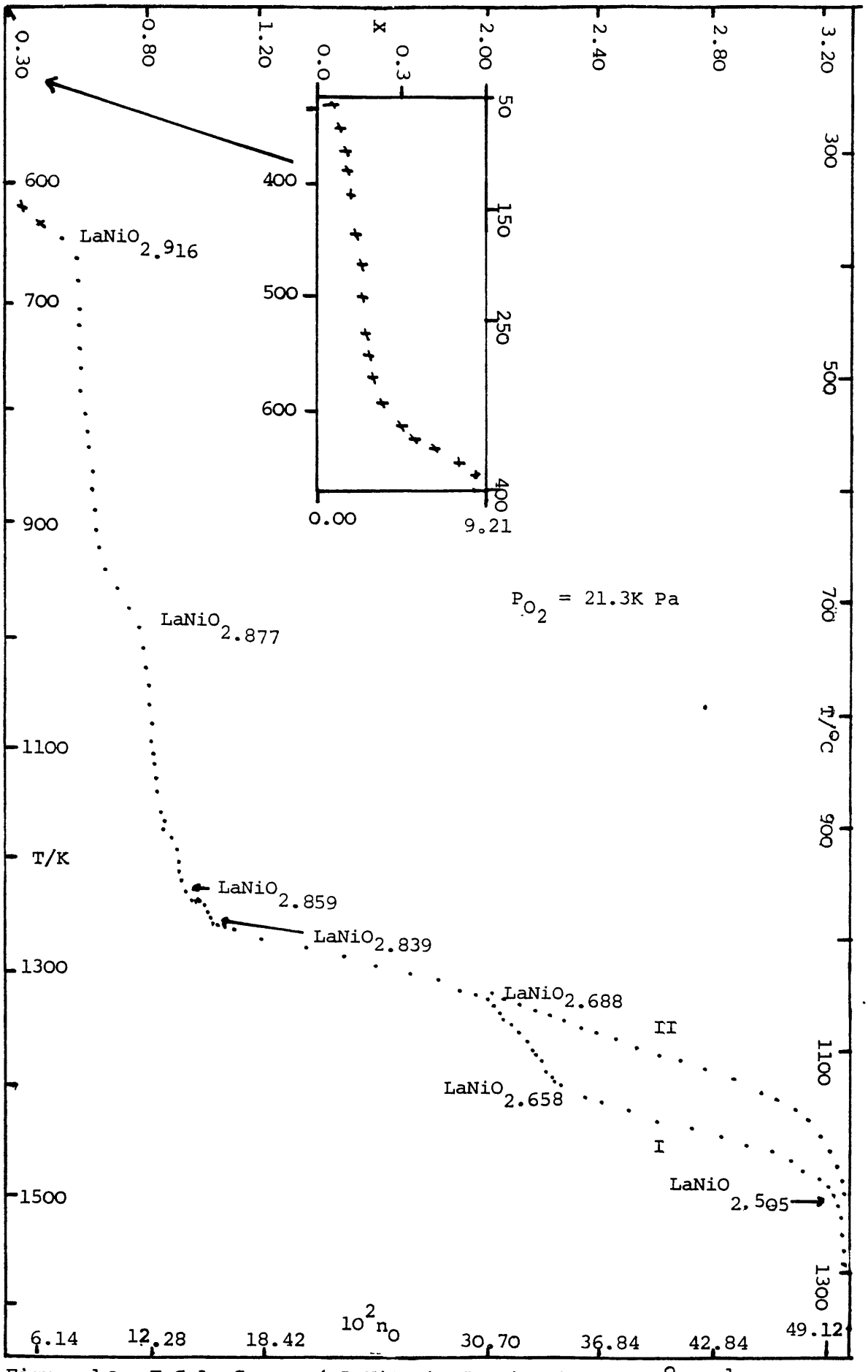

Figure 19 - T.G.A. Curve of $LaNiO_3$ in Static Air: I, $1^{o}min^{-1}$.
II, $3^{o}min^{-1}$.

Figure 19 confirms the oxygen loss in steps. The decomposition was complete at x = 3.25% (n_O = 0.500) for temperatures greater than 1250°C. X-ray analysis confirmed the final product to be a mixture of La_2NiO_4 and NiO. Gai and Rao[56] carried out a study to x = 1% (T = 1000°C) and suggested phases of the type $La_NNi_NO_{3N-1}$ with N = 7, 9 and 13 were formed. They added that the rhombohedral cell was retained at all compositions; its volume increasing only slightly upon oxygen loss. Obayashi et al.[4] performed both T.G.A. and D.T.A. reporting that the latter technique showed an exothermic peak at 335°C and endothermic peaks at 940°C, 1120°C and 1200°C. They explained the T.G.A. Curve in air on the following scheme :-

$$2LaNiO_3 \xrightarrow{940^\circ C} \underset{\text{cubic (Pm3m)}}{2LaNiO_3} \xrightarrow{1120^\circ C} La_2NiO_4 + NiO + \tfrac{1}{2}O_2$$

$2LaNiO_3$ (R3m)

$La_2NiO_4 + NiO + \frac{1}{2}O_2 \xrightarrow{1200^\circ C} La_2O_3 + NiO$

They concluded that $LaNiO_3$ decomposed at $LaNiO_{2.75}$ rather than $LaNiO_{2.5}$ because the La and Ni coordination numbers in $LaNiO_{2.5}$ change from 12 to 10 and 6 to 5 respectively in spite of the fact that the tolerance factor for $LaNiO_{2.5}$ falls within the range where the perovskite structure was stable.

The author's explanation of the T.G.A. profile is at variance with the major part of those given by both schools.[4,56]

The thermal scan rate might be faster than the inherent phase transformation. Nevertheless we can to a first approximation assume that there are basically two types of regions in the T.G.A. profile :-

a) The 2 phase regions where the system is univarient (V = 1) and $\frac{\partial T}{\partial n_O} \sim 0$

b) The 3 phase regions where the system is invarient (V = 0)

$$\frac{\partial T}{\partial n_O} \sim \infty$$

Ideally the T-X (T.G.A.) curve is a series of steps (Figure 19) (T = a step function of n_o) as v oscillates between 0 and 1, but hysteresis is observed for reasons of fast thermal scan which may result in non-equilibrium situations and the thermal broadening of phase fields at high temperatures. Figure 19 shows the effect of thermal scan rate (curves I and II) where significant detail is lost in the region $1000K \leqslant T \leqslant 1200K$ at a heating rate as low as $3^{o}min^{-1}$.

If there are p-1 intermediate compounds formed the T-X curve can be considered as the sum of p-1 T-X curves of the intermediate phases. Accordingly each is separable by an amount in n_o units - Weppner et al.[62] . Figure 20 shows the effect of thermal broadening on Δ .

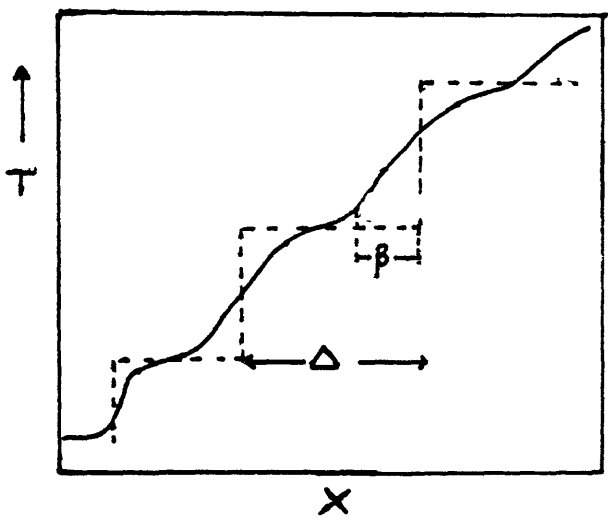

Figure 20 - Typical T-X plot of systems with a due succession of phases showing 'phase broadening' at higher temperatures.

Whether the composition hysteresis β can be interpreted as 'the width of the stoichiometry' or as a metastable phase is dependent on the free energy of mixing of the phases at the triple point. This view will be expanded on in Chapter 5.

Table 13 summarises T and n_o taken at triple points in Figure 20.

TABLE 13 Oxygen Deficient Phases in the T.G.A. of $LaNiO_3$

T/K	n_O	Formula on $LaNiO_3$ basis
1505	0.4946	$LaNiO_{2.5054}$
1423	0.3420	$LaNiO_{2.658}$
1340	0.3120	$LaNiO_{2.688}$
1268	0.1602	$LaNiO_{2.8398}$
1243	0.1409	$LaNiO_{2.8591}$
1000*	0.1230	$LaNiO_{2.877}$
653*	0.0840	$LaNiO_{2.9160}$

* only major peaks shown in this region.

Taking the suggestion of Obayashi et al.[4] that $LaNiO_{2,5}$ 'decomposes' according to the following scheme :-

$$LaNiO_{2.5} = \tfrac{1}{2}La_2NiO_4 + \tfrac{1}{2}NiO$$

the first peak (T = 1505K) can be explained. If this is true for N=1 (La_2NiO_4) then it should be true for N+1 ($La_3Ni_2O_7$). If peak 2 (T=1423K) corresponds to the formation of $La_3Ni_2O_7$ then the following is valid :-

$$La_3Ni_2O_7 + NiO = La_3Ni_3O_8 = LaNiO_{2.666}.$$

The agreement is fair considering the possible effect of thermal broadening. It therefore appears that $La_{N+1}Ni_NO_{3N+1}$ phases are formed in decomposition process and we shall carry out further analysis.

4.1.1 Analysis of the T-X (T.G.A.) profile of $LaNiO_3$

If we start with $LaNiO_3$ (N = ∞) then equation (60) is valid

$$LaNiO_3 \xrightarrow{\text{Heating}} \frac{1}{N+1} La_{N+1}Ni_NO_{3N+1} + \frac{1}{N+1} NiO + \frac{1}{2(N+1)} O_2 \quad \ldots\ldots\ldots (60)$$

and the 'formula' of each phase is :-

$$f = LaNiO_{\frac{3N+2}{N+1}} \quad \ldots\ldots\ldots (60a)$$

At each triple point

$$n_O = \frac{1}{N+1} \text{ and } \left\{n_{O_2} = \frac{1}{2(N+1)}\right\} \quad \ldots\ldots\ldots (61)$$

For 'coexisting' phases $[N_i]$ and $[N_f]$ (i.e. $N_i - N_f = 1$)

$$n_O = = \left\{ \frac{1}{(N_i+1)} - \frac{1}{(N_f+1)} \right\} \quad \ldots\ldots\ldots\ldots\ldots\ldots\ldots\ldots\ldots\ldots (62)$$

$$= \frac{1}{(N_i+1)(N_f+1)}$$

The above is meaningful only if we start at $N = \infty$ ($LaNiO_3$). If we start at the right side of equation (60) for overall transitions from 'defect composition' $LaNiO_{\frac{3N+2}{N+1}}$ then equation (63) applies.

$$\frac{1}{N+1} La_{N+1}Ni_N O_{3N+1} \longrightarrow \frac{1}{n+1} La_{n+1}Ni_n O_{3n+1} + \frac{N-n}{(N+1)(n+1)} NiO + \frac{N-n}{2(N+1)(n+1)} O_2 \quad \ldots\ldots (63)$$

$$n_O = \frac{N-n}{(N+1)(n+1)} \text{ and } \left\{ n_{O_2} = \frac{N-n}{2(N+1)(n+1)} \right\} \quad \ldots\ldots\ldots\ldots\ldots\ldots (64)$$

$$\text{Now } \lim_{N\to\infty} \frac{N-n}{(N+1)(n+1)} = \frac{1}{(n+1)} \left[\lim_{N\to\infty} \frac{N}{(N+1)} - \lim_{N\to\infty} \frac{n}{(N+1)} \right] \quad \ldots\ldots\ldots (64a)$$

$$= \frac{1}{(n+1)} \left[1 - 0 \right] .$$

So that equation (64) approaches equation (61) for $LaNiO_3$.

For $N < \infty$ but large $\frac{N}{(N+1)} \neq 1$ and the approximation $\frac{n}{(N+1)} = 0$ might be too rough. Since by definition $n \geqslant 1$, $\frac{1}{(N+1)}$ seems a better approximation (say for $N \gtrsim 20$) for the last term in equation (64a) for $N < \infty$ but large. Equation (64) can therefore be written :-

$$n_O = \left[\frac{N-1}{N+1}\right] \frac{1}{(n+1)} \text{ and } \left\{ n_{O_2} = \tfrac{1}{2} \frac{N-1}{N+1} \frac{1}{(n+1)} \right\} \quad \ldots\ldots\ldots (64b)$$

and

$$= \left[\frac{N-1}{N+1}\right] \frac{1}{(n_i+1)} - \frac{1}{(n_f+1)}$$

$$= \left[\frac{N-1}{N+1}\right] \frac{1}{(n_1+1)(n_f+1)} \quad \ldots\ldots\ldots\ldots\ldots\ldots\ldots\ldots (64c)$$

(remembering also that $\Delta_{O_2} = \tfrac{1}{2} \Delta_O$)

Returning to Table 13 we see that the transition N=1⟵N=2 (formation of La_2NiO_4) occurs at $n_O = 0.4946$ (T=1505K). Putting n_O and n=1 in equation (64b) gives :-

$$2(0.4946) = \left[\frac{N-1}{N+1}\right] \quad \text{i.e. } N = 180$$

and therefore from equation (60a) f = $LaNiO_{2.9944}$ as the stoichiometry of the starting material. To all intents and purposes this can be considered as $LaNiO_3$ (i.e. N is very large) and we can use equations (60)-(62) as the basis of further calculations. Table 14 compares the observed 'transitions' in the range 1200K$<$T$<$1510K against those calculated on the basis of equations (60)-(62).

TABLE 14 Intermediate $La_{N+1}Ni_NO_{3N+1}$ Phases in the T.G.A. of $LaNiO_3$

N	Transition $N_f \leftarrow N_i$	Calculated (N = ∞)			Observed		
		n_O	$10^2\Delta_O$	f	n_O	T_d/K	T_d^*/K
1		0.500		$LaNiO_{2.500}$	0.494	1505	1500
	1 ← 2		16.67				
2		0.333		$LaNiO_{2.666}$	0.342	1423	1434
	2 ← 3		8.33				
3		0.250		$LaNiO_{2.750}$	(0.312)	1340	1360
	4 ← 3		5.00				
4		0.200		$LaNiO_{2.800}$	-	-	-
	5 ← 4		3.34				
5		0.166		$LaNiO_{2.833}$	0.160	1268	-
	6 ← 5		1.93				
6		0.143		$LaNiO_{2.856}$	0.140	1243	-

T_d is the decomposition temperature

* taken from Ξ(T) thermodynamic studies (Chapter 3 - Table 10)

We note that in Table 14 certain transitions appear to be masked and indeed there appears to be a 'carrying over' of certain transitions to the final N=1←N=2 transition. The thermodynamic reasons for this are not obvious but they are probably two-fold :-

(i) Fast thermal scan may lead to premature decomposition and in consequence poor resolution of the profile;

(ii) Thermodynamic properties of the N$>$1 phases are similar ($\bar{G}_{O_2}$ steps are small) and random mixing occurs. In other words solid solution (metastable) phases are formed as a consequence of thermal broadening of the phase fields and β (Figure 20) is significant.

The fact, however, that the N = 3 and 4 phases are not well resolved

while the N = 5 and 6 appears to be, poses a contradiction. Figure 21 shows the part of the T-X curve of interest $900^{o}C < T < 1400^{o}C$.

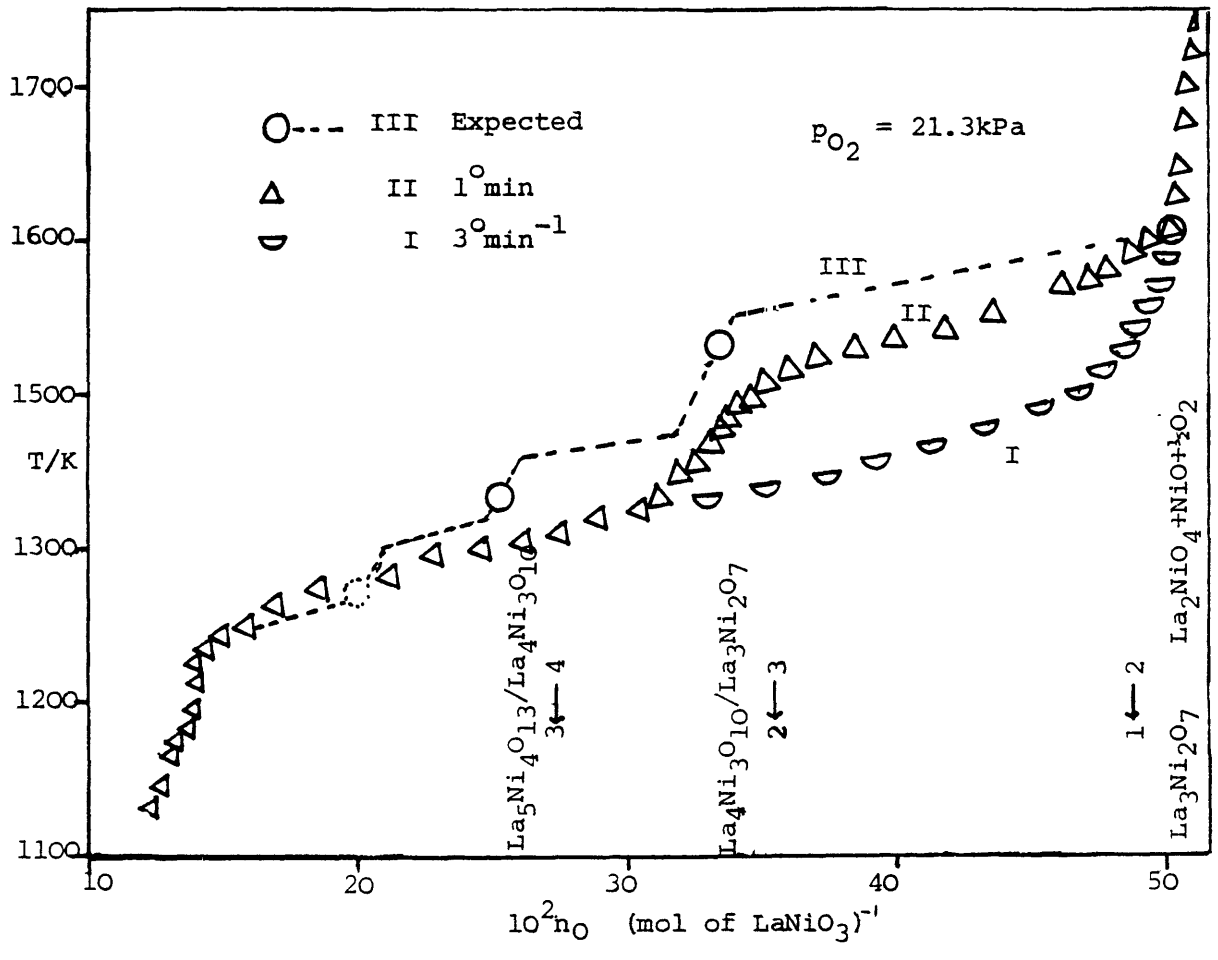

Figure 21 - The T.G.A. Curve of $LaNiO_3$ $900^{o}C < T < 1400^{o}C$.

Figure 21 (III) shows the 'expected' behaviour of the $La_{N+1}Ni_NO_{3N+1}$ oxides. In working up the 'expected' curve a straight line is drawn between the decomposition temperature of the phases that coexist as determined in Chapter 3 plotted against n_O shown in Table 14. Noting that the important N=2← N=3 transition is masked and the N=1← N=2 appears at 1470K instead of at 1500K at $3^{o}min^{-1}$ the idea that the beforementioned transitions are thermally masked seems reasonable. Accordingly the idea of the 'expected' T-X curve has some plausibility.

The foregoing analysis is reasonably consistent with findings on the thermodynamic properties of the isolated La-Ni-O compounds

(i.e. decomposition temperatures determined in Chapter 3). The suggestion by Obayashi et al.[4] that La_2NiO_4 decomposes into La_2O_3 and NiO at 1200°C is in direct contradiction, firstly, with the age-old preparative technique for La_2NiO_4 which is by heating La_2O_3 and NiO at (1200-1400)°C and secondly, with the work of Timofeeva et al.[26b] who melted the material at 1670°C. . In addition that $LaNiO_3$ tolerates point defects up to $LaNiO_{2.75}$ is questionable. The above formula is explainable on the basis of equation (60a) and Table 14 i.e. N = 2 for the defect phase above. Gai and Rao's[56] suggestion of $La_NNi_NO_{3N-1}$ with N = 7, 9 and 13 does not explain the absence of N = 1 - N = 6 phases for N = 8,10,11 and 12. These authors also suggested that superlattice reflections in the electron diffraction pattern of the 'oxygen deficient' phases gave the following cell dimensions :

$a = c \quad \sqrt{2}a_c$ and $b = 2a_c$ (either orthorhombic or body centred tetragonal symmetry)

This appears to be partially correct as we know from Chapter 1 that $a \simeq b \simeq \sqrt{2}a_c$ and $c = (2n+1)a_c$ ($a_c = 3.85\text{Å}$) holds for the intermediate La-Ni-O compounds (having Fmmm symmetry). The preceding analysis is also supported by the fact that X-ray analysis of $LaNiO_3$ heated to 1050°C and 1150°C in air showed equilibrium mixtures of N=1,2,3 and NiO and N=1,2 and NiO respectively. This was previously outlined in Section 2.5.

There still remains one important question. Why is there preferential NiO formation? The answer simply is that we are moving to the La_2O_3 rich side of the phase diagram as we know from the crystallography of the compounds. We know from equation (12) that La_2O_3 is consumed (not produced) as one approaches the thermodynamically more stable oxides (ie $N \longrightarrow 1$).

4.2 Coulometric Studies

If the assumption concerning the unresolved band in the T-X curve of $LaNiO_3$ (Figure 21 - 1270K < T < 1340K) is correct then in principle resolution is possible by electrochemical means. The technique has the following advantages :-

i) Electrical quantities (E and i) can be measured with greater precision.

ii) Small quantities of oxygen are titrable (e.g. 1mC = 10^{-9} moles of O_2).

iii) Finer control of experimental variables ($E = f(p_{O_2})$ and $i = f(n_{O_2})$ is possible.

iv) Actual equilibrium measurements can be obtained under open circuit conditions the only tedium being the equilibration time.

In principle both T-X and P-X curves are obtainable. A large part of this Chapter is devoted to an apparatus designed with this in mind.

4.2.1 The Electrochemical Oxygen Pump and Gauge

(i) The Gauge :-

The gauge is a solid electrolyte galvanic cell that measures the equilibrium oxygen partial pressure against a suitable reference according to Nernst Law - $E = \frac{RT}{4F} \ln p_{O_2}/p_{O_2}$ (ref).....(65). A 'minigauge' (in situ) was adopted - Figure 22. The reference electrode was the Ni/NiO equilibrium and the electrolyte was YSZ.

Now the Ni/NiO electrode is by reputation a slow electrode.[45] As a general case for solid state reactions, equilribium attainment is limited by the diffusion of particles in a concentration gradient. According to Kofstad[57] vacancies are the main diffusing species in NiO. At 1200K the chemical diffusion coefficient $\tilde{D}_{NiO} = 7.7186 \times 10^{-8}$ $cm^2\ s^{-1}$ where $\tilde{D}_{NiO} = 2D_{V_{Ni}'}$ and $3D_{V_{Ni}'}$ for singly and doubly charged vacancies respectively. Gauge response should be sufficiently fast (of the order of minutes) if the electrode microsystem[63] involves a small area of electrode surface.

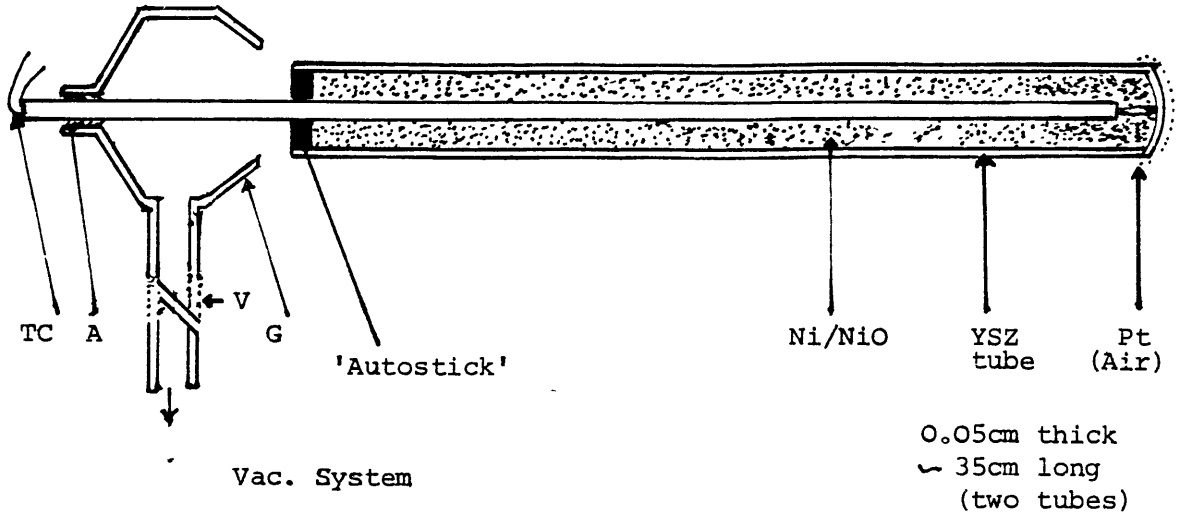

Figure 22 - Ni/NiO minigauge G = Ground Glass Cone
V = vacuum stopcock
A = Araldite seal

The response time of a gauge ideally should be as small as possible.[64] This is a subject now undergoing intensive development. The Kleitz school[60,61,63] have studied sensing time as a function of electrode configuration for air gauges and recently by Haaland[65] for 'nonequilibrium' oxygen gauges. Although the Ni/NiO gauge has not undergone such an intensive 'kinetic' study the E(T) is well known; materials are cheap and minigauge construction simple. The gauge calibration against air (p_{O_2} = 21.3kPa) is shown in Figure 23 below.

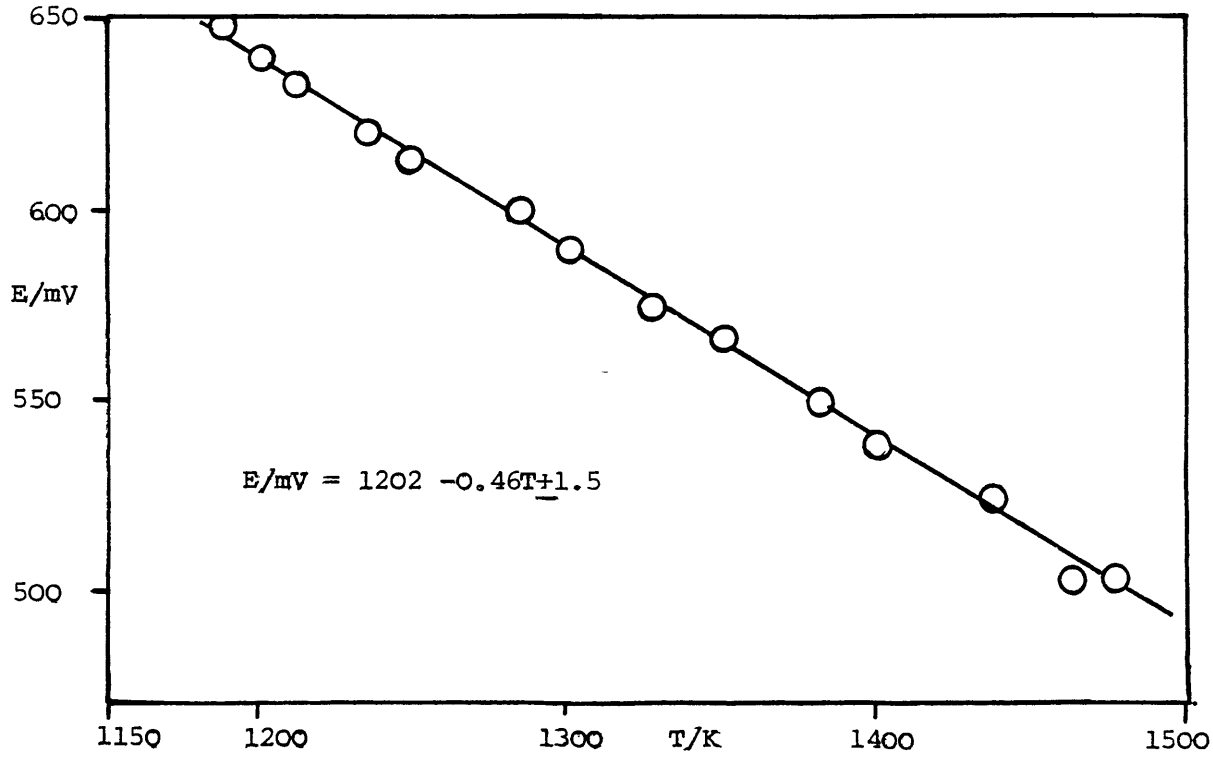

Figure 23 - Minigauge Calibration

(ii) The Pump

The pump is a secondary oxygen 'battery' - a solid electrolyte galvanic cell - which can deliver a quantity of oxygen Q according to Faraday's Law.

$$4O^{2-} \longrightarrow 2O_2 + 4e^-$$

$$n_{O_2} = \frac{Q}{4F} \qquad \text{.....(66)}$$

Q = charge = $\int i\,dt$
F = 96450C

Figure 24 shows the pump design adopted. The unusual feature is that the Ni/NiO electrode rather than air was adopted as a source/sink of Oxygen. The reason for this is primarily to 'kill two birds with one stone'. Commercially available electrolyte (YSZ) tubes are very often porous at the temperature range required; with a metal/metal oxide electrode therefore there is no need for surrounding electrolyte tubes with an outer annulus.

Equilibration in analytical pump-gauge systems is largely controlled by the hydrodynamics of the system and the response time of the gauge. Pump speed is usually low on the list of priorities.

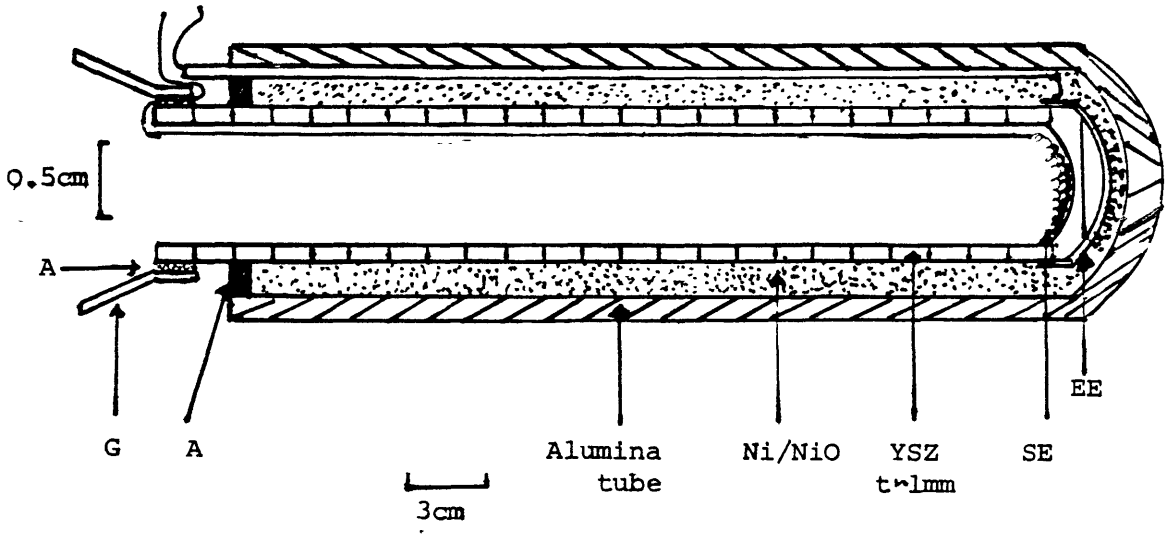

Figure 24 - The Ni/NiO pump. G = Ground glass cone A = Araldite Seal SE = Sample Electrode EE = Exterior Electrode

The Ni/NiO pump has one poor feature in that the equilibrium cell voltage at 1200K is about 69mV relative to oxygen; for electrodes of high oxygen potentials such as $LaNiO_3$ and the other La-Ni-O compounds (Chapter 3) the over potential at which electrolysis of the YSZ electrolyte occurs (Ni/NiO + ve) might be low. Against air (P_{O_2} = 21.3kPa) at 1200K electrolysis set in at E ∿ 0.8V(Ni/NiO + ve) and E ∿1.2V (Ni/NiO - ve)[58]. Electrolysis results in $t_{O^{2-}} \neq 1$ because of the high electronic conductivity of the species so formed.

(iii) The 'Pump and Gauge'

The minigauge fits into the pump as is shown in Figure 25 leaving only a small gap for the sample to be studied. The apparatus has a very small internal volume, it is robust primarily because of the Ni/NiO annulus and it is portable. Because the La-Ni-O compounds are very soluble in dilute acid, the apparatus can be cleaned and reused several times. There is nevertheless one unsatisfactory feature of the design in the use of a common between the pump anode (sample electrode) and the gauge. This can result in polarisation of the gauge voltage during pumping cycles.

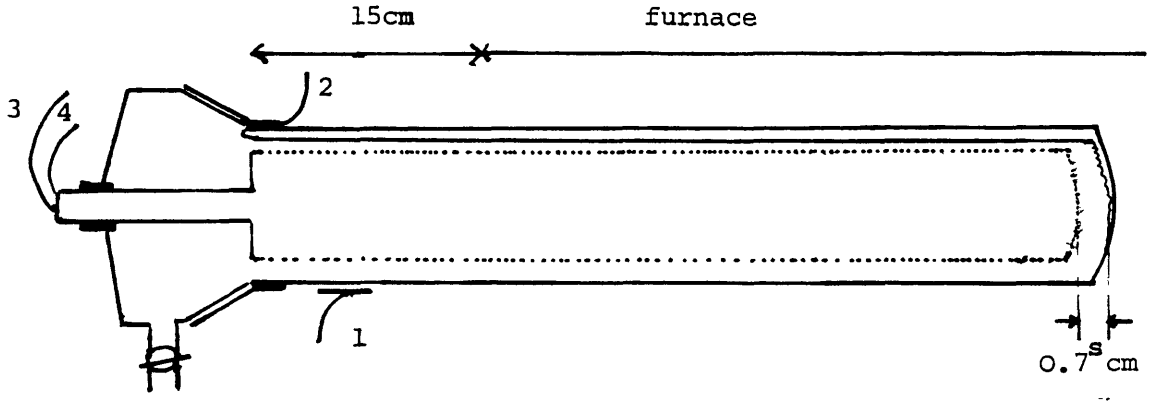

Figure 25 - The 'Pump and Gauge'
s = space reserved for sample -
3 and 4 are thermocouple leads
2 is the common connection between pump and gauge.

Equations (65)and(66) tell us that pump and gauge modulation depends on the choice of experimental variables and in consequence on the types of experiments required. We have the following variables at our disposal :-

(a) Temperature - by and large independent of the net electrochemical reaction.

(b) $E_g = f(p_{O_2})$ - since $E_g = A - \gamma T$ (i.e. gauge temperature varies with sample temperature), for studies involving constant p_{O_2} (i.e. a T-Q profile) modulation of E is essential. For the corresponding P-Q (T=const.) profile modulation is elegant but not essential.

(c) $i_p = f(Q) = f(n_{O_2})$ - modulation is not necessary if we modulate E_g but for reasons outlined above concerning the electrolysis of the electrolyte it is desirable to have a voltage limit or simply to use a constant voltage especially if E_g is modulated by simple proportional control.

We adopt two modes of operation : (1) E = f(Q),T = const.
(2) T = f(Q) (and so E = f(T))

Mode 1 We adopt the configuration shown in Figure 26.

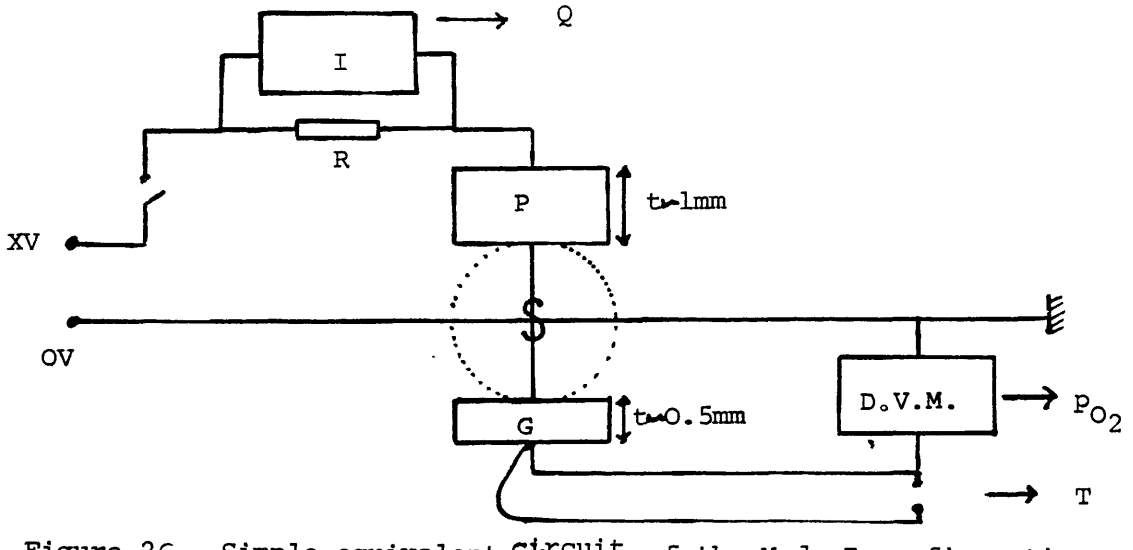

Figure 26 - Simple equivalent circuit of the Mode I configuration.
I = Time;Electronic T.S.100n Digital Integration
DVM =(Data Precision 2005 type 2400)
R = 1~ P = Pump; G = Gauge. Normally
300mV < X < 900mV

The arrangement amounts to a simple titration cell. Automation was not included in the circuitry because the small internal volume should facilitate rapid equilibration after pumping cycles.

The magnitude of gauge polarisation will depend on the electrode kinetics of the sample S (Figure 26). This should have little effect on the final steady state value of the e.m.f.

Measurements on the $LaNiO_3$ samples (Sections 4.3 and 4.4.) revealed that the gauge voltage polarisation depended on the stoichiometry of the sample. This was largest for samples containing a higher concentration of Ni^{2+} - i.e. the more reduced samples.

Mode 2 For $T = f(Q)$ (p_{O_2} const. so that $E = f(T)$) we adopt the configuration shown in Figure 27. Accurate control of both T and p_{O_2} is necessary. The former is afforded by a commercially available (Eurotherm type 015) P.I.D. temperature controller and the latter by a simpler proportional controller.

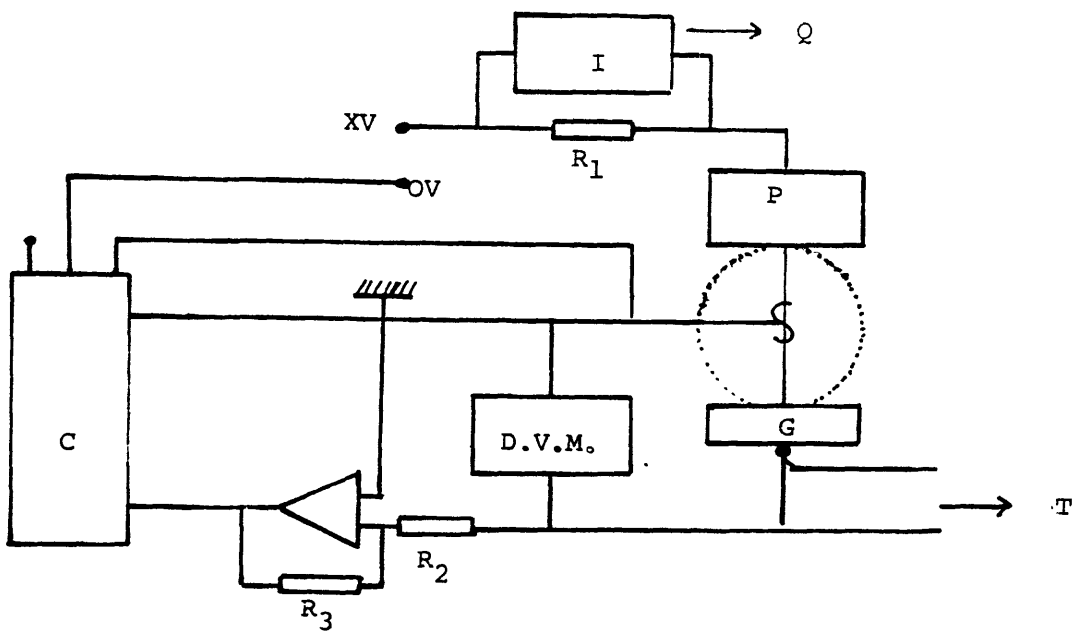

Figure 27 - Equivalent circuit - $T = f(Q)$ operation

Normally $\frac{R_2}{R_3} = \frac{1}{40}$. C = Proportional Controller

All other symbols have the same meaning as in Figure 25.

The controller has a 0-19mV input and maximum input impedance of 1kΩ the operational amplifier is merely to make E_g fall within this range. The controller is a wire wound potentiometer connected to a millivolt set pointer. The pre-set output of this potentiometer is connected in series with the gauge voltage (E_g) amplified down (as shown) by the buffer amplifier. The error difference ($E_g - E_{set}$) is amplified by a chopper amplifier which controls a relay in a manner so that the relay is energised when E_g is above set point. This is a very simple form of modulation but the mainstay of this work was not the design and evaluation of 'pump gauge' systems, but rather the application of one.

4.2.2. Calibration of the Apparatus

One important property of the system must be its internal volume (capacity). This in principle is determinable by filling the gap reserved for the sample (Figure 24) with an inert material such as platinum gauze having a shape and compactness similar as far as possible to that of a typical 'non-inert' sample to be studied. Reproducible and meaningful results can be obtained only from electrochemically 'clean' apparatus. Clean means free from carbonaceous matter which are oxygen scavengers at low oxygen potentials (i.e. the CO/CO_2 equilibrium). In this connection the separation of the araldite seal shown in Figure 24 from the end of the furnace was more than adequate for the above requirements for operations of up to 5 days.

(i) Mode 1

According to Meas[60] at time t = 0 if P_o, E_o and n_o are the initial values of oxygen pressure, cell voltage, and number of moles oxygen in the system respectively and at time t $P_o \rightarrow P_o + \Delta P$, $E_o \rightarrow E$ and $n_o \rightarrow n$ then from equation (65)

$$E = \frac{RT}{4F} \text{ Ln } \frac{P_o + P}{P_o} = \frac{RT}{4F} \frac{P}{P_o} \quad \text{(if changes are small)} \quad \ldots\ldots\ldots\ldots\ldots\ldots\ldots\ldots\ldots\ldots (67)$$

and since $PV = nRT$ ..... (68)

$$\Delta PV = \Delta nRT \quad \ldots\ldots\ldots\ldots\ldots\ldots\ldots\ldots\ldots\ldots\ldots\ldots\ldots\ldots (68a)$$

and from equation (66)

$$\Delta n = \frac{\Delta Q}{4F}$$

Putting equations (66a) and (68a) into equation (67) gives :

$$\frac{\Delta E}{\Delta Q} = \left[\frac{RT}{4F}\right]^2 \frac{1}{P_o V_{eq}} \quad \ldots\ldots\ldots\ldots\ldots\ldots\ldots\ldots\ldots\ldots\ldots\ldots (69)$$

Figure 28 shows a typical response time of the system at 1211K when S is a clean piece of Pt gauze.

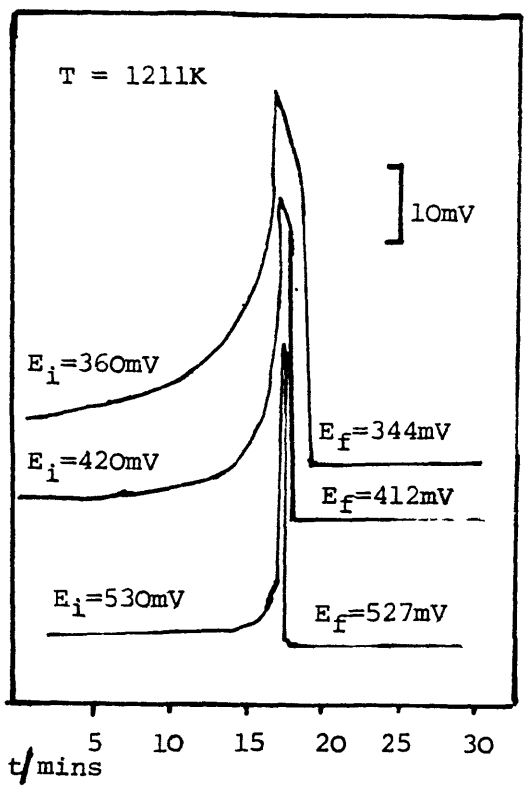

Figure 28 - (Pumping in) Gauge Response. Voltage Peaks correspond to polarisation during pumping cycles some is however due to a genuine concentration gradient. At E = 360mV and below we observe a gradual voltage rise due to buffering effect of carbonaceous species.

The response time is moderate considering the small volume of the system. The shape may be a factor that enlarges the response time, i.e. two large volumes separated by small diffusion pathways.

A typical E(Q) plot for the system when clean is shown in Figure 29. The cleaning procedure involves evacuating the apparatus when cold to 5 X 10^{-6} Torr using a silicone oil diffusion pump. This is followed by degassing at (300-400) ^{o}C under the dynamic vacuum using a liquid nitrogen trap. From the calibration graph (Fig. 29) :-

$\frac{\Delta E}{\Delta Q} = 9.5\ VC^{-1}$

At T = 122OK E_o = 42OmV

Where p_{O_2} x/kPA = 21.3 exp $\frac{4E'_g FF}{R\ T}$

Where E'_g is the gauge calibration voltage at 122OK as is shown in Figure 22. P_o can therefore be calculated.

$P_{O_2}/P_a = 21278 \exp 4F(E'_g - E_o)/RT = 4.7929Pa$

Putting T, P_o, and $\frac{\Delta E}{\Delta Q}$ in equation (69) gives : V_{eq} = 14.9 cm3

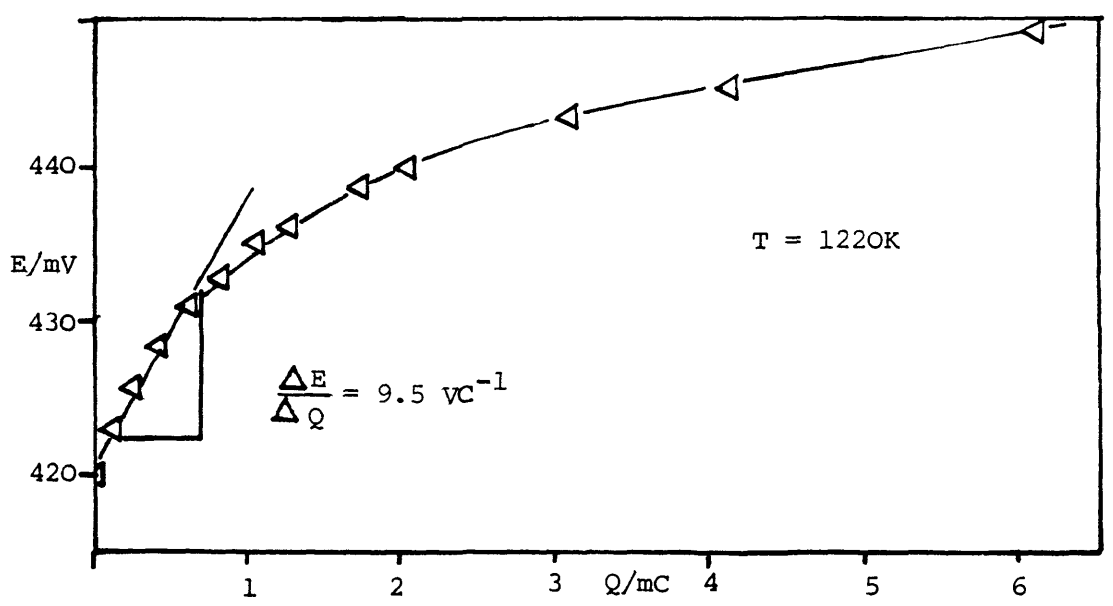

Figure 29 - E(Q) plot for the system at 122OK

According to Meas the reciprocal of equation (69) is a capacitance in Farads (CV^{-1})

$$c/CV^{-1} = \frac{\Delta Q}{\Delta E} = \left[\frac{4F}{RT}\right]^2 P_o V_{eq} \quad \ldots\ldots\ldots\ldots\ldots\ldots\ldots\ldots\ldots\ldots\ldots\ldots (70)$$

For a clean system it is possible to determine its volume from a Frequency vs Time constant study.

(ii) Mode 2

Putting equation (68) into equation (66) gives :

$$\left[\frac{4FP}{R}\right] V_{eq} = Q_o T_o \quad \ldots\ldots\ldots\ldots\ldots\ldots\ldots\ldots\ldots\ldots\ldots\ldots\ldots\ldots (71)$$

$$\frac{\Delta Q}{\Delta(1/T)} = \left[\frac{4FP}{R}\right] V_{eq} \quad \ldots\ldots\ldots\ldots\ldots\ldots\ldots\ldots\ldots\ldots\ldots\ldots\ldots\ldots (72)$$

At time t = 0, T_o and Q_o are the initial values of temperature and 'quantity' of oxygen so that $\Delta Q = Q - Q_o$ and $\Delta(1/T) = (1/T_o) - (1/T)$ after time t. Therefore from the slope of the Q(1/T) plot the equivalent volume V_{eq} can be determined. Operation is more complex than for Mode 1. The basic difficulty is the polarisation of the gauge voltage E_g during pumping cycles especially for applied pump voltages $E_p \backsim$ 700mV (Ni/NiO + ve). The 'Mode 2' operation is in effect an electrochemical microbalance. Ideally T and Q should change simultaneously but this requires much more sophisticated circuitry and controller than shown in Figure 27. For the present design it was best operationally to let Q lag behind T. Figure 29(a) shows E_g = f(time) (the voltage peaks correspond to the controller relay energised).

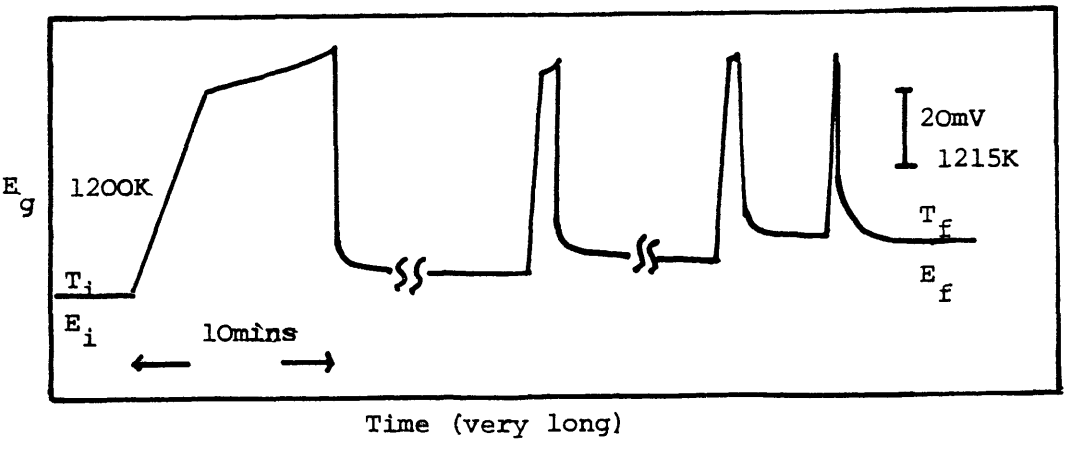

Figure 29(a) - E_g=f(t) - Mode 2 - For E_i=438mV; E_f=426mV (holding at 10Pa)

Times were very long primarily because of polarisation of E_g so that on cycles were overtly short. To overcome this the controller had to be 'helped' along by manually setting set point above the required pre-set voltage (i.e. for the maintenance of constant p_{O_2}) until about 90% of the required charge Q (estimated from previous experimental runs) was passed. This therefore corresponds to a 'semi-automatic mode of operation. Figure 30 shows a typical Q vs 1/T plot for the system cleaned as described earlier.

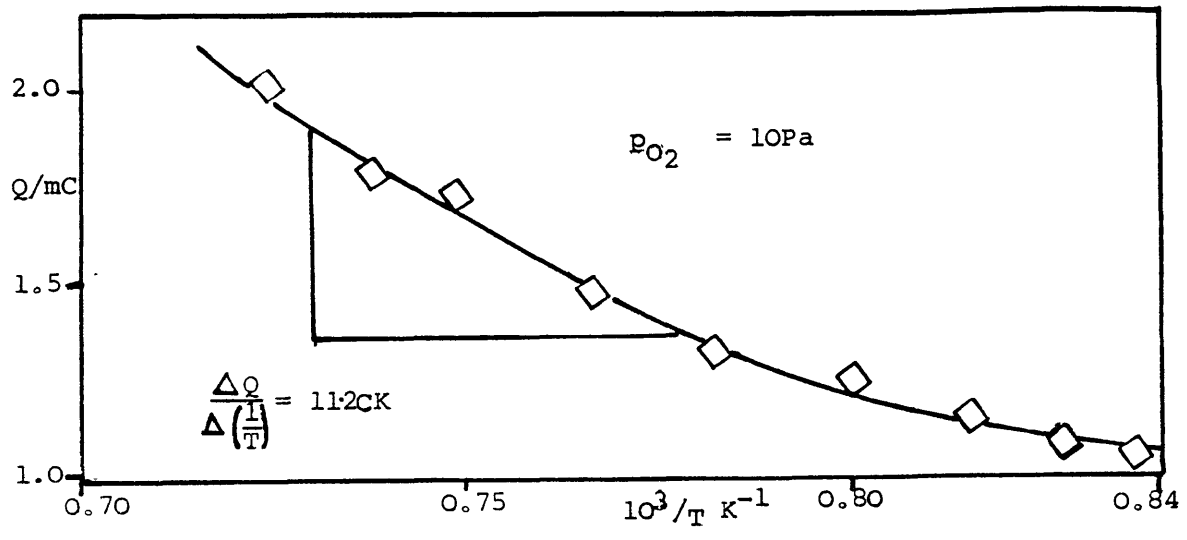

Figure 30 - $Q(^1/_T)$ plot for the system when clean

Putting $\frac{\Delta Q}{\Delta(1/T)}$ and P in equation (72) gives - $V_{eq} = 23.8cm^3$ which is in fair agreement the calibration results of the Mode 1 experiments.

4.3. The (Electrochemical) P-X Curve of Lanthanum Trioxo-nickelate III - $LaNiO_3$ -.

The P-X (E(Q)) curve of $LaNiO_3$ can be considered as N-1 P-X curves of the phases $La_{N+1}Ni_NO_{3N+1}$ and therefore ideas for the analysis follows directly from Section 1 of this Chapter. For 1 mole of 'pure' $LaNiO_3$ as starting material we obtain discontinuities at $\frac{1}{2(N+1)}$ moles of O_2 - equation (61) in the E(Q) plot. Putting equation (61) into equation (66) gives - $Q_N = \frac{2F}{(N+1)}$ .....(73) and correspondingly the separation along Q for coexisting phases

$[N]$ and $[N+1]$ are given by putting equation (66) into equation (63)

i.e. $$\Delta O_2 = \frac{2F}{(N_i+1)(N_f+1)} \quad \ldots\ldots\ldots\ldots\ldots\ldots\ldots\ldots\ldots\ldots\ldots\ldots (74)$$

Identical analysis for 'impure' $LaNiO_3$ as starting material

(i.e. $\frac{1}{N+1}$ mol of $La_{N+1}Ni_NO_{3N+1}$) gives :-

$$Q_N = \left[\frac{N-1}{N+1}\right] \frac{2F}{(n+1)} \quad \ldots\ldots\ldots\ldots\ldots\ldots\ldots\ldots\ldots\ldots\ldots\ldots (75)$$

and putting equation (66) into equation (64c) gives :-

$$\Delta O_2 = \left[\frac{N-1}{N+1}\right] \frac{2F}{(n_{i+1})(n_f+1)} \quad \ldots\ldots\ldots\ldots\ldots\ldots\ldots\ldots\ldots\ldots (76)$$

As before 3 and 2 phase regions are distinguishable by the slope of the E(Q) curve being 0 and ∞ respectively as the variance oscillates between 0 and 1 respectively. Figure 31 shows the E(Q) curve of flux prepared $LaNiO_3$ at 1214K. We note firstly that the slopes and shapes are different from the calibration curve suggesting that an active sample is being investigated. Equilibrium was rapidly established at high p_{O_2} ($611mV \leqslant E \leqslant 530mV$ - $6.130kPa \leqslant p_{O_2} \leqslant 0.277kPa$ - typically $t \backsim (30 - 60)$ mins. but became progressively sluggish with decreasing p_{O_2} (e.g. $t \backsim 5$ hours at $E = 490mV$ - $p_{O_2} = 0.075kPa$). The latter part of the profile was not studied primarily because of lack of time. We also note that β the 'compositional hysteresis' is large. This means that the E(Q) slopes of 2 and 3 phase regions are $< \infty$ and > 0 respectively. This is indicative of either -

(i) Equilibrium not being fully established after titrating cycles, or

(ii) Metastable phases being formed as a result of phase broadening at the temperature of the experiment. Chapter 5 discusses this phenomenon.

The triple points in Figure 31 could not be explained on the basis of equation (73) (i.e. $LaNiO_3$ as starting material). The starting stoichiometry is calculable from equation (75) provided a particular transition (decomposition) is correctly assigned. Table 15 summarises

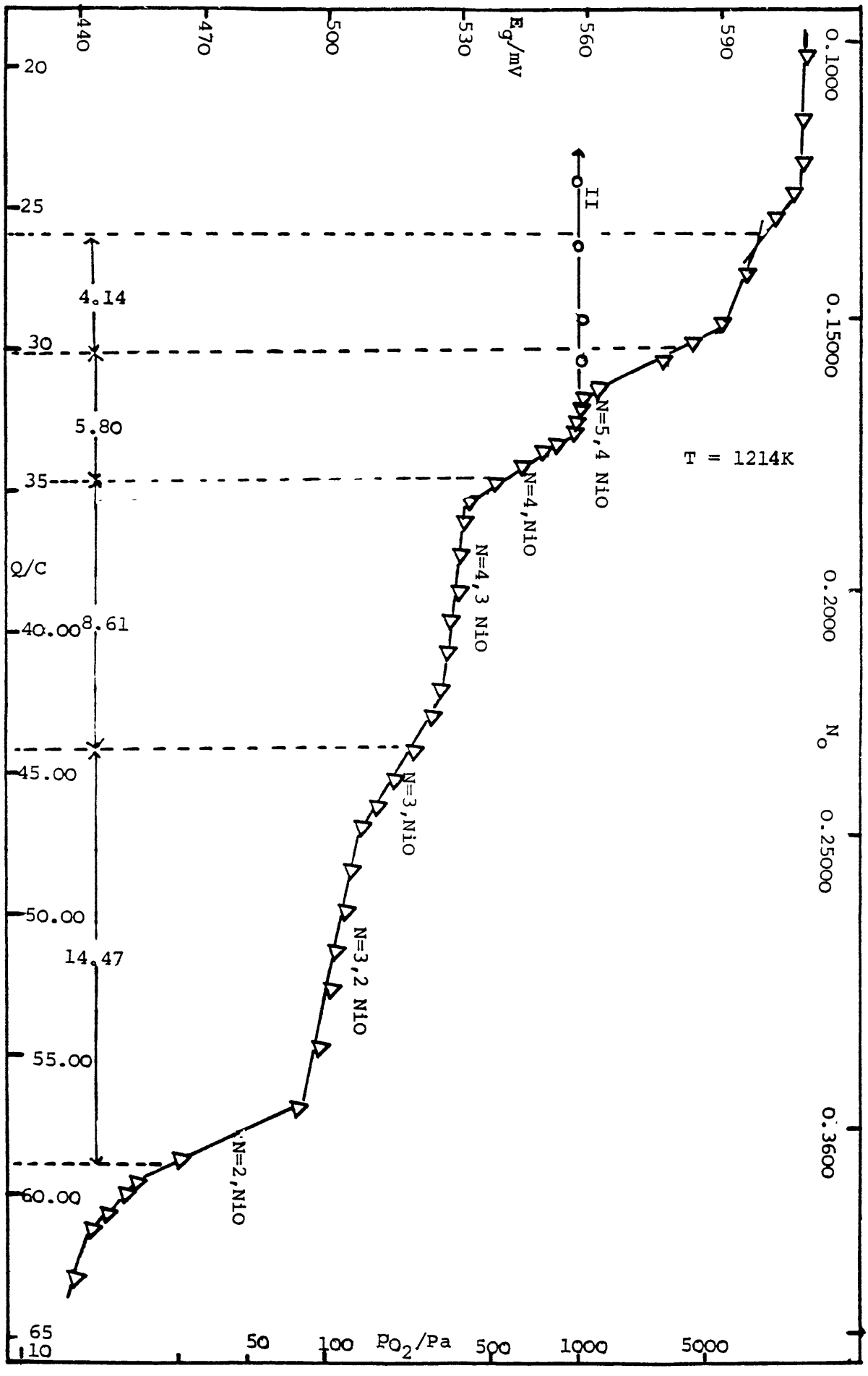

Figure 31 - The Electrochemical G(X) Curve of $LaNiO_3$

N calculated according to equation (75).

TABLE 15 N calculated from triple points (Q_n) in the E(Q) curve (Fig. 31) using equation (75)

n*	$^{**}10^{-3}Q_n$/C	N
2	58.569	22
3	44.150	22
4	38.541	25
5	29.735	25

* n of $La_{n+1}Ni_nO_{3n+1}$

** Q_n taken at a point near the mid-point of the 2-phase regions

Taking N = 23 from equation (60) :-

f = $LaNiO_{2.9583}$ is the stoichiometry of the starting material.

Table 16 below compares calculated and observed values of Q_n and O_2 on the basis of equations (73) and (74) ($LaNiO_3$ (N = ∞) as starting material) and on the basis of equations (75) and (76) (i.e. $LaNiO_{2.9166}$ (N = 23) as starting material).

TABLE 16 Transformation in the E(Q) curve (Fig.31) of "$LaNiO_3$"

n	$^*n_f-n_i$	N=∞ Q_n/kC	N=23 Q_n/kC	Obs Q_n/kC	N=∞ Δ/kC	N=23 Δ/kC	Obs Δ/kC
1		96.45	88.73	-			
	1←2				32.150	28.578	-
2		64.30	59.15	58.56			
	2←3				16.075	14.789	14.47
3		48.22	44.36	44.15			
	3←4				9.645	8.874	8.609
4		38.58	35.49	35.54			
	4←5				6.431	5.915	5.806
5		32.14	29.57	29.73			
	5←6				4.592	4.226	4.145
6		27.57	25.35	26.76			
	6←7						

Δ is Δ_{O_2}, $^*n_f-n_i$ are decompositions shown in equation 9.

The agreement between the calculated and observed values are fair and equations (75) and (76) seems reasonable approximations.

4.3.1. Thermodynamic Properties of Unisolated Phases

In 3 phase regions the p_{O_2} is constant. For example the region bounded by N = 4 and N = 5 is represented below :-

$$\frac{1}{6}La_6Ni_5O_{16} + \frac{1}{6}NiO + \frac{1}{12}O_2$$

$$\downarrow$$

$$\frac{1}{5}La_5Ni_4O_{13} + \frac{1}{5}NiO + \frac{1}{10}O_2$$

Along the path of the coulometric titration

$$dG = dn_{N=5}\bar{G}_{N=5} + dn_{N=4}\bar{G}_{N=4} + dn_{NiO}\bar{G}_{NiO} + dn_{O_2}\bar{G}_{O_2} \quad \ldots\ldots\ldots\ldots\ldots\ldots (77)$$

Now $\frac{n_{O_2}}{n_{NiO}} = \text{const.}$

$$\left(\frac{\partial G_{O_2}}{\partial G_{N=5}}\right)_{n_{NiO}, n_{O_2}} = -\left(\frac{\partial n_{O_2}}{\partial n_{N=4}}\right)_{\bar{G}_{O_2} n_{NiO}} \quad \ldots\ldots\ldots\ldots\ldots\ldots (78)$$

Following the arguments in Lewis and Randall[55] and Darken and Gurry[83]:-

$$\log \gamma_{N=4} - \log \gamma_{N=5} = -\int_{\log \gamma'_{O_2}}^{\log \gamma''_{O_2}} \left(\frac{\partial n_{O_2}}{\partial n_{N=4}}\right)_{\bar{G}_{O_2} n_{NiO}} d\log \gamma_{O_2} \quad \ldots\ldots\ldots (79)$$

$$\log \frac{\gamma}{1-\gamma} = \log \frac{a_{N=4}}{a_{N=5}} = \Delta G_{N=4 \leftarrow N=3}$$

and $\gamma_{O_2} a_{O_2} = p_{O_2}$

$$G_{N=4 \leftarrow N=5} = -\frac{2.303RT}{N(N+1)} \int_{\log p_{O_2}(N=5)}^{\log p_{O_2}(N=4)} \left(\frac{\partial n_{O_2}}{\partial n_{N=5}}\right)_{\bar{G}_{O_2} n_{NiO}} d\log p_{O_2} \quad \ldots\ldots\ldots (80)$$

Now $\left(\frac{\partial n_{O_2}}{\partial n_{N=5}}\right)$ has to be evaluated as a function of p_{O_2} from the coulometric titration curve. The integrand approaches ∞ as $n_{N=5}$ approaches zero, but this is a two-phase region and should not affect our ESTIMATE. Figure 32b shows the plot of $\frac{X_{O_2}}{X_{N=4}}$ vs log p_{O_2}; the former being calculated on the following basis :-

(i) Allowance is made for the fact that the starting material was not $LaNiO_3$ but $La_{24}Ni_{23}O_{70}/NiO$ (i.e. N = 23).

(ii) $X_{O_2} = \frac{n_{O_2}}{600}$ where $50 \leqslant n \leqslant 60$

and $X_{N=4} = \left(1 - \frac{n_{O_2}}{600}\right) \frac{1}{6}$

From Figure 32b - $\frac{X_{O_2}}{X_{N=4}} = 11.47 - 4.73 \log p_{O_2}$ .....(81)

and so $\Delta G = \frac{2.303RT}{30} \int_{-2.08}^{-1.70} 11.47 - 4.73 \log p_{O_2} \, d\log p_{O_2}$

$= \frac{2.303RT}{30} (0.600)$

so $\Delta G_{1214K} = 465J$ and ΔG that corresponds to equation (9) is 25 times this value

i.e. $\Delta G_{N=4 \leftarrow N=5} = 11.64kJ$ .....(81a)

From equation (11) :- $\Delta G = 6\Delta G_f^{\circ} N=4 + \Delta G_f^{\circ}(NiO) - 5\Delta G_f^{\circ}(N=5)$ ....(82)

Putting $\Delta G_f^{\circ}(N=4)$ from Table 10 and the data of Steele[45] for $G_f^{\circ}(NiO)$ gives :-

$\Delta G_f^{\circ}(La_6Ni_5O_{16}) = -5101 \text{ kJmol}^{-1}$ (at 1214K) .....(83)

Similar techniques have been used by Weppner et al.[62] in the Cu-Ge-O system and in the Li-Sb and Li-Bi systems[79].

Equations (81a) and (83) were the values tabulated in Tables 10 to 12 respectively and were both used in Section 3.4.

According to equation (79) $\log \gamma_{N_i} = f(p_{O_2})$. The preceding arguments have also suggested that as $n \rightarrow \infty$ in $La_NNi_NO_{3N+1}$ then the separation $a_{N_{i+1}}$ should become progressively smaller. Accordingly log "$\Delta\gamma$" - the separation of three phase regions (which are a series of parallel slopes) - is reflected in the voltage separation. Although the activity of at least one solid phase would be required to calculate the activity of all the other phases that coexist within the series we make the following deductions from Fig.32a:-

i) $\Delta E_{N=1/N=2}$ 50mV very approximately as the final decomposition was not studied.

ii) $\Delta E_{N=2/N=3}$ 31mV $69.5 \text{ Pa} \leqslant p_{O_2} \leqslant 253.4\text{Pa}$.

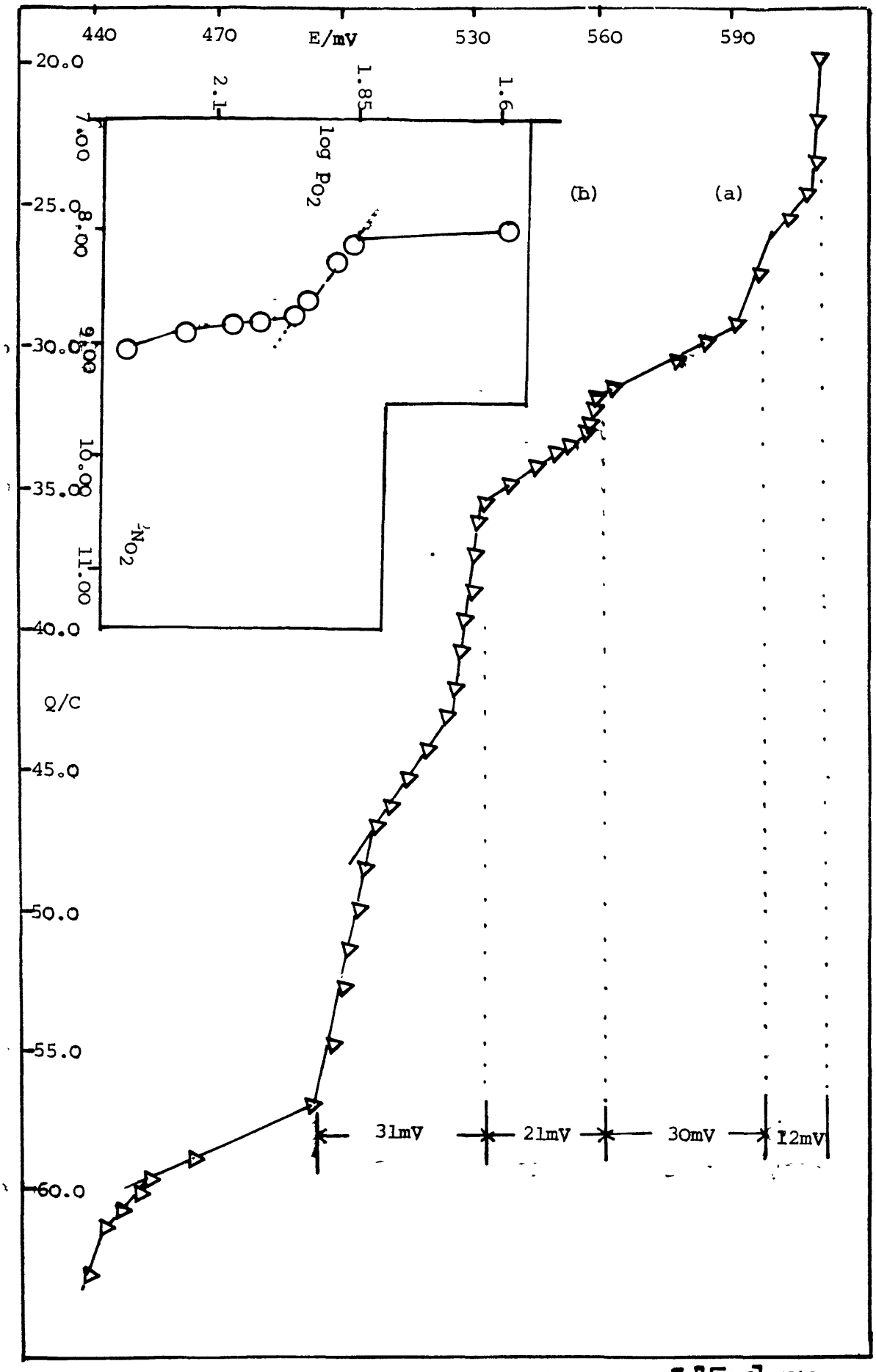

Fig. 32 - (a) Voltage Separation of Triphasic Regions [N],[N+1] NiO in the E-Q Curve of $LaNiO_3$
(b) log p_{O_2} (10Pa) vs n_{O_2} for the N=5,4(011) Region

iii) $\Delta E_{N=3/N=4}$ 21mV 253.4Pa $\leqslant p_{O_2} \leqslant$ 524Pa

iv) $\Delta E_{N=4/N=5}$ 30mV 524 .Pa $\leqslant p_{O_2} \leqslant$ 3282Pa

v) $\Delta E_{N=5/N=6}$ 12mV 328.2Pa $\leqslant p_{O_2} \leqslant$ 6049Pa

From Figures 14 and 15 (Chapter 3) the voltage separation at 1214K for $E_{N=2/N=3}$ and $E_{N=3/N=4}$ from galvanic cell studies are in good agreement with ii) and iii) respectively. This indicates that the minigauge is accurate. The argument does not appear to hold for the final two three phase equilibration. This is primarily because titration steps were large (~5C) and therefore a more detailed study of these regions is necessary. Obayashi et al.[4] reported that the T-X (T.G.A.) curve was reversible below 1140°C ("where $LaNiO_3$ decomposes"). This suggests similar thermodynamic properties for the intermediate phases. Figure 31 (II) however shows the absence of reversible behaviour in the P-X curve at the three phase region bounded by N=3, 4(011). Presumably reversibility is concentration dependent and is attainable at higher p_{O_2}.

Nakamura et al.[33a] have studied the P-X profile of $LaNiO_3$ by gas equilbration. They reported that :

i) at 1273K $LaNiO_3$ decomposed into La_2NiO_4 and NiO via an intermediate X phase at $101.325kPa \leqslant p_{O_2} \leqslant 1.01325Pa$.

ii) the decomposition :- $NiO \longrightarrow Ni + \frac{1}{2}O_2$ at $p_{O_2} = 0.68\mu Pa$ ($10^{-11.7}$ atmos)

iii) the decomposition :- $La_2NiO_4 \longrightarrow La_2O_3 + Ni$ at $p_{O_2} = 32nPa$ ($10^{-12.5}$ atmos).

For the first observation we know that the 'X phase' is a family of closely related phases which the thermogravimetric balance presumably could not resolve. They assumed also that at 25.45kPa ($10^{-0.6}$atmos) that the following is true :

$$2\ LaNiO_3 \longrightarrow La_2NiO_4 + NiO + \tfrac{1}{2}O_2$$

$$\Delta G = RT\ln p_{O_2} = 3.64\ kJmol^{-1}$$

which we know is not true.

Using the same relationship between free energy and decomposition pressure they calculated ΔG for the transformations in (ii) and (iii) above. We also know that ΔG at a triple point in the G-X curve is zero - Weppner et al.[79] The author is not sure of the basis of any calculations as those, which are not based on the Gibbs-Duhem relationships.

4.4. The (Electrochemical) T-X Curve of Lanthanum Trioxonickelate III ($LaNiO_3$)

The 'Mode 2' operation of the apparatus (i.e. as a microbalance) necessitates the use of an isobar. In other words γ from $E = A - \gamma T$ was not included in the circuitry (Figure 27). Isobar for 101.325Pa (10^{-3}atmos) is shown in Figure 33 below.

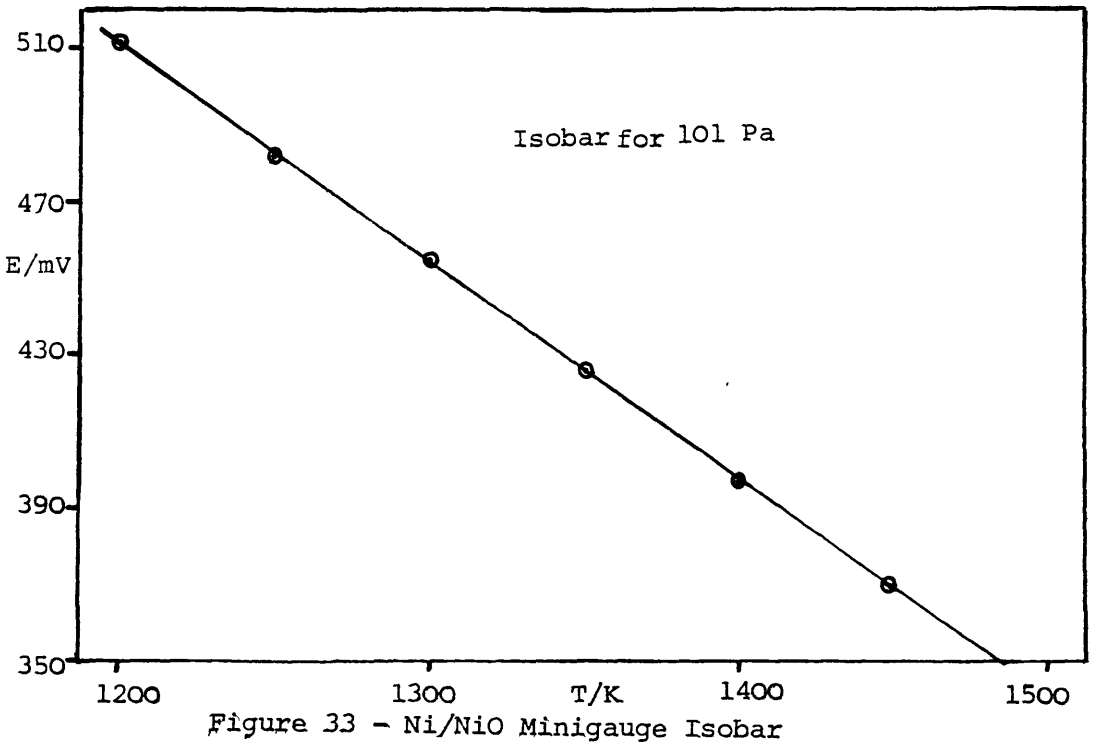

Figure 33 - Ni/NiO Minigauge Isobar

Ideally an offset voltage would have been preferred at the amplification stage to increase the sensivity of the controller, but this would probably would have left the system floating.

Figure 34 shows the T-X curve of $LaNiO_3$ at 1.0132kPa (10^{-3}atmos). The profile was studied as before only to $La_3Ni_2O_7$ because of the extremely long equilibrium times. The resolution is fair when the effect of phase broadening is considered.

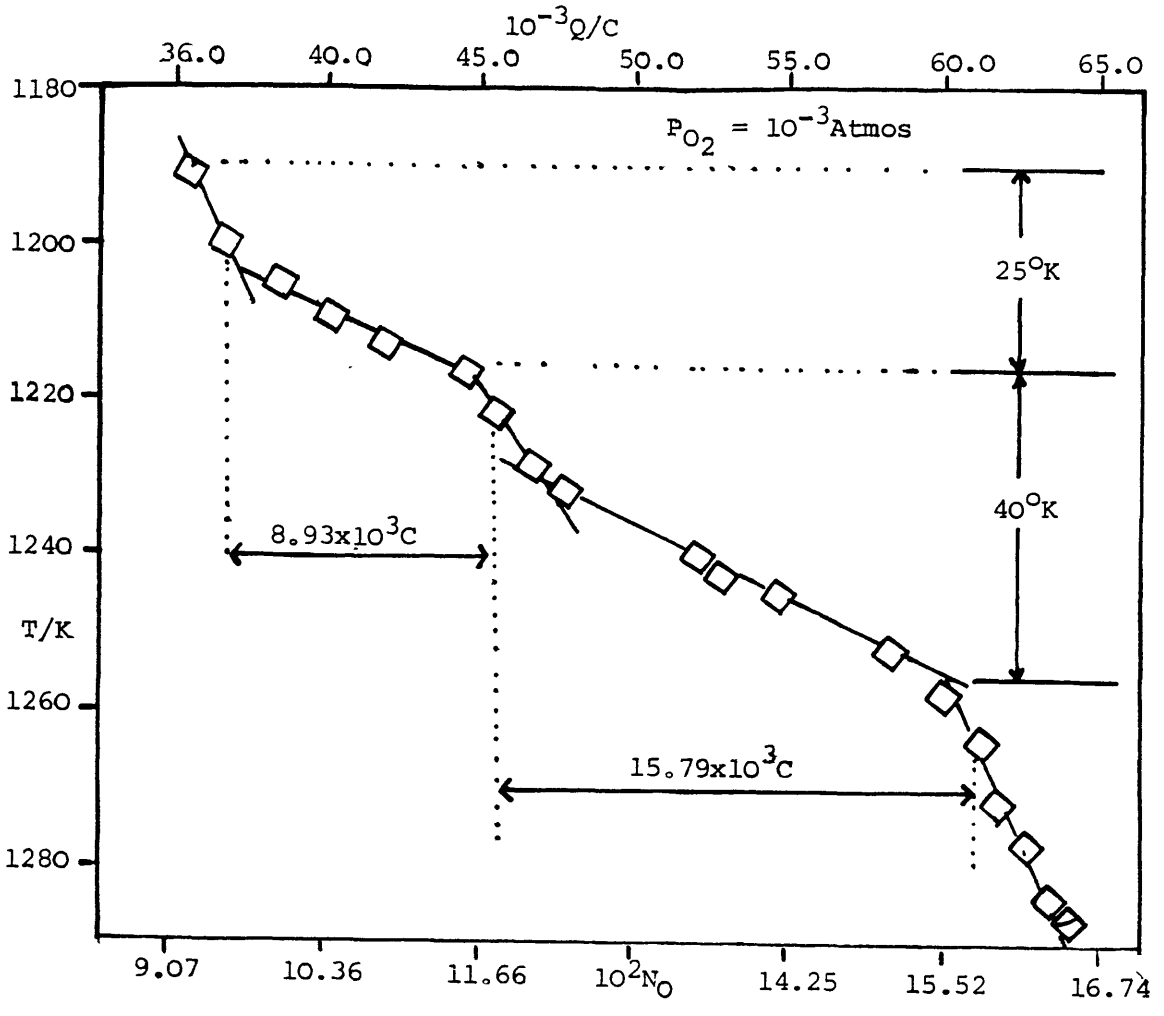

Figure 34 - Electrochemical T.G. Curve of $LaNiO_3$ at 10^{-3}Atmos

As in the previous case the separations and triple points (n_{O_2}) could not be explained on the basis of equations (73) and (74) (i.e. $LaNiO_3$ as starting material) so the starting stoichiometry is calculable from equations (75) and (76).

TABLE 17 Q_n for $La_{n+1}Ni_nO_{3n+1}$ compounds in the T-X curve of $La_{N+1}Ni_NO_{3N+1}$ (Figure 34)

n	Q_n/kC	N*
2	61.00	32
3	45.40	30
4	35.10	-

* N calculated from equation (75)

Taking N = 31 and putting this into equation (60a) gives :-

f = $LaNiO_{2.9687}$ for the sample of flux prepared '$LaNiO_3$' used.

Table 18 compares calculated and observed (Equation (75) and (76)) for Q_n in Figure 34.

TABLE 18 Transformations in the T-Q curve (Fig. 34) of '$LaNiO_3$'

N	Transition n_f n_i	calc. (N=31) Q_n/kC	obs Q_n/kC	calc. (N=31) Δ/kC	obs Δ/kC
1		90.604	-		
	1 ⟵ 2			30.201	-
2		60.403	61.00		
	2 ⟵ 3			15.103	15.000
3		45.402	45.40		
	3 ⟵ 4			9.061	8.940
4		36.241	-		

Allowing for the quantity of each phase since $\overline{G}$ is an extensive property, $\overline{G}$ at triple points should be the same in both T-X and P-X profiles.

ie. $\overline{G}_{P-X} \backsim \overline{G}_{T-X}$

or $\frac{RT_1}{Z_1} \log p_{O_2} \backsim \frac{RT_2}{Z_2} \log p_{O_2}$

where Z = $\frac{N-1}{N+1}$: Z_1 = 0.9399 (T-X) and Z_2 = 0.9166 (P-X)

Table 19 below summarises $\overline{G}$ from the two techniques.

TABLE 19 Transitions in P-X and T-X profiles of '$LaNiO_3$' (a comparison)

Transition N_f N_i	T-X (p_{O_2} = 10^{-3}atmos) T/K	$\overline{G}$/kJ	P-X (T = 1214K) p_{O_2}/atmos	$\overline{G}$/kJ
2 ⟵ 3	1260	80.403	7.422×10^{-4}	79.318
3 ⟵ 4	1217	69.899	2.272×10^{-3}	65.035

It must be emphasised that these are values relative to starting material 'pure $LaNiO_3$'. Fuller analysis on the basis of equation (80) is needed to calculate approximate enthalpies of transformation on the T-X curve.

Although resolution of the T.G.A. profile was advanced a step further it was originally hoped to resolve the pattern more completely. The experimental programme had to be curtailed because of the very long equilibration times.

4.5. Experimental

(1) Thermogravimetric Studies :

These were performed on a Stanton 707 Electromicrobalance fitted with a platinum furnace and running at maximum sensivity. The thermocouple was ~ 1mm vertical to the sample. Measurements shown in Figure 19 were in static air, typically (5-10)mg samples of oxide were used. These samples were from re-oxidised (240 atmos O_2) $LaNiO_3$ prepared as described in Chapter 2.

For the higher temperature range $1000\ C < T < 1450^{o}C$ the T.G.A. profile was scanned rapidly ($(5\text{-}6)^{o}min$) up to about $970^{o}C$ then held at this temperature for about an hour. The remainder of the profile was scanned at $1^{o}min^{-1}$ ((or $3^{o}min$) as is shown in Figure 19 The low temperature range $50^{o}C < T < 1000^{o}C$ was scanned normally at $2^{o}min^{-1}$. Typically a profile under a given atmosphere (say air) took up to 2 days to obtain in its entirety.

The author believes more work is needed at even slower thermal scan - say $0.5^{o}min^{-1}$ to elucidate the T.G.A. profile of $LaNiO_3$ more completely.

(2) The Oxide ion 'pump and gauge' :

Electrolyte tubes were manufactured by Zircoa Corporation. They were quoted as having a 1% Fe^{2+} impurity - this imparted a yellow colour to the tube. The pump tube was about 0.1cm in thickness and the gauge tube approximately 0.05cm. Platinum paste electrodes were made using Englehard (type 6082) paste firing as recommended by the manufacturers. Better adherence on the gauge

tube was obtained when the paste was applied into a pre-sputtered film of platinum (t~1μm).

The Ni/NiO electrode used in both the pump and the gauge was from a mixture of Ni (Johnson Matthey - specpure -) and NiO (Koch Light 99.9%) in a 10:6 ratio. The reason for this ratio is to overcome any moisture that may be present in NiO and indeed any Ni^{III} oxides.

The Ni/NiO mixture was packed firmly into the gauge tube (in the gauge application) around the thermocouple. The holes within the thermocouple sheath (Figure 22) were sealed off at the hot end with the Ni/NiO mixture and with araldite at the cold end. The gauge was sealed from air using 'autostick' sealing agent.

No carbonaceous matter from this material or indeed the araldite seal were observed to affect the results for 'clean' systems. For example when erroneous results were obtained they were due to carbon from solvents such as acetone e.g. from rotary pump oil.

(2.1.) Setting Up Procedure

After an experiment was over, the cell was washed with dilute HNO_3 and then distilled water and blow-dried using a hot air blower. Carbonaceous solvents such as ether, acetone etc. were avoided as they tend to 'dirty' the system.

For all measurements the system was evacuated down to about 5×10^{-6} Torr using a silicone oil diffusion pump having a liquid nitrogen cold trap.

The cell had an internal volume of about 13cm (determined via the 'water' experiment - See 3.5) and typically 1.3-1.5g of samples of $LaNiO_3$ were used. These were very large samples and in consequence equilibrium times were longer than they would otherwise have been.

Equilibrium times were of the order of 30 minutes at ~600mV but became progressively longer reaching about

5 hours at 490mV, and thereafter increasing as the percentage of N^{III} in the oxide(s) decreases.

The profile was studied three times (twice to the formation $La_3Ni_2O_7$) and it was hoped to resolve the higher 'p_{O_2} branch' of the profile (i.e. $611 < E < 530$ mV more completely but there was insufficient time.

(2.2.) Voltage and Current Measurements :

Voltage was measured on a Data Precision (Series 200 Model 2400) with a maximum input impedance of 10^{10} Ω. Current was integrated automatically with a Time Electronic (type TS100n) digital integrator. The input was voltage developed across a high accuracy 1Ω resistor rated at 0.75 watts. For the range of current ($0.1mA < i < 20mA$) the voltage drop was assumed to be negligible. The proportional controller used in the 'Mode 2' operation was manufactured by Control Instruments (type B P11) with a quoted control sensivity of 25-40μV.

(3) Furnace and Temperature Controller :

All measurements were made in an inductively wound platinum furnace. These were effectively noise free primarily because the output impedance of the gauge was low. Furnace temperature was controlled to $\pm 2^{\circ}$ by a P.I.D. Controller (Eurotherm type 015).

CHAPTER 5

Stoichiometry of $La_{N+1}Ni_NO_{3N+1}$ Phases

5.1. Résume on some Defect Models of A-B-O Systems

It is known that perovskite oxides show both oxidative and reductive nonstoichiometry i.e. ABO_{3+x} and ABO_{3-x} respectively. Tolfield et al.[66] have studied $LaBO_{3+x}$ systems (B = Ti - Fe) by neutron diffraction. They suggested that the 'nonstoichiometry' could be explained on the basis of defects on both A and O sites. Galy et al.[67] and Nanot et al.[68] proposed that structures $A_nB_nO_{3n+2}$ were rational in the systems $Ca_2Ni_2O_7$ $NaNbO_3$ and $La_2Ti_2O_7$ - $CaTiO_3$ (i.e. pyrochlore - perovskite). On the reductive side Jacobson and Horrox[69] studied $Ba_{1-x}Sr_xMnO_{3-x}$ by neutron diffraction proposing a model based on ordering of oxygen point defects ordering along certain crystallographic directions. Later Hutchison et al.[70] confirmed the 'preferred ordering' of cation and oxygen defects although they did not propose a model involving any 'phase formation'. In the $SrFeO_{3-x}$ system Tolfield et al.[71] isolated the compound $SrFeO_{2.75}$ ($Sr_4Fe_4O_{11}$). Grenier et al.[72], subsequently, rationalised such ABO_{3-x} systems on the basis of phases $A_nB_nO_{3n-1}$ intermediate between perovskite (ABO_3(n = ∞)) and brownmillerite ($A_2B_2O_5$ (n = 2)).

It is clear that in such ternary system description of non-stoichiometry on one sublattice and in many cases on two sublattices is an inadequate if not inappropriate formalism. In A-B-O systems removal of one component, say oxygen, leads to a rearrangement and redistribution of cations A and B. A description in terms of anion and cation arrangement and distribution is a necessary condition for full appreciation of the equilibrium situation with such compounds.

5.2 B - Phase Width or Metastable Phase?

Provided there are no phase transformations, there is a broader composition range of existence for refractory compounds at high temperatures. The G-T-X surface for a system A-B-O having a succession of

phases say $A_{N+1}B_NO_{3N+1}$ is shown in Figure 35.

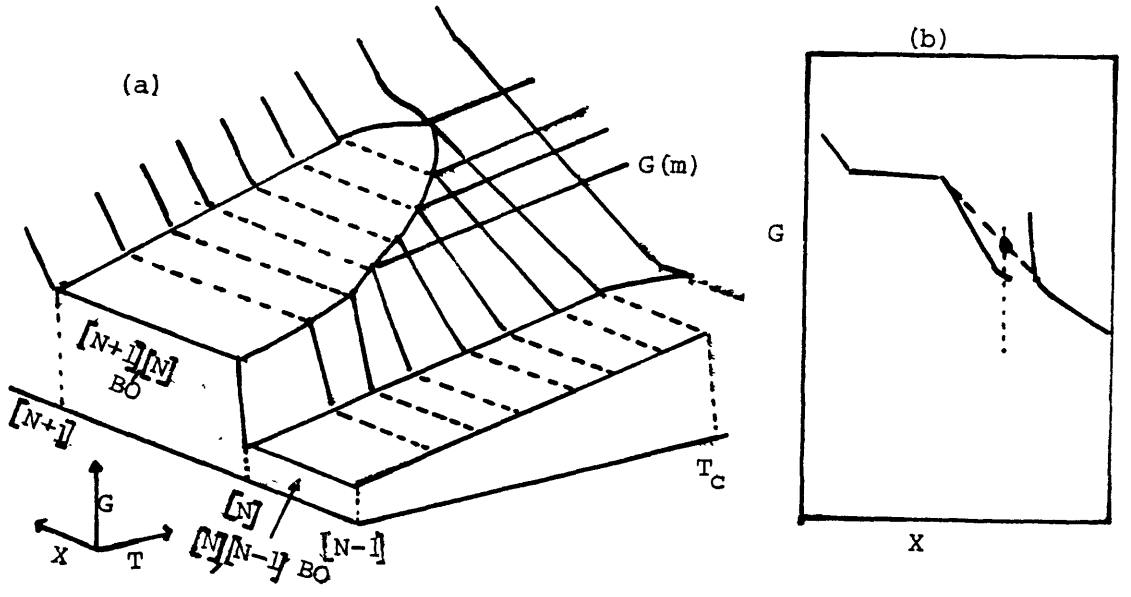

Figure 35 - (a) General G-T-X surface of a system A-B-O with a succession of phases
(b) G-X curve for two 'common tangent' phases that accept defects unequally.

The envelope within which the system is invarient (i.e. N+1, N+2 and BO coexist) closes at some critical temperature T_c above which one ternary nonstoichiometry phase, m and possibly a binary BO_z phase exists.

The G-X curve of each ternary phase will depend on the "flexibility" of its composition. For similar phases (in the thermodynamic and crystallographic sense) sharing a common tangent, a regular solution should be formed above T_c - the G-X curve should be symmetrical about its mid-point. In practice one structure accumulates defects more readily. According to Anderson[52] such a phase will have a less well defined G-X curve about the 'univarient composition' (X_o^b Fig. 35b). The mutual but unequal displacement of the two curves about X_o^b widens the co-existence ranges but under these conditions the G-X curve is asymmetrical about its mid-point.

In Figure 31 (the G-X curve of $LaNiO_3$ at1214K) we saw the broadening of diphasic regions especially the N = 3/NiO region. Between two triphasic regions the "state of affairs" is shown in Figure 36.

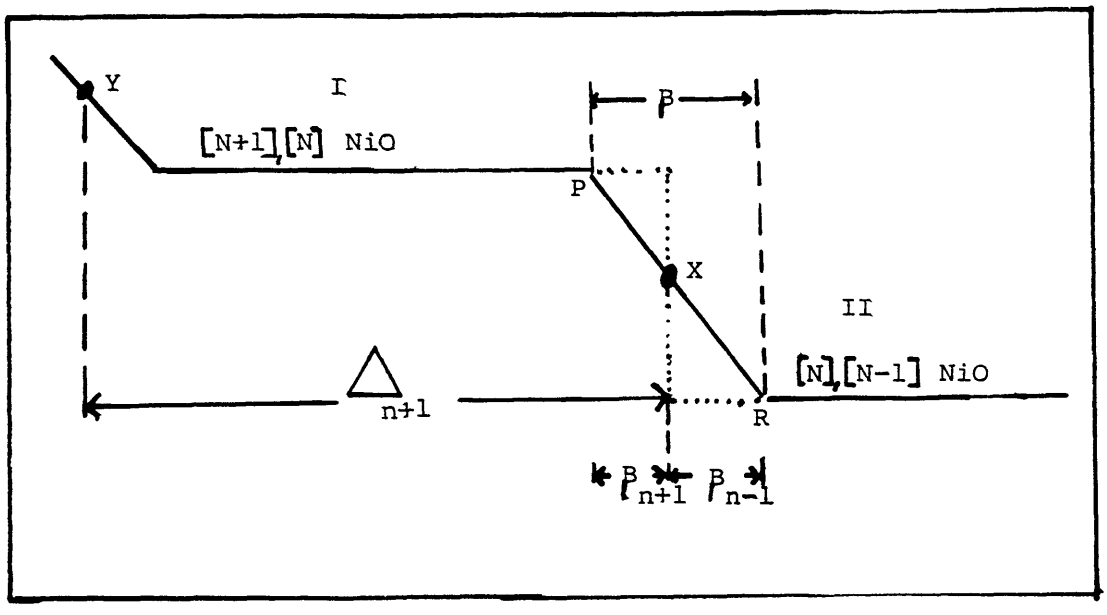

Figure 36 - Broadening of diphasic regions N /BO involving disolution of other ternary phases.

The ideal composition of phases N+1 and N are at Y and X respectively. The quantity of each phase is some function of the quantity of oxygen i.e. along the path of the decomposition of the $La_{N+1}Ni_NO_{3N+1}$ phases. Along I this amounts to :-

$$\frac{1-X_1}{N+1}\,[N+1]\ ,\quad \frac{X_1}{N}\,[N]\ ,\quad \frac{X_1}{N(N+1)}\,[NiO]\quad \text{at } \frac{X_1}{2N(N+1)} \text{ moles of } O_2$$

where $0 < X < 1$

And along II :-

$$\frac{X_2}{2}\,[N]\ ,\quad \frac{1-X_2}{N-1}\,[N-1] \text{ and } \frac{1-X_2}{(N-1)N}\,[NiO] \text{ at } \frac{X_2}{2(N-1)N}\,O_2$$

To a first approximation the quantity of each phase [N+1] (at P) and [N-1] (at R) that mixes intimately with [N] in the pseudo-univarient region is given by :-

$$\frac{\beta_{n+1}}{\Delta_{n+1}}\,[N+1] \times \frac{1}{N+1} \quad \text{and} \quad \frac{\beta_{n-1}}{\Delta_{n-1}}\,[N-1] \times \frac{1}{N-1}$$

This treatment avoid the necessity of using absolute quantities of oxygen, therefore data from T.G.A. studies as well as data from coulometric studies can be treated. Treatment of data taken from Figure 31 is shown in Table 20. Also tabulated is Δ_i (obtained from equation (74)).

TABLE 20 Phase Width of $La_{N+1}Ni_BO_{3N+1}$ Phases at 1214K

Region	β/kC	β_{N+1}/kC	β_{N-1}/kC	Δ_{N+1}/kC	Δ_{N-1}/kC
N=2,NiO	3	1	2	14.78	29.23
N=3,NiO	5	2	3	8.874	14.78
N=4,NiO	2.3	1	1.3	5.916	8.874

The actual composition of the 'univarient' can be described as a ratio $Q'_{N+1}:Q_N:Q'_{N-1}$ where Q_i is calculable from equation (73) and $Q'_i = \frac{B_i}{\Delta_i} Q_i$. An approximate free energy of formation of these compositions can be calculated from the relationship :-

$$G_f^\circ(\text{soln}) \leq X_{N+1}\Delta G_f^\circ(N+1) + (1-X_{N+1}-X_{N-1})\Delta G_f^\circ(N) + X_{N-1}\Delta G_f^\circ(N-1)$$

where X_i is the mole fraction of phase i and is related to Q'_i. Table 21 summarises the calculated composition and free energy of formation of the regions listed in Table 20. Data for the thermodynamic calculations are taken from Table 11.

TABLE 21 Composition and Free Energy of Formation of $La_{N+1}Ni_NO_{3N+1}$ Phases at 1214K

Ideal Composition	Composition of 'univarient'	ΔG_f°/kJmol^{-1}
N = 2	$0.088La_4Ni_3O_{10}:0.867La_3Ni_2O_7:0.044La_2NiO_4$	-2534, -2499*
N = 3	$0.155La_5Ni_4O_{13}:0.689La_4Ni_3O_{10}:0.246La_3Ni_2O_7$	-3586, -3361*
N = 4	$0.109La_6Ni_5O_{16}:0.776La_5Ni_4O_{13}:0.113La_4Ni_3O_{10}$	-4220, -4232*

* ΔG_f° calculated for the ideal $La_{N+1}Ni_NO_{3N+1}$ phases (Table 11).

The foregoing analysis assumes zero or small enthalpy of mixing. The actual enthalpies of transformation have been tabulated in Table 9. The enthalpy of solution ΔH_{sol} can be calculated from the relation :-

$$\Delta H_{sol} = X_{N+1}\Delta H_{N+1} + X_{N-1}\Delta H_{N-1}$$

where ΔH_i is the transformation enthalpy listed in Table 9.

This analysis also omits the effect of the binary phase NiO. Whether it enters the common pool must ultimately be a matter of structural compatibility and free energy. This will be reviewed later.

If such an intimate mixture, as just described, is possible then β (Section 4.1) represents a metastable phase and the 'phase width' description is inadequate.

5.3. Conditions for Metastable (Solid Solution) Phase Formation

According to Anderson[52,73] the necessary conditions for such an intimate mixing of phases are :-

(i) The thermodynamic criterion. This is such that there is a net gain in free energy when any single phase enters the 'solution' phase $[G(sol) \leqslant G(single\ phase))$. This condition appears to be satisfied for the compounds listed in Table 21. A fuller analysis of the prevailing equilibrium processes involve principles developed for Subdivision or Operational Equilibrium[52] which is outside the scope of this text. However the following may serve as a useful, if not over-simplistic example:-

At lower temperatures (below T_c - Fig. 35) the equilibrium process shown in (a) is operative.

$$(a)\ (N+1)La_{N+2}Ni_{N+1}O_{3N+4} \rightarrow (N+2)La_{N+1}Ni_{N}O_{3N+1} + NiO + \tfrac{1}{2}O_2$$

The system is invarient, the equilibrium composition of each phase is given by :-

$$\frac{(1-X)}{(N+2)}[N+1] \ ,\ \frac{X}{(N+1)}[N] \ ,\ \frac{X}{(N+2)(N+1)}[NiO] \ \text{at} \ \frac{X}{2(N+2)(N+1)}O_2$$

and $\mu_{O_2} \neq f(X)$ but $\mu_{O_2} = f(T)$ in accordance with (a).

At higher temperature, above T_c, coexistence ranges become broadened and (b) is operative.

$$(b)\ (N+1)La_{N+2}Ni_{N+1}O_{3N+4} \rightarrow (N+2)La_{N+1}Ni_{N+1}O_{3N+1} + NiO + \tfrac{1}{2}O_2$$

$$\downarrow$$

$$NLa_{N}Ni_{N-1}O_{3N-2} + NiO + \tfrac{1}{2}O_2$$

i.e. There are two competing equilibrium processes.

The equilibrium composition of each phase is given by :-

$$1-\delta \quad \frac{(1-X)}{N+2}\,[N+1] \;,\; \frac{\upsilon X}{(N+1)}\,[N] \;,\; \frac{\upsilon X}{(N+2)(N+1)}\,[NiO] \text{ at } \frac{\delta X}{(N+2)(N+1)}\,O_2$$

$$1-\delta \quad \frac{W}{N}\,[N-1] \;,\; \frac{(1-\delta)W}{N(N+1)}\,[NiO] \text{ at } \frac{(1-\delta)W}{2N(N+1)}\,O_2$$

A nonstoichiometric phase is formed with the above quantities of phases [N+1] and [N-1] intimately mixed with, or dispersed in, phase [N] . Under these conditions $U_{O_2} = f(\delta)$ and the slope of the U(T) changes above T_c (variance changes). This phenomenon is observed in Figure 37 for triphasic mixtures N=2,3 with NiO and N=3,4 with NiO previously studied in Chapter 3 (Figure 14).

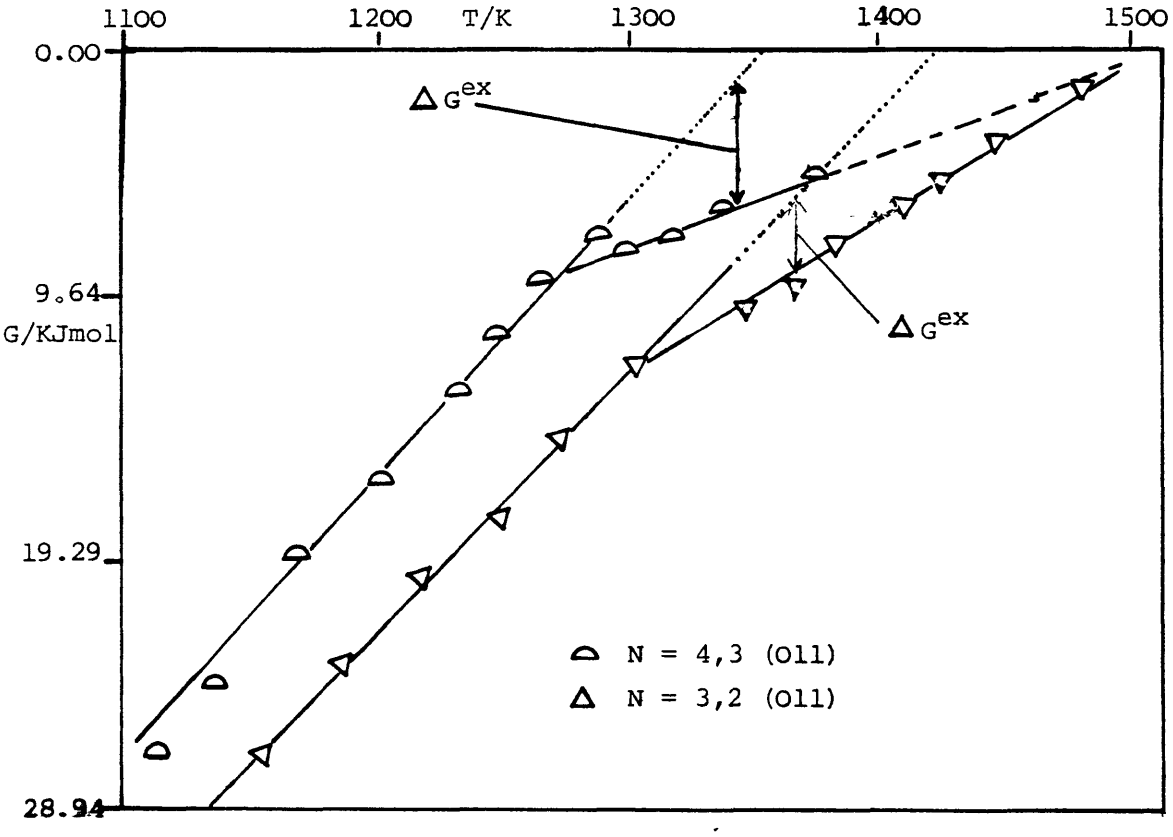

Figure 37 - G(T) plots showing Change of Variance at High Temperature for N+1 N (O11) mixtures indicating formation of a grossly defective nonstoichiometric phase.

ΔG^{ex} after Anderson[52] represents the decrease in free energy in transforming mixture into the "metastable" nonstoichiometric phase.

(ii) The structural criterion. The primary reason for terming the pseudo univarient range metastable is that it should be monophasic. Structures must be compatible for solid solution formation i.e. possesses at least one sublattice in common. It is becoming increasingly acceptable that such phases possess a high degree of local order - regions of phases [N+1] and [N=1] dispersed in phase [N].

Coherent intergrowth is possible between ABO_3 (Pm3m) and its I4mmm polytypes (Figure 8) along two interfaces. The same is true for the rhombohedrally distorted analogues $R\bar{3}m$ and Fmmm (Section 1.4) respectively. The remaining boundaries of each phase may remain coherent or involve an edge dislocation. This, as will be seen later, is important for phases with only two unit cell edges in common e.g La_2NiO_4 (N=1) and $La_3Ni_2O_7$ (N=2) having I4mmm and Fmmm symmetries respectively.

The effect of NiO d(Ni-O-Ni)= 4.177Å as a solute will depend on whether coherence is possible along the perovskite sublattice of the $La_{N+1}Ni_NO_{3N+1}$ (d(Ni-O-Ni) = 3.85Å) compounds. It is only speculation that NiO might intergrow coherently probably separating out as Guinier-Preston Zones. The 'concentration' of these zones might be low because of the appreciable lattice constant variation.

Twinning of NiO and $La_{N+1}Ni_NO_{3N+1}$ compounds might also become important. The $c \backsim (2N+1)a$ "lattice constant rule" outlined in Section 1.4. shows that (2N+1) NiO unit cells are just as compatible with the c axis of the ternary compounds.

5.4. Nonstoichiometry - The low temperature situation -

At higher temperatures the 'solid solution formation' range should be widened, under the conditions outlined in Section 5.3. At these temperatures there may also be :-

(i) Solute and solvent decomposition, for example a fraction of the solvent phase [N] decomposing into Phase [N-1].

(ii) Solubility of other phases say [N+2] and [N-2] albeit in lower concentrations. This situation arises because of the widening of the 'univarient condition'.

Any quantitative treatment meets formidable theoretical difficulties, for example how is the solubility related to anion and cation diffusion etc.

Under normal conditions where quenching can be drastic, i.e. removal from furnace, some of the solid solution can be frozen. The amount of each phase which separates out must largely be a matter of quenching speed and solubility product. The expression for the mole fraction of each phase as a function of temperature, according to Anderson[52] is :

$$X_{(\text{solute})}^{N+1} = X_{(\text{solvent})}^{N} \exp \frac{k\Delta G^{ex}}{RT}$$

where $k = f(1-X_{N+1})$. Since ΔG^{ex} is a function of temperature (Fig. 37) it is impossible to say, from these simplistic considerations, how much the fraction X_{N+1}/X_N (i.e. the ratio of solute to solvent) will decrease from, say, 1200K to 300K. But even if it is as large as 50% i.e. 50% each of phases [N+1] and [N-1] respectively, this still represents a considerable stoichiometric broadening. The case for phase N=2, $La_3Ni_2O_7$ (Table 21) is shown below:-

$$0.088La_4Ni_3O_{10}:0.867La_3Ni_2O_7:0.044La_2NiO_4 \quad 1214K$$

$$\downarrow$$

$$0.044La_4Ni_3O_{10}:0.934La_3Ni_2O_7:0.022La_2NiO_4 \quad 300K$$

corresponding to a composition $La_{3.154}Ni_{2.022}O_{7.066}$. This composition is monophasic but a typical diffraction pattern contains two sets of spots :-

(i) Strong reflections from the parent subcell, $La_3Ni_2O_7$, and is independent of composition.

(ii) Weak superlattice reflections indicating rational multiplicities i.e. the presence of other $La_{N+1}Ni_NO_{3N+1}$ cells which according to Anderson[73,87] change with composition and is indicative of a single mode of defect ordering.

The author refers to Plate 2(a-e) where such superlattice reflections were observed. They have not been analysed in detail, but it can be inferred that they indicated adaptive ordering along the perovskite subcell of either ternary La-Ni-O phases, as exemplified in Figure 38 and/or of NiO, as discussed in Section 5.3.

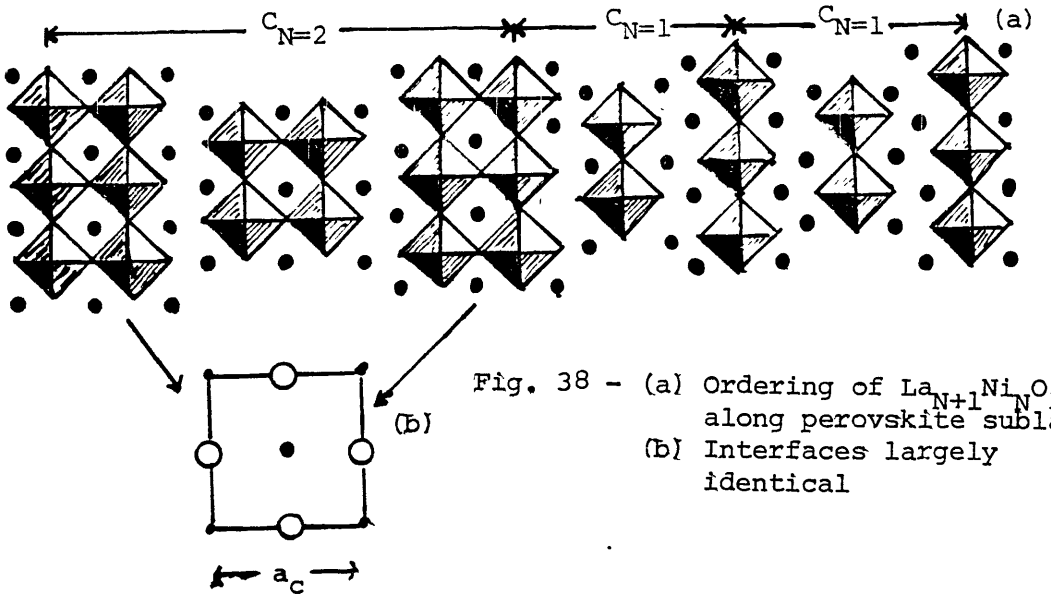

Fig. 38 - (a) Ordering of $La_{N+1}Ni_NO_{3N+1}$ along perovskite sublattice
(b) Interfaces largely identical

5.5. Electron Microscopic Study of the La-Ni-O Phases

Modern electron microscopy is such that it is now possible to study materials on the unit cell level. It is well known that a fringe image is formed by recombining, through the objective aperture, the transmitted electron beam and some or all of the diffracted beams.

There is, however, not necessarily a one to one correspondence between fringe spacing and the lattice planes which gave rise to the diffraction [75]. In an excellent review Allpress and Sanders[74] outlined the conditions under which there is a one to one correspondence.

(i) The use of very thin crystals.

(ii) The use of n, where $n > 2$, diffracted beams to form the image.

(iii) The use of an objective aperture which restricts the number of beams in (ii) according to its diameter. This arises because although in principle the more diffracted beams used to form the image the greater the image detail, in practice objective lens spherical abberation increases for beams with increasing Bragg angle.

$$\Omega = \frac{C_s \lambda^3}{2d^4}$$

C_s = Spherical abberations (typically 3-5mm)

λ = Wavelength (typically 0.037Å)

Ω = Retardation

Lattice spacings, $d \sim 50$Å will suffer a phase retardation of π or more, which will modify the contrast in the image and hinder or prevent successful interpretation.

(iv) Because of the objective aperture, amplitude contrast from excluded beams will appear in the image. Experience has shown that this effect is minimised at slightly under-focussed conditions, i.e. image possesses maximum contrast.

(v) Careful control of the specimen orientation so that the structural features which are of interest lie exactly parallel to the direction of the incident beam. This is achieved by the use of a goinometer stage in the microscope. The two possible types of orientation are :-

(a) The Systematic orientation is such that the

specimen is tilted so that a single line of reflections such as hOO, OkO, OOl etc. dominates the pattern. The image then contains a set of fringes lying parallel to the diffracting planes. In brief this is the condition for a one dimensional lattice image.

(b) The Zone Axis orientation is such that the incident beam is parallel to a crystallographic direction UVW and the section of reciprocal lattice containing a set of spots so that hV + kV + lW = O. Thus for example B = [OlO] the diffraction pattern will contain hOl reflections and the resulting lattice will be two dimensional.

Lattice imaging is now accepted as one of the most powerful tools for the investigation of the microstructure of real crystals. To date most of the work on ternary or pseudoternary systems appear to be on perovskite polytypes. For example, Hutchison et al.[70] on the $Ba_{1-x}Sr_xMnO_{3-x}$ family of phases, Horiuchi et al.[76] on the $Bi_2CaNa_{n-2}Nb_nO_{3n+3}$ phases and Grenier et al.[72] on the perovskite - brownmillerite ($CaTiO_3$-$Ca_2Fe_2O_5$ - $Ca_n(FeTi)_nO_{3n-1}$) system. For "pure" A^{n+}-B^{m+}-O systems the work appear to centre around 1:5 and 2:4 systems. For example the work of Tilley[3] on the Sr-Ti-O system and Hervicu et al.[77] on the Ca-Nb-O system.

The author is aware of only two reports of the study of a 3:3 e.g. $La^{3+}B^{3+}O_3$ oxide. These were short notes by Marquis et al.[78] on the oxide $LaCoO_3$ and by Gai et al.[56] on $LaNiO_3$. The author believes that there are two principal reasons why many of the important 3:3 perovskite systems have escaped attention. The first is a historical one in that the first defect oxides studied were the CS phases of TiO_2, Nb_2O_5, and WO_{3-x}[86,90] etc. and there was a natural extension of ideas

to ternary oxides such as $CaNbO_3$, $KTaO_3$, $SrTiO_3$, etc. which were known to be defective. The second reason is the belief that the greater the formal charge on B, the greater the tendency to reside in distorted polyhedron environment. By this scheme the larger B^{3+} cations of the first row (e.g. Co, Ni and Cu) would resist the formation of CS type phases.

5.5.1 Lattice Images of the La-Ni-O Perovskite Related Phases

The types of images obtained in this study were by using the 001 systematic orientation - Section 5.5(v)(a). Therefore under conditions outlined above a one to one correspondence is possible.

Lattice images were obtained on a JEOL 120CX Electron Microscope at 100kV (λ = 0.037Å), fitted with a double tilt stage (α = $\pm 60^{\circ}$) and anticontamination unit. Specimens were crushed under butan-1-ol or liquid nitrogen and dispersed on holey carbon films.

(i) Well ordered $La_{N+1}Ni_NO_{3N+1}$ - Plate 4

Plate 4 shows one dimensional (001) lattice images of N = 1 (La_2NiO_4), N = 2 ($La_3Ni_2O_7$) and N = 3 ($La_4Ni_3O_{10}$). Remembering from Chapter 1 that results of X-ray diffraction of these oxides gave c = 12.65Å, 20.509Å and 27.94Å respectively the agreement is fair. The transition N = 1, $\longrightarrow$ 2, $\longrightarrow$ 3 is clearly shown in the fringe spacing and corresponds to the reciprocal lattice spacings shown in Plates 2(b) -2(d).

In Plate 4(b) we observe a lamella of N = 3 intergrown coherently within the N = 2 matrix. This makes the overall stoichiometry of the crystal $(La_3Ni_2O_7)_Z(La_4Ni_3O_{10})_Y$ where $Z \gg Y$.

(ii) Disordered N = 2 ($La_3Ni_2O_7$ - c = 20.509Å).

Plate 5 shows a section of a highly disordered N = 2 crystal. There are intergrown lamellae of N = 4, N = 3 and N = 1. It is difficult to deduce a stoichiometric formula since the size of U,V,X and Y

Plate 4

ID Lattice images of "well ordered" N = 1, N = 2 and N = 3 crystals using the 00L systematic orientation.

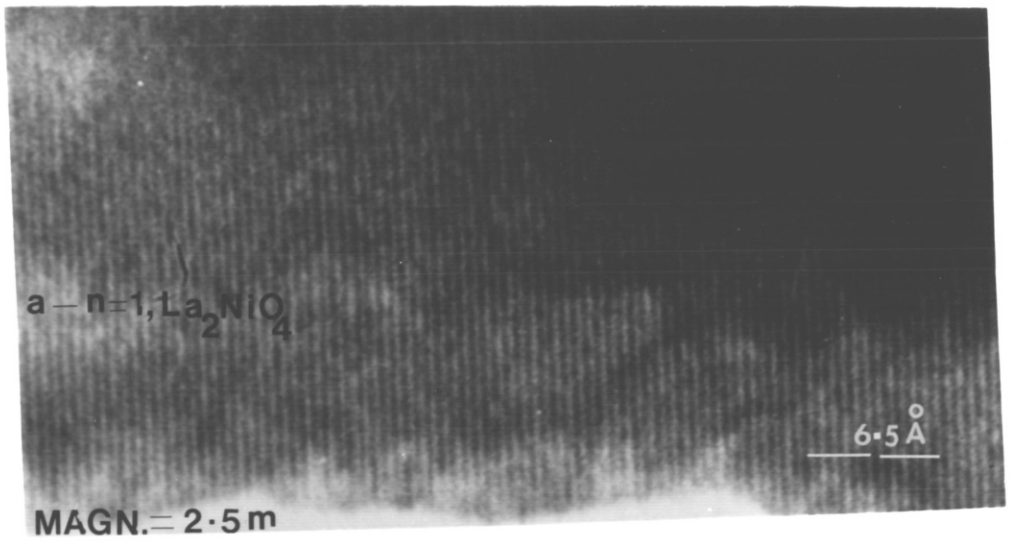

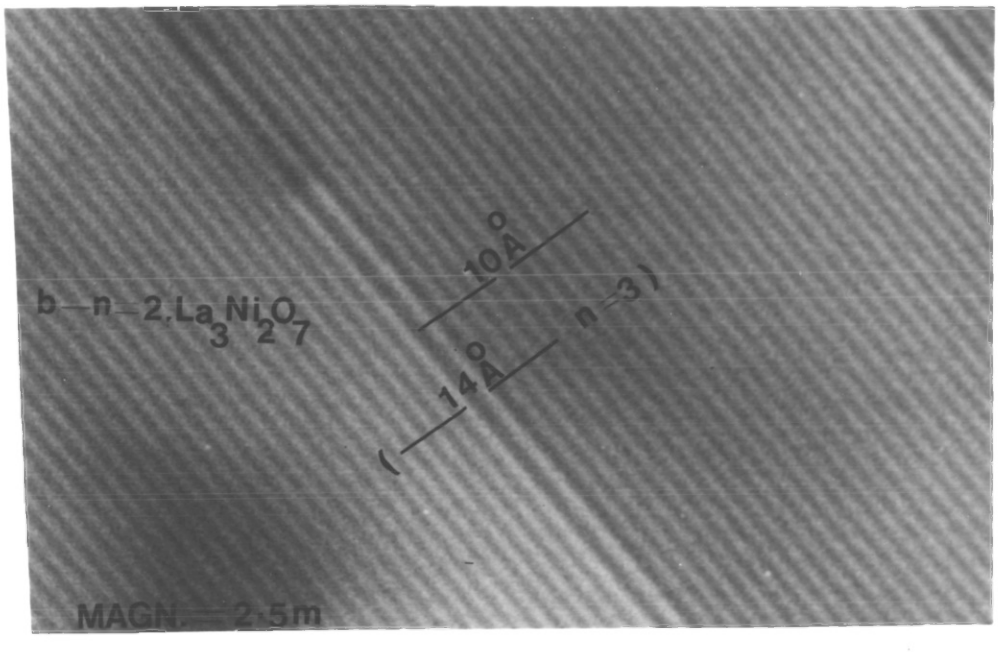

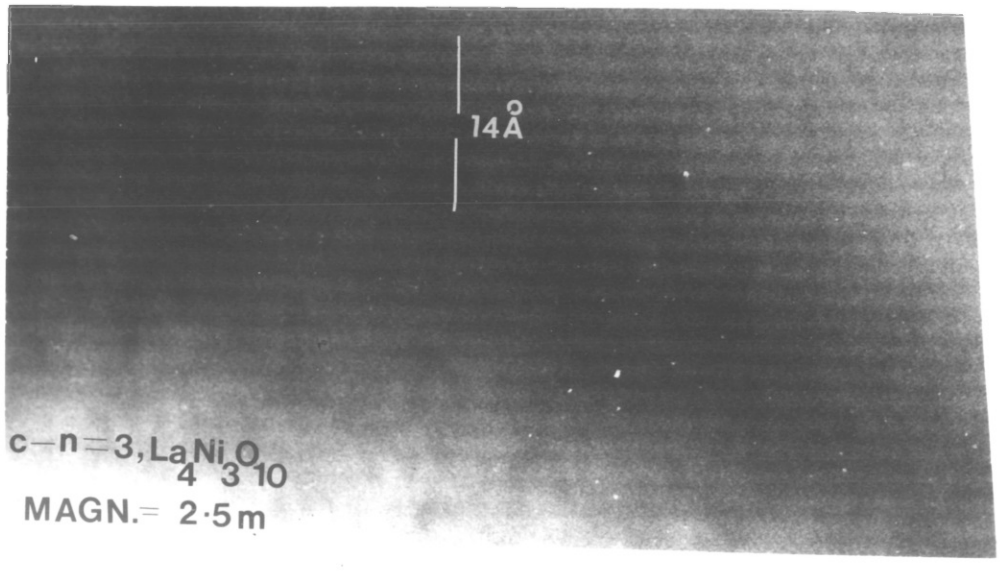

Plate 5

ID Lattice image of disordered N=2 ($La_3Ni_2O_7$)

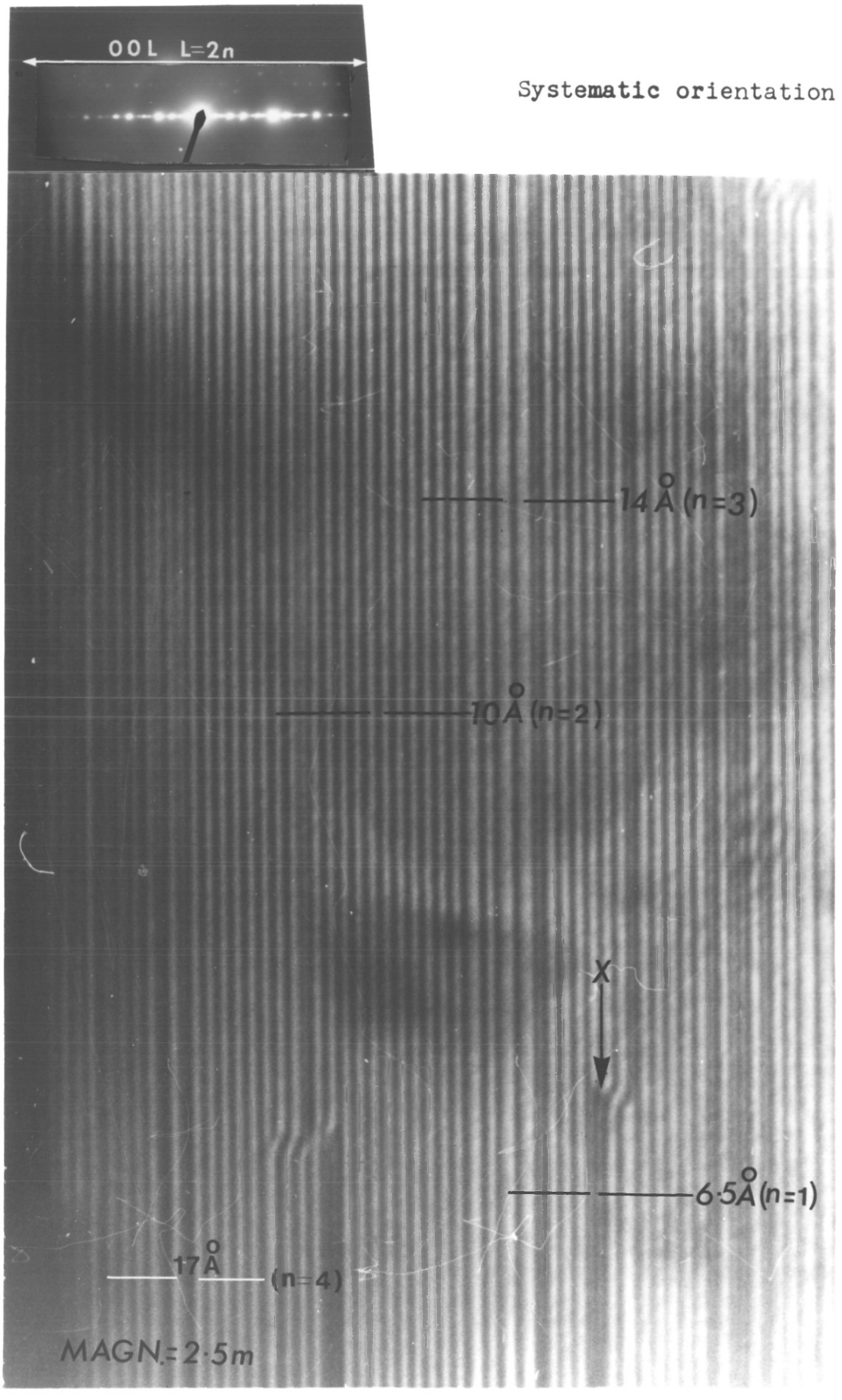

of U(N=4):V(N=3):X(N=2):Y(N=1) depend on the area of the specimen chosen. Overall V > Y and the specimen might be loosely named "oxygen rich $La_3Ni_2O_7$". Coherence does not appear to be restricted to phases with $\Delta N = 1$. For example areas of N = 3 are shown to intergrow coherently with N = 1. Thus all the phases are very similar as they all have the perovskite subcell.

Another interesting feature of Plate 5 is where the N = 1 fringes terminate within the crystal there seems to be an edge dislocation - labelled as x. The fact that the N > 1 phases are distorted to the orthorhombic may result in all interfaces not being coherent with those of the N = 1 phase and dislocations at these interfaces are therefore energetically favourable.

(iii) Disordered N = 3 ($La_4Ni_3O_{10}$ - 27.94Å)

Plate 6(a) and (b) are images of different crystals of $La_4Ni_3O_{10}$ taken at 250000 magnification. The latter shows lamellae of intergrown N = 2 and N = 4 making the overall composition somewhere between N = 3 and N = 2 since Z/X of X(N=4):Y(N=3):Z(N=2) is a very large ratio. The regions marked X and Y are probably G.P. zones but these were not studied in any detail. The crystal in the latter picture was sliced into two as shown with the crystal on the right being better oriented.

(iv) Disordered N = 4 ($La_5Ni_4O_{13}$ - c = 34.99Å -)

Plate 7 is the image taken of a crystal (of $La_5Ni_4O_{13}$) at 250000 magnification. The specimens were of extremely small grain size. The photograph shown approximates to about 90% of the actual size of typical crystal.

There is evidence of intergrown lamellae N = 2 and N = 3 and larger slabs of, what can be described as N = ∞ ($LaNiO_3$), since resolution of these regions were not possible. There is a huge

Plate 6

Lattice image of disordered N = 3 ($La_4Ni_3O_{10}$)

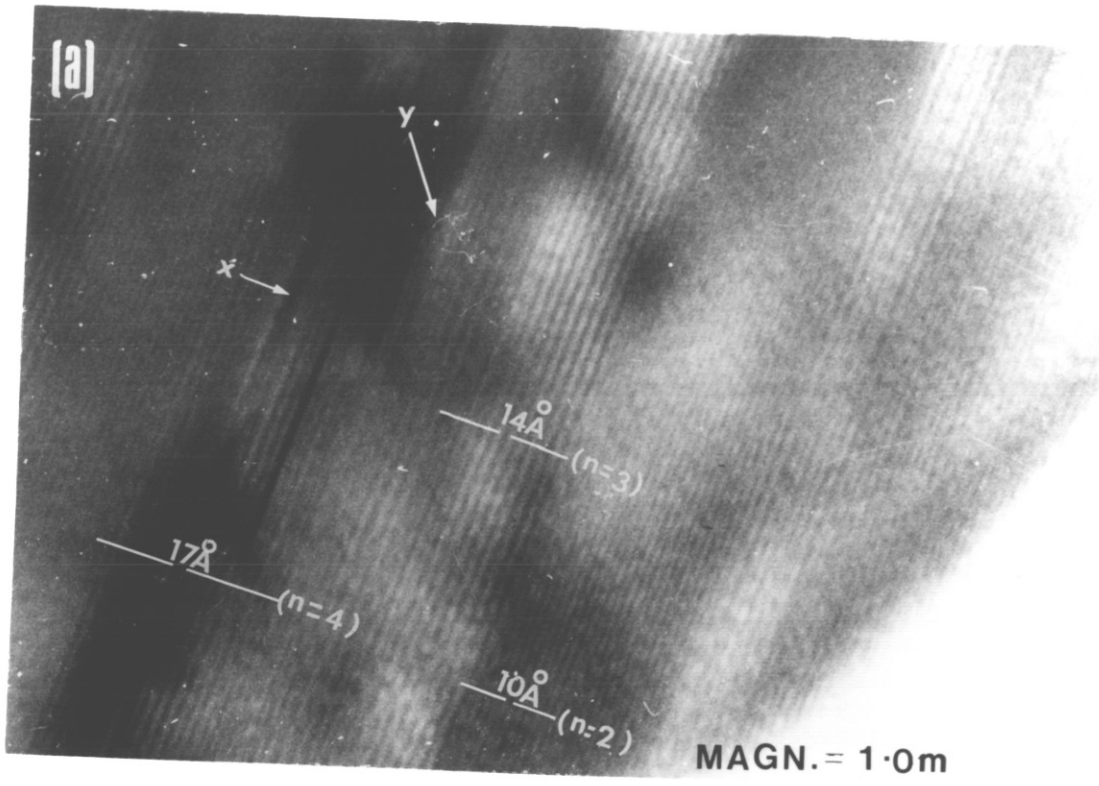

X & Y show what are probably GP zones.

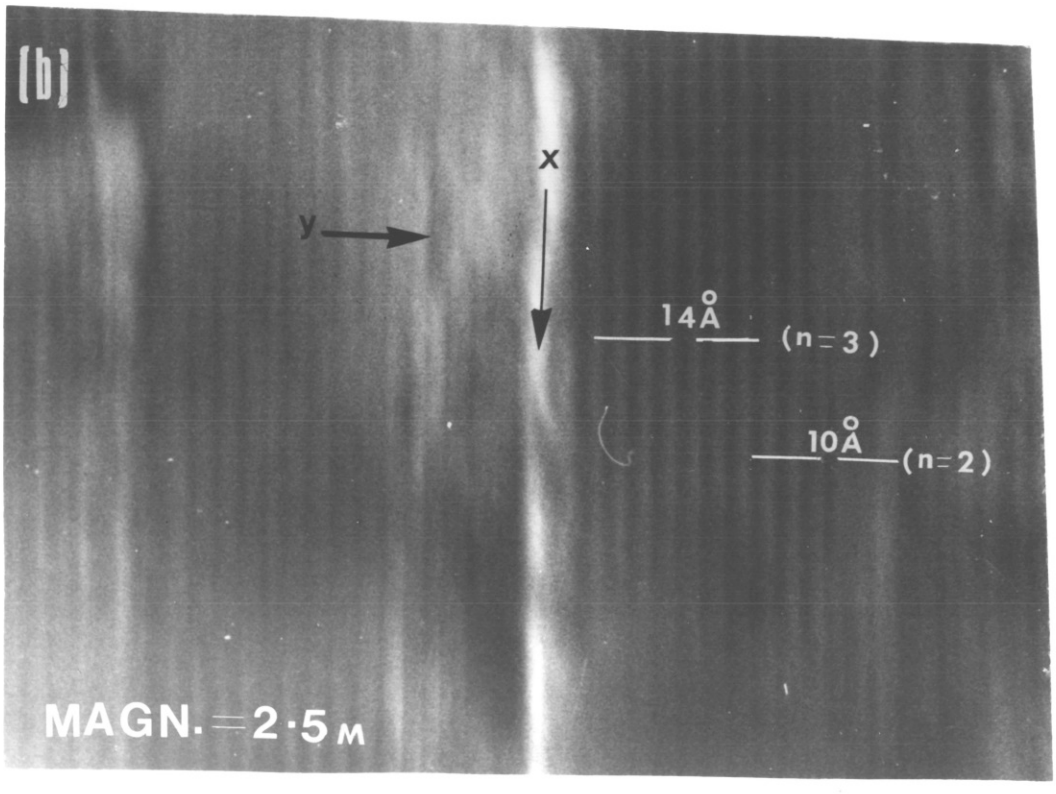

X shows boundary between two small crystals.
Y is probably a GP zone.

Plate 7

Lattice image of highly disordered N = 5 ($La_5Ni_4O_{13}$)

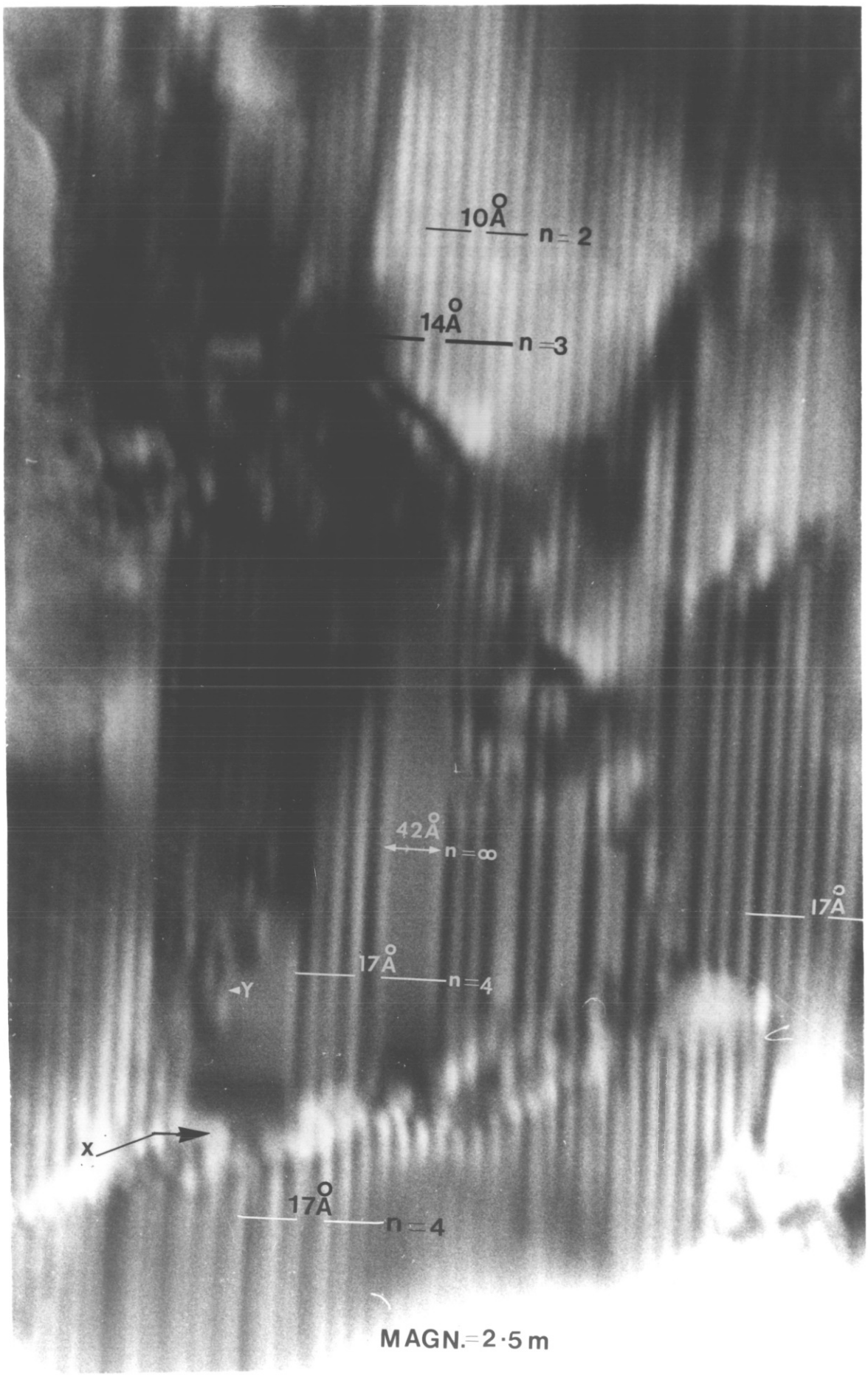

Plate 8

ID Lattice image of disordered $LaNiO_3$ showing intergrown lamellae of $La_{N+1}Ni_NO_{3N+1}$

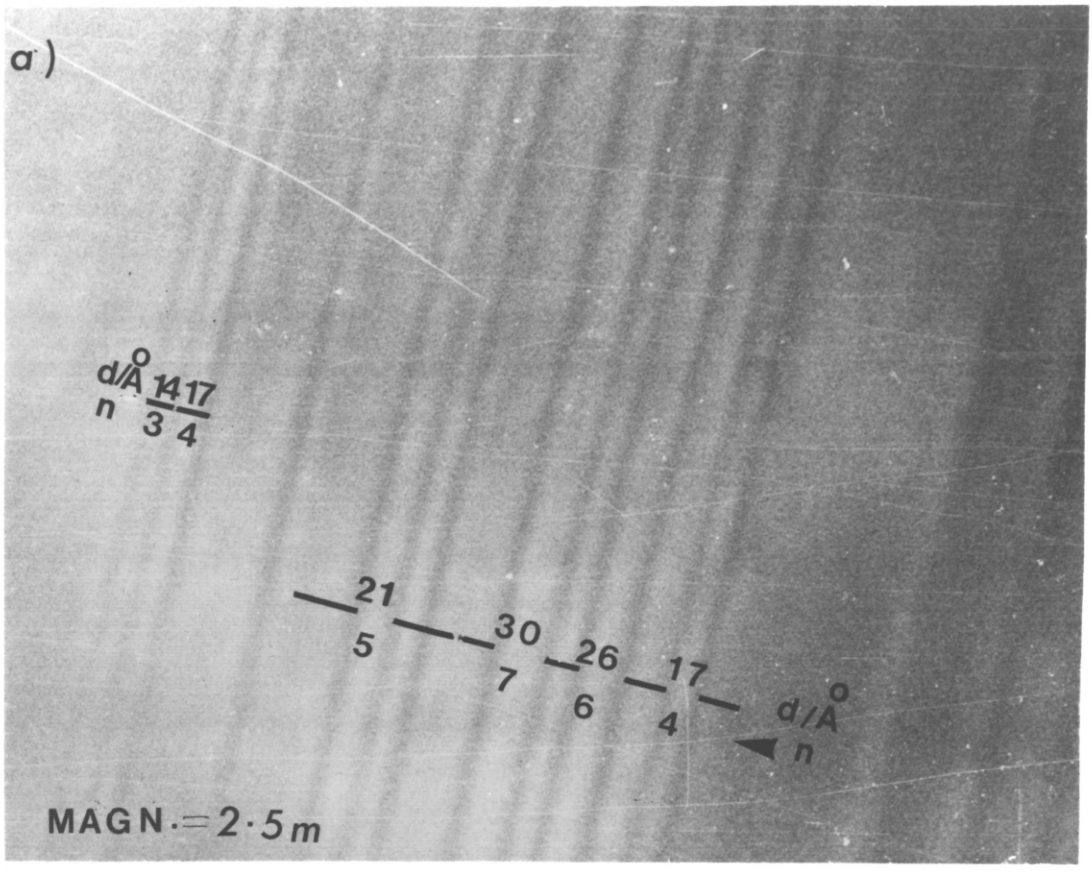

a) From caption shown in b) below

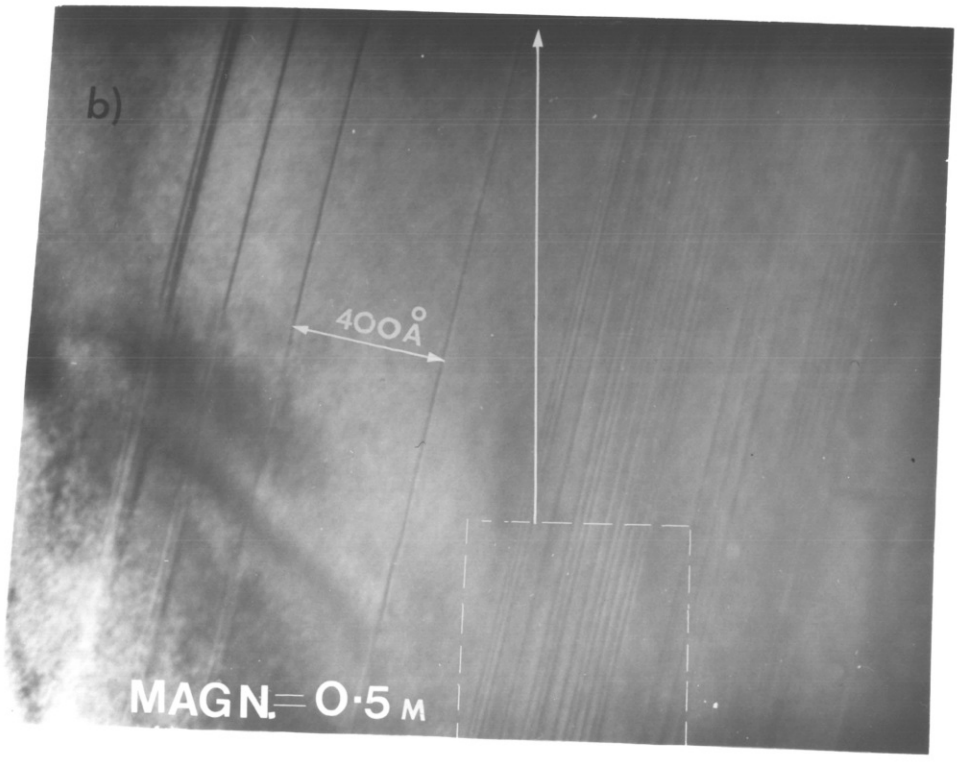

The sample was flux prepared then hot pressed at 1000°C under oxygen. Finally argon ion thinned.

dislocation running at the foot of the picture and there is a strange feature at Y which seems to be a dislocation loop (parallel to the reflecting planes) having a diameter of $\sim 14\text{Å}$.

(v) Disordered N = ∞ ($LaNiO_3$)

Plate 8 shows the image of disordered $LaNiO_3$. Specimens were from fluxed prepared $LaNiO_3$ which was then hot pressed at 1000°C in pure oxygen and then Argon-Ion thinned. This sample had the X-ray diffraction pattern of $LaNiO_3$ as reported in the literature[5].

Tilley[3], on the $Sr_{N+1}Ti_NO_{3N+1}$ phases, has stated his preferences for the interpretation of the fringes in the perovskite (N=∞) as planar faults rather than coherently intergrown phases. The author believes that this is an unnecessary formalism as coherence is possible on all interfaces of all phases sharing the perovskite subcell, although the best strain free coherence is between phases where ΔN is small, so therefore unresolved slabs can be interpreted as regions where N is large.

Generally $c_N \sim (2N+1)a_c$ where $a_c \sim 3.9\text{Å}$ so that $c_N = f(N)$ is calculable for the $La_{N+1}Ni_NO_{3N+1}$ phases, and is shown in Table 22.

TABLE 22 Approximate Unit Cell Parameter c for the $La_{N+1}Ni_NO_{3N+1}$ Compounds

N	c/Å	c/Å (observed by X-ray)
1	12	12.658
2	20	20.509
3	27	27.94
4	35	34.99
5	43	-
6	51	-

Plate 8(a) shows that areas with N= 3,4,5,6,7 and possibly 8 and 9 are present in $LaNiO_3$ prepared under the conditions discussed above. If ΔN is the principal criterion for strain free coherence then it must get larger as N increases and phases gradually become indistinguishable.

CHAPTER 6

Discussion

6.1. The validity of the formula $La_{N+1}Ni_NO_{3N+1}$ and a critique of the experimental methods in the evaluation of N.

The method of identifying the compounds was by comparing X-ray crystallographic data of isolated phases with the data of known and similar phases of other systems. Since no chemical analysis data were presented in the text, this could seemingly pose a question as to the validity of an assumed formula. By similar arguments the absence of density measurements which would have been checks on the number of formula units per unit cell are not supportive of the assumptions based on the X-ray powder diffraction data.

The fact however that lattice imaging studies indicated the grossly defective nature of the compounds shows that such data could well have been misleading.

Data from coulometric and thermogravimetric studies in Chapter 4 shows that NiO is produced at every phase transformation tending towards the more stable oxides (i.e $N \rightarrow 1$). Accordingly the formula $La_{N+1}Ni_NO_{3N+1}$ is plausible - for example the separation along the absissa in Figures 19, 31 and 34 - although N could not be determined with any great certainty because of the broadening of phase fields within the temperature range of interest i.e. $1000^oC < T < 1450^oC$. The occurrence of NiO in most, if not all, of the prepared oxides shows that N cannot be determined simply from an assessment of the macroscopic ratios of the amounts of both metal oxides used in any preparation although the X-ray detection limit of NiO in such compounds may be quite low.

Gai and Rao[56] suggestion that the intermediate phases in the La-Ni-O system were of the type $La_NNi_NO_{3N-1}$ is at variance with the structural findings in this work. These authors did not consider that

the segregation of the NiO phase accompanies all the phase transformation shown in the T.G.A. of $LaNiO_3$, and consequently writing a defect formula purely on the basis of oxygen loss was over simplistic.

The isolation and identification of $La_3Ni_2O_7$ and to a lesser extent $La_5Ni_4O_{13}$ provide vital evidence as to the existence of a family based on the formula. Seppanen's[29] suggestion that from his T.G.A., studies on $LaNiO_3$, $La_3Ni_2O_7$ did not exist especially at high temperatures, was perhaps an oversight. The findings in this work on the T.G.A., coulometric and structural studies refute this argument completely. However the structural data collected for $La_5Ni_4O_{13}$ is not very convincing. Synthesis of $N \geq 4$ phases in the La-Ni-O system appear to demand new sets of experimental guidelines and procedure. The author believes in the authenticity of the compound (e.g its decomposition temperature (Figure 14) has been determined) but further believes that purer samples and correspondingly better X-ray and electron diffraction patterns are needed for fuller characterisation.

No structural evidence of a phase $LaNi_2O_4$ (as reported by Von Sieler et al.[32]) has been observed during this study.

6.2. Factors controlling the formation of $La_{N+1}Ni_NO_{3N+1}$ phases and their coherent intergrowth

Only in the N = 1 compound was La_2O_3 ever detected (by X-ray) throughout this study. In addition, NiO is present as a decomposition product of $LaNiO_3$ and all the intermediate compounds. The preferential retention of La^{3+} must be due to the energy barrier for the formation of La_2O_3 being larger than that for the formation of NiO. The ion La^{3+} normally sits in ten or twelve-fold coordination while Ni^{2+} or Ni^{III} normally sits in six or four-fold coordination (six-fold normally with oxygen).

The long axis of all the $N < \infty$ phases have strings of N+1 La^{3+} ions not sandwiched by oxygen ions - Figure 8. Coulombic forces of repulsion might become great at large values of N so that such phases might not be obtainable without the use of dopants such as Sr^{2+} which has a similar size to La^{3+}. Other $A^{n+}_{N+1}B^{m+}_{N}O_{3N+1}$ intermediate phases have been characterised but predominantly in 2:4 (i.e. n:m) systems (for example Ruddelesden et al.[92] on the Sr-Ti-O system) and in doped 1:5 systems, e.g.Carpy et al.[88] on the (Ca)Na-Nb-O system. The a cations in these systems have a smaller charge to radius ratios. It is plausible that the coulombic repulsive forces along the c axis will not develop as rapidly (with increasing values of N) as it does in 3:3(2) systems. This is probably why the 2:4 and doped 1:5 compounds were the first to be discovered historically.

The compounds in the Sr-Ti-O and (Ca)Na-Nb-O are known to be microstructurally defective. They are also known to have a high permittivity ε[3]. There is a modern held view that a high ε is diagnostic of defect accumulation by intergrowth (extended defect) formation. The high ε is dominated by the ionic polarizibility term according to Tilley[3]. On the ultra-microscopic scale small highly charged B cations (i.e Ti^{4+} and Nb^{5+}) can occupy a distorted polyhedron environment. By this argument stabilisation of intergrowth interfaces requiring only minimal shifts in atomic positions (and free energy) would be favourable. It is known however that covalency increases with ionic charge[93] - the Ti-O bond is estimated to be 50% covalent - and Goodenough[8,11] makes the point that this markedly affects the band structure of $SrTiO_3$. It is therefore unwise to discuss this phenomenon purely on the basis of ionic charge to radius ratio.

Nevertheless Ni^{III} has an e/r of 4.8/0.60 nCm^{-1}[38] while for Ti^{4+} and Nb^{5+} it is 6.4/0.60 nCm^{-1} and 8.0/0.64 nCm^{-1}[38] respectively.

Secondly Ni^{2+} ($e/r = 3.20/0.74\ nCm^{-1}$)[38] is to varying degrees incorporated in all the $N < \infty$ compounds. A concomitant argument is that all the La-Ni-O oxides are metallic conductors or semi-conductors of low activation energy. These factors may represent significant departures from the rules that have been applied to explain the intergrowths in the insulating Sr-Ti-O and Na(Ca)-Nb-O compounds.

On the unit cell level a more general condition for the occurrence of such phases and their intergrowth appear to fit the Anderson[52,73] model more closely. That is to say two or more phases should have at least two crystallographic directions (one sublattice) in common.

6.3. Interpretation of non-stoichiometry in La-Ni-O Compounds

The compounds $LaNiO_3$ and La_2NiO_4 have been studied extensively (the former more so) for electrochemical applications[1,2a,17,18,36]. As a result their stoichiometry has, from time to time, been scrutinized. Matsumoto et al.[18,36] have suggested that the formula of $LaNiO_3$ as prepared by the flux method[5] was $LaNiO_{2.84}$. Cong et al.[89] have suggested that La_2NiO_4 prepared by the method of Rabenau et al.[19] had a formula $La_2NiO_{4+\frac{x}{2}}$ where $x \sim 0.186$. Similar observations have been forwarded by Gopalakrishaan et al.[27] All these schools suggested that nonstoichiometry involves a variable $Ni^{3+}:Ni^{2+}$ ratio.

Although the Matsumoto school[2a,18,19] has on several occasions observed the formation of NiO in $LaNiO_3$[36] they did not suggest that the oxygen nonstoichiometry of the ternary phase included the 'separating out' of the NiO phase and in consequence a La-Ni ratio greater than one in the 'defective compound'. Lattice Imaging studies (Chapter 5) have shown that nonstoichiometry in such A-B-O systems is a multiple sublattice problem and in accordance a nonstoichiometric formula is best written using the scheme developed in Section 5.2.

6.4. Correlation of microstructural and thermodynamic observations on the La-Ni-O Compounds

To reconcile structural studies and thermodynamic findings is a speculative exercise. The major difficulty in correlating the two approaches for refractory materials is the difficulty in obtaining reliable thermodynamic data at low temperatures and paradoxically obtaining detailed microstructural data at high temperatures.

In the ideal world N of $La_{N+1}Ni_NO_{3N+1}$ is both a macroscopic and a microscopic entity explainable on both structural and thermodynamic grounds. We know from our microstructural studies in Chapter 5 that in all the isolated compounds, there is always a perturbation in the mean value of N. This is inspite of the fact that the materials on the macroscopic level (i.e. from their X-ray powder diffraction studies) behave monophasic. The thermodynamic properties evaluated in Chapter 3 relies on the assumption of monophasic behaviour i.e. N being invarient.

Thermodynamic measurements on triphasic mixtures show that there is an intimate mixing of phases at higher temperatures. The random motion of ions at these elevated temperatures breaks down the uniqueness between the lattices. This is primarily due to the fact that all the phases have two common crystallographic directions. A problem arises on how to describe the phase mixing on an Operational or Subdivision Equilibrium Model as explained by Anderson[52] and others. The problem is made more intractable by the fact that we are dealing with a three component system. We can, to a first approximation, assume that two ternary N phases will intergrow in another N phase matrix so that Δ N = 1 $\pm$ 1. The possibility exists that a fourth phase (NiO) also participates.

The formation of a high temperature solid solution based on a mixing of sublattices as shown in Figure 8 is either a catastrophic or gradual process. In the former case the temperature must be such that ionic vibrations break down uncommon crystallographic directions. This is similar to the melting of a solid. The e.m.f. vs temperature curves for triphasic mixtures should show a sharp deviation at the temperature of solution formation. On the other hand if the latter case is operative, there should be a gradual solvation of solute species as solubility increases with temperature. We also know that as the temperature increases both the solute and the matrix are decomposing to the more stable phase(s) - i.e. $N \rightarrow 1$. We would under these conditions expect curveture in the E(T) plots. The data collected shows a sharp break in the E(T) plots - Figure 37. This points to a catastrophic process although this behaviour is unexpected. The data points collected are probably too widely spaced to rule out (for certain) the case of gradual solvation.

Structurally the data collected on cold, as it were, quenched samples showed evidence of intergrowths not restricted to the $\Delta N = \pm 1$ rule. Thus the assumptions in the penultimate paragraph are not wholly valid. By analogy the composition of the high temperature solid solution is more complex than that described by the simplistic thermodynamic model developed in Section 5.3.

The microstructural data collected in this work could best be described as preliminary. No satisfactory explanation of the superlattice reflections present in Plate 2 - Chapter 1 - has been given. In consequence there is a probability that 2 dimensional disorder exists in the compounds investigated. These reflections show that there are structural features along the perovskite [010] and [100] directions in all the I4mmm and Fmmm structures of the $N < \infty$ phases. The

reflections represent the breakdown of unit cell centering conditions. Now this could take the form of adjoining perovskite type subcell without the heavier La ion or in other words blocks of NiO intergrown on the unit cell level. They could also signify the intergrowth of other N phases having slightly different symmetries. Studies are now in progress to investigate these assumptions.

The occurrence of intergrowths in all the compounds investigated questions the validity of the E(T) plots for triphasic N-phase mixtures given in Chapter 3 (Figure 14a). The validity rests on the assumption that for all phases, the concentration of matrix is high in relation to solute species. This is supported by low temperature X-ray data. For the $N > 1$ phases we do not know the extent of matrix decomposition at high temperatures or how the E(T) relations are affected by any concentration of solutes. This requires analysis outside the scope of a macro-thermodynamic model.

On the experimental front the $N > 4$ oxides have smaller enthalpies and entropies of transformation. They have correspondingly smaller voltage separations in the general E(T) plot for all triphasic mixtures as exemplified in Figure 14. The problems of theoretical analysis could be mitigated if those regions of the phase diagram could be investigated at lower temperatures. It is a parodody however that from an analogy with the microstructural data collected on $La_5Ni_4O_{13}$ and $LaNiO_3$ - Plates 7 and 8 - these phases are probably more apt to be grossly defective.

6.5. The Electrocatalytic effect of $LaNiO_3$ - The probable operational situation

The electrocatalytic effect of $LaNiO_3$ has been well studied by Matsumoto et al.[2a,17,18,36]. These authors have on several occasions claimed the preparation of Cubic $LaNiO_3$[2a,36] having a lower catalytic activity for oxygen reduction than the normal

hexagonal $LaNiO_3$ prepared by the flux method[5]. The author has observed no such 'cubic' $LaNiO_3$ and believes the fuzzy X-ray diffraction pattern for poorly crystalline $LaNiO_3$ as was shown in Plate A)(d) might well have been mistaken for 'cubic' $LaNiO_3$

Matsumoto et al.[36] suggested that the rate of low temperature oxygen reduction on $LaNiO_3$ (in alkaline solution) is controlled by oxygen absorption into oxygen vacancies within the first few monolayers. This is probably interpretable in terms of thick layered perovskite $La_{N+1}Ni_NO_{3N+1}$ phases (i.e. N large) forming and decomposing under the applied electrochemical field. The speed of such processes might be rapid as enthalpies and entropies of transformation would necessarily be small. Experiments are now in progress in collaboration with the Chemistry Department of the College to investigate this assumption.

If catalytic activity is dependent on the concentration of Ni^{III} in the La-Ni-O compounds and consequently on electrode conductivity which should increase with the size of the perovskite building blocks (i.e. N), from the results obtained in Section 4.3. we can say that $LaNiO_3$ is not suitable for high temperature electrode application under oxygen pressures less than one atmosphere. This is because at these temperatures, under atmospheres with a p_{O_2} as high as air (p_{O_2} = 21.3kPa) $LaNiO_3$ does not exist. Catalytically less active $La_5Ni_4O_{13}$, $La_4Ni_5O_{10}$ and $La_3Ni_2O_7$ exist in this region of the phase diagram.

CONCLUSION

New ternary $La_{N+1}Ni_NO_{3N+1}$ compounds have been prepared. The N = 2 and 3 phases were fully characterised structurally (by X-ray diffraction) but more structural data is needed for the N = 4 phase. Thermodynamic measurements indicated that differences in thermodynamic

properties (ΔH_f^o and S^o) of phases sharing the common tangent ($\Delta N = 1$) decreases as $N \rightarrow \infty$ (perovskite building blocks become larger). However more data (investigation of more phases) is needed to fully elucidate this phenomenon.

Nonstoichiometry involves coherent intergrowth of $La_{N+1}Ni_NO_{3N+1}$ phases and in consequence is a multiple sublattice problem. Above about (1270-1310)K nonstoichiometry appears to involve one grossly defective 'metastable phase'. Full theoretical description of this on an Operational Equilibrium Model[52,90b] is beset by difficulties primarily the multiplicity of sublattices.

No electrokinetic studies on $LaNiO_3$ have been discussed in this text, but the author believes that mechanism of the reported excellent electrocatalytic effect of $LaNiO_3$[11,17] might involve formation, decomposition and reformation of thick layered perovskite $La_{N+1}Ni_NO_{3N+1}$ phases (i.e. N large) in the electrochemical reaction.

A P P E N D I X

A1 The $LaNiO_3$ Powder Diffraction Pattern :

TABLE A1 - Indexing of the X-ray Powder Diffraction of $LaNiO_3$ on the Hexagonal (H) and Rhombohedral (R3m) Basis

$d_{obs}/\AA$	$d_{cal}/\AA$	$hkl_{(R)}$	$hkl^{(5)}_{(R)}$	$hkl_{(H)}$	$hkl^{(5)}_{(H)}$	I/I_o	$I^{(5)}$
3.829	3.828	020	100	012	101	29	S
2.718	2.721	$\bar{2}20$	$10\bar{1}$	110	110	100	VS
2.696	2.693	220	110	104	012	86	VS
2.312	2.315	$\bar{1}31$	-	113	-	2	-
2.298	2.294	131	-	015	-	1	-
2.223	2.223	$\bar{2}22$	$11\bar{1}$	202	021	21	M
2.188	2.189	222	111	006	003	8	W
1.9183	1.9179	040	200	024	202	51	S
1.7223	1.7234	$\bar{2}40$	$20\bar{1}$	122	211	6	VW
1.7089	1.7089	240	210	116	113	6	W
1.5744	1.5751	$\bar{4}22$	$21\bar{1}$	300	122	12	S
1.5690	1.5690	$\bar{2}42$	-	214	-	32	-
1.5508	1.5512	242	211	018	104	12	M
1.3631	1.3640	$\bar{4}40$	$20\bar{2}$	220	220	11	M
1.3485	1.3484	044	220	208	024	11	M
1.2779	1.2786	060	300	306	303	3	VVW

$\lambda = 1.7902\AA$ (Co K_α); KCl used as internal Standard.

The diffraction pattern was indexed using the programmes EGUIN and LSUCRE.

(5) Indexing after A. Wold et al.[5]

$a_H = 5.4538\AA$, $c_H = 13.128\AA$ $\quad \left\{ a_H = 5.456\AA,\ c_H = 13.122\AA \right\}$[5]

$a_R = 7.672\AA$, $\alpha = 90^\circ 32'$ $\quad \left\{ a_R = 7.676\AA,\ \alpha = 90^\circ 43' \right\}$

A2 Calculation of ΔG°_{f} (La_2O_3) at 1200K

For the reaction -

$$2La + \frac{3}{2} O_2 \longrightarrow La_2O_3$$

$\Delta H^{\circ}_{f298} = 1758.5 \pm 13$ kJmol
$\Delta S^{\circ}_{298} = 124.9 \pm 3$ $JK^{-1}mol$ } 46,49

$$\Delta S^{\circ}_{1200} = \Delta S^{\circ}_{298} + \int_{298}^{1200} \Delta Cp \frac{dT}{T} = -289 \text{ } Jk^{-1}mol$$

$$\Delta H^{\circ}_{f1200} = \Delta H^{\circ}_{298} + \int_{298}^{1200} \Delta Cp \, dT = -1818 \pm 15 kJmol$$

Where Cp is of the form $aT + bT + \frac{c}{T^2}$ $(JK^{-1}mol^{-1})$.

Taken from Kubachewski et al.[46]

TABLE A2 - Heat capacities used in evaluation of $\Delta G^{\circ}_{f}(La_2O_3)$

	a	10^3 b	10^{-5} c
La_2O_3 (298-1171)K	120.75	12.886	-13.723
*La (298-800)K	25.18	6.694	-
O_2 (298-3000)K	29.957	4.184	- 1.673

* The assumption is made that no phase change takes place up to 1200K.

A3 Third Law Entropies

TABLE A3 - S° for components in the La-Ni-O- phase diagram

Phase	$S^{\circ}_{298}/JK^{-1}mol^{-1}$	$S^{\circ}_{1050}/JK^{-1}mol$	$S^{\circ}_{1200}/JK^{-1}mol$
O_2	205.10	246.02	250.06
NiO	38.07	94.90	102.47
Ni	27.79	70.03	74.44
La	56.90	94.44	98.89
La_2O_3	124.90	289.73	308.24

S° is calculated from Cp data in (48) and (49) and the 'Third Law Treatment' (Chapter 2).

REFERENCES

1. T.H. Estell - Proc. Workshop High Temp Solid Oxide Fuel Cells (Ass. Univ.-Ed H.S. Issacs, S. Srinivasan and I.L. Harry -) p66 (1977)

2.(a) H. Tamura, H. Yoneyama and Y. Matsumoto - Electrodes of Conductive Metallic Oxides (Elsevier - Ed. S. Trassatti -). A 261 (1980)

(b) E. Honig - Electrodes of Conductive Metallic Oxides (Elsevier) Ed. S. Trassatti -). A 83 (1980)

3. R.D.J. Tilley - J. Solid State Chem. 21 293 (1977)

4. H. Obayashi and T. Kudo - Jap. J. Appl. Phys. 14(3) 330 (1975)

5. A. Wold, B. Post and E. Banks - J Amer. Chem. Soc. 79 4911 (1957)

6. G. Demazeau, A. Morbeuf, M. Pouchard and P. Hagenmuller - J. Solid State Chem. 3 582 (1971)

7. C.N.R. Rao - J. Indian Chem. Soc L1 979 (1974)

8. J.B. Goodenough and J.M. Longo - Landolt Bernstein Tableau (New Jersey 111/4a) Springer Verlag Berlin (1970)

9. J.B. Goodenough, N. Mott, M. Pouchard, G. Demazeau and P. Hagenmuller - Mater. Res. Bull 8 647 (1973)

10. P. Ganguly and C.N.R. Rao - Mater. Res. Bull 8 405 (1973)

11. J.B. Goodenough and P.M. Raccah - J. Appl. Phys. 36(4) 1031 (1965)

12. J.B. Goodenough - J. Appl. Phys. 37(3) 1425 (1966)

13. W.C. Koehler and E.O. Wollan - J. Phys. Chem. Solids 2 100 (1957)

14. J. Gopalakrishnan, G. Colsman and B. Reuter - Z. Anorg. Chem 424 155 (1976)

15. G. Demazeau, C. Parent, M. Pouchard and P. Hagenmuller - Mater. Res. Bull 7 913 (1972)

16.(a) M. Arjomand and P.J. Machin - J.C.S. (Dalton) 1055 (1975)

(b) M. Arjomand and P.J. Machin - J.C.S. (Dalton) 1061 (1975)

17. Y. Matsumoto, H. Yoneyama and H. Tamura - J. Electroanal Chem. 83 167 (1977)

18. Y. Matsumoto, H. Yoneyama and H. Tamura - J. Electroanal Chem. 80 116 (1977)

19. V.A. Rabenau and P. Eckelin - Acta Crystallog. 11 304 (1958)

20. G. Demazeau, M. Pouchard and P. Hagenmuller - J. Solid State Chem. 18 159 (1976)

21. G. Blasse - J. Inorg. Nucl. Chem. 27 2683 (1963)

22. G. Thornton, A.F. Orchard and C.N.R. Rao - J. Phys (Solid State) 9 1991 (1976)

23. J.B. Goodenough - Mater. Res. Bull 8 423 (1973)

24. G.A. Smolenskii, V.M. Yudin and E.S. Sher - Fiz. Tver. Tela. 4(11) 3350 (1962)

25. E. Legrand and M. Ver Schveren - J. Physique 25 578 (1964)

26.(a) H. Kleinsmager and A. Reich - Z. Naturforsn. 27a 363 (1971)

(b) N.I. Timofeeva and I.V. Romanovich - Izv. Akad. Nauk. SSSR Neorg. Mater. 7(11) 2104 (1971)

27. J. Gopalkrishnan, G. Colsman and B. Reuter - J. Solid State Chem. 22 145 (1977)

28. G.J. McCarthy, W.B. White and Roy - J. Inorg. Nucl. Chem. 31(12) 329 (1969)

29. M. Seppanen - Scan. J. Metal. 5 191 (1979)

30. J.J. Janeck and G.P. Wirtz - J. Amer. Ceram Soc. 61(5) 242 (1978)

31. M. Seppanen and M.H. Tikkanen - Acta. Chem. Scand Ser A 30(5) 389 (1976)

32. Von J. Seiler and J. Kaiser - Z. Anorg. Chem. 371 316 (1970)

33.(a) T. Nakamura, G. Petzow and L.G. Gaukler - Mater. Res. Bull 14 649 (1979)

(b) A. Wold and R.J. Arnott - J. Phys. Chem. Solids 9 1976 (1959)

34.(a) O. Greis and H. Andress "EGUIN" - Program for Length Corrections of X-ray Guinier Patterns - Freiburg i Br (1972)

(b) O. Greis "LSUCRE" - Program for Least Squares Unit Cell Refinement Freiburg i Br (1970)

35. D. Mekhandzhiev - Dolk. Bolg. Akad. Nauk 22(11) 1253 (1969)

36. Y. Matsumoto, H. Yoneyama, H. Tamura - Bull Chem Soc. Japan 51(7) 1927 (1978)

37.(a) A.M. Golub, L.S. Sidorik, S.A. Nedilko and T.T. Fedorick - Izv. Akad. Nauk, SSSR Neorg. Mater. 14(10) 1866 (1978)

37.(b) P.K. Gallagher - Mater. Res. Bull 3 225 (1968)

38. R.D. Shannon and C.T. Prewitt - Acta. Crystallog. B25 925 (1969)

39. D.M.L. Goodgame and M.A. Hitchman - Inorg. Chem 3(10) 1389 (1964)

40. K. Boguslawska and A. Cyganski - Rocz. Chem. 49 1079 (1976)

41. K. Boguslawska and A. Cyganski - Chem. Anal (Warsaw) 20(4) 893 (1975)

42. M.B. Davies and J.W. Lethbridge - J. Inorg. Nucl. Chem 34 2171 (1972)

43. M.V. Kniga and R. Zaretskaya - Izv Akad. Nauk. SSSR. Neorg. Mater 7(3) 2164) (1971)

44. Chan Li Chuan and W. Weppner - Naturwiss (Springer Verlag) 65(S) 595 (1978)

45. B.C.H. Steele - Electromotive Force Measurements at High Temp. (Ed. C. Alcock.) (Inst. Mining and Mettallurgy) p12 (1968)

46. O. Kubaschewski and C.B. Alcock - Metallurgical Thermochemistry 5th Edition (Pergamon) p392-447 (1979)

47. M. Seppanen - Thesis for Doctor of Technology - Helsinki University of Technology (1979)

48. O.M. Sreedharan, M.S. Chandrasekharaiah and M.D. Karkhanavala - High Temp. Sci. 8 179 (1976)

49. I. Barin, Knack and O. Kubaschewski - Thermochemical Properties of Inorganic Substances (Springer Verlag Berlin) p395 (1975)

50. Glassner - Thermochemical Props. of Oxides, Fluorides and Chlorides to 2500K Argonne National Laboratory publn. ANL (5750)

51. J. Cassendane - An. da. Braselaria-de Ciencias 36(1) 13 (1964)

52. J.S. Anderson - Problems of Nonstoichiometry (North Holland - Ed. A. Rabenau) p22 (1970)

53.(a) Balhauson - Introduction to Ligand Field Theory - (McGraw Hill) p99 (1966)

(b) E. Konig and Kremer - Ligand Field Theory (McGraw Hill) 8 397-403 (1977)

54. J.B. Goodenough, A. Wold, R.J. Arnott and N. Henyuk - Phys. Rev. 124(a) 373 (1961)

55. G.W. Lewis and M. Randall - (Rev. K. Pitzer and L. Brewer) - Thermodynamics (McGraw Hill) Chapt. 34 p551 (1961)

56. P.L. Gai and C.N.R. Rao - Z. Naturforsch (30a) 1092 (1975)

57. Per Kofstad - Nonstoichiometry, Diffusion and Electrical Conductivity in Binary Metal Oxides (John Wiley) p258 (1972)

58. B.C.H. Steele and R.W. Shaw - Solid Electrolytes 28 483 (1978)

59. B.C.H. Steele - N.B.S. Special Publ^{n} 296 165 (1968)

60. Y. Meas - These, Docteur-Ingenieur E.N.P.G. Grenoble (France) (1978)

61. J. Fouletier and M. Kleitz - J. Electrochem. Soc. 125(5) 751 (1978)

62. W. Weppner, Chan Li Chuan and W. Pickarczyk - Electrochemical Determination of Phase Diagrams and Thermodynamic Data of Multicomponent System - Electrochimicia Acta - Submitted for Publication 1980.

63. J. Fouletier, P. Fabry and M. Kleitz - J. Electrochem. Soc. 123(2) 204 (1978)

64. R.T. Dirstine and C.J. Rosa - Z. Metalkde 43(70) 152 (1979)

65. D. Haaland - J. Electrochem. Soc. 127(4) 796 (1980)

66. B.C. Tolfield and W.R. Scott - J. Solid State Chem. 10 183 (1974)

67.(a) J. Galy and A. Carpy - Phil. Mag. 29 1207 (1974)

(b) R. Portier, A. Carpy, M. Fayard and J. Galy - Phys. Stat. Sol (a) 30 683 (1975)

68. M. Nanot, F. Queyroux, J.C. Giles, R. Portier and M. Fayard - Mater. Res. Bull 10 313 (1975)

69. A.J. Jacobson and A.J.W. Horrox - Acta. Crystallog. 332 1503 (1976)

70. J.L. Hutchison, A.J. Jacobson - J. Solid State Chem. 20 117 (1977)

71. B.C. Tolfield, C. Greaves and B.E.F. Fender - Mater. Res. Bull 10 737 (1975)

72. J.C. Grenier, G. Schiffmacher, P. Caro, M. Pouchard and P. Hagenmuller - J. Solid State Chem 20 365 (1977)

73. J.S. Anderson - J.C.S. Dalton p1107 (1973)

74. J.G. Allpress and J.V. Sanders - J. Appl. Crystallog. 6 165 (1975)

75. J.W. Edington - Pract. El. Microscopy (Macmillan) 3 p(75-82) (1976)

76. S. Horiuchi, K. Muramatsu and M. Shimager - J. Solid State Chem. 34 51 (1980)

77. M. Hervicu, F. Studer and B. Raveau - J. Solid State Chem. 22 272 (1977)

78. P. Marquis and L.B. Sis - J. Mater. Sci. 12 1484 (1977)

79. W. Weppner and R.A. Huggins - J. Electrochem Soc. 125(1) 7 (1978)

80. M. Foex - Bull Soc. Chemique France 109 (1970)

81. W.B. Parsons - Treatise on Solid State Chem. - Ed. B. Hannay p115 (1971)

82. H. Obayashi, Y Sakurai and T. Gejo - J. Solid State Chem. 17 299 (1976)

83. L.S. Darken and R.G. Gurry - Physical Chem. of Metals (McGraw Hill) Chapt. 10 - (1953)

84. T. Wolfram, E.A. Krant and F.J. Horin - Phys. Rev B 7(4) 1677 (1973)

85. D.B. Meadowcroft - Nature 226 847 (1970)

86. E. Iguchi - J. Solid State Chem 23 231 (1978)

87.(a) J.S. Anderson - (Plenum Publ^{n} - Modern Aspects of Solid State Chem. - Ed. C.N.R. Rao -) p29 (1970)

(b) J.S. Anderson - J.C.S. Publ^{n} - Surface and Defect Props. of Solids (I) p5 (1972)

88. A. Carpy, P. Amestoy and R. Portier - Comp. Rend. Acad. Sc. Paris 278(c) 1256 (1974)

89. H.N. Cong, P. Chartier and J. Brenet - Comp. Rend. Acad. Sc. Paris 279(c) 1085 (1974)

90.(a) E. Iguchi and R.D.J. Tilley - J. Solid State Chem. 21 49 (1977)

(b) R.D.J. Tilley - J. Solid State Chem. 19 53 (1976)

91. W.M.H. Sachlter and P. Van der Pank Surf. Sci 18 62 (1969)

92. S.N. Ruddlesden and P. Popper - Acta. Crystallog. 10 538 (1957)
11 54 (1958)

93. E. Mooser and W.B. Parsons - Acta. Crystallog. 13 1015 (1959)